Introductions to crystal structure using X-ray Diffraction methods

Ian Robinson
Brookhaven National Lab
University College London
School of Materials, TongJi

+Als-Nielsen and McMorrow Book

+Prof. Jeremy Cockcroft, UCL Chemistry

+Emil Bozin talk at ADD 2013 (Grenoble)

Class Outline

- Crystal structure (using VESTA software)
- Surface diffraction and surface structure
- Powder diffraction methods
- Williamson-Hall analysis of size and strain
- Pair Distribution Function (PDF)

Generations of Synchrotron

- 2nd: Storage Ring Dedicated to X-rays
  - NSLS Surface X-ray Diffraction 1987
- 3rd: Undulators in "Straight Sections"
  - APS Coherent X-ray Diffraction 2001
  - NSLS-II 2015
- X-ray Free Electron Lasers
  - LCLS Ultrafast Coherent Diffraction 2008

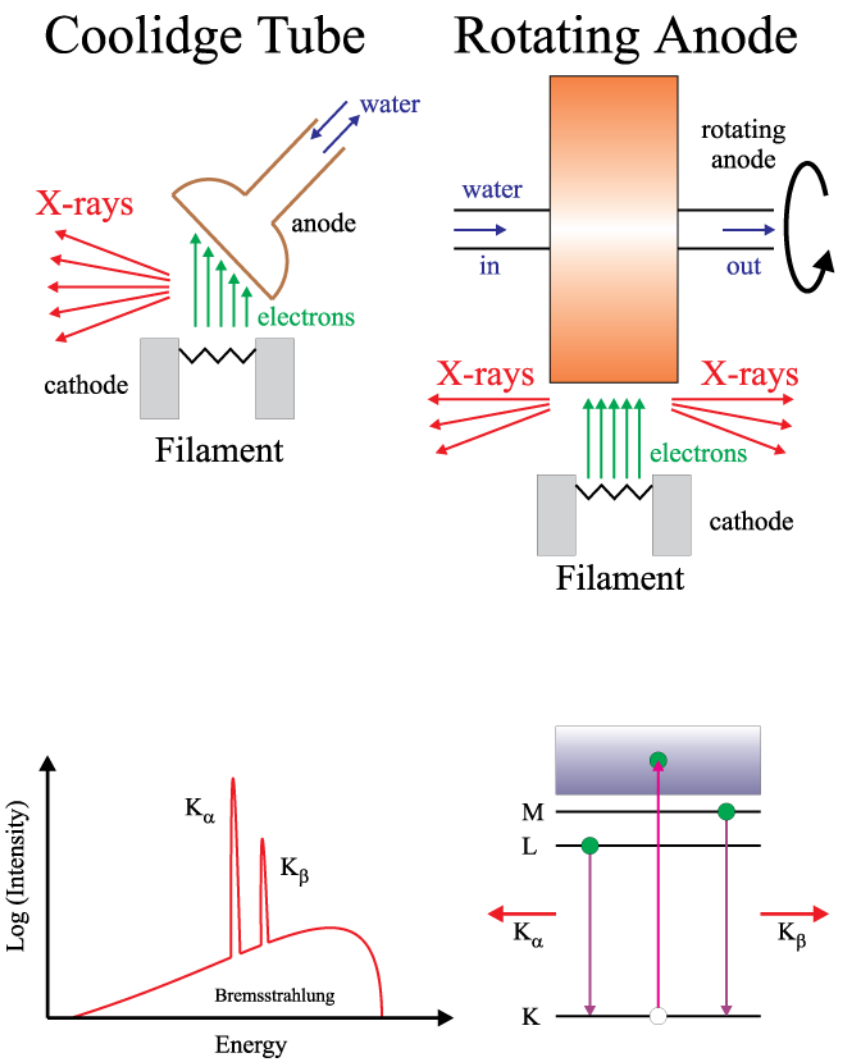

Fig. 2.1 The standard X-ray tube (upper, left) was developed by Coolidge around 1912. The intensity limitation is set by the maximum power a cooled metal anode can withstand. The power can be increased by dissipating it over a larger volume which is achieved by rotating the anode (upper, right). The spectrum from an X-ray tube has discrete fluorescent lines superimposed on the continuous bremsstrahlung radiation (bottom, left). Schematic atomic energy level diagram (bottom, right): the K_α line results from transitions between an L and K shell, whereas the K_β comes from an M to K transition.

X-ray Scattering vs Diffraction

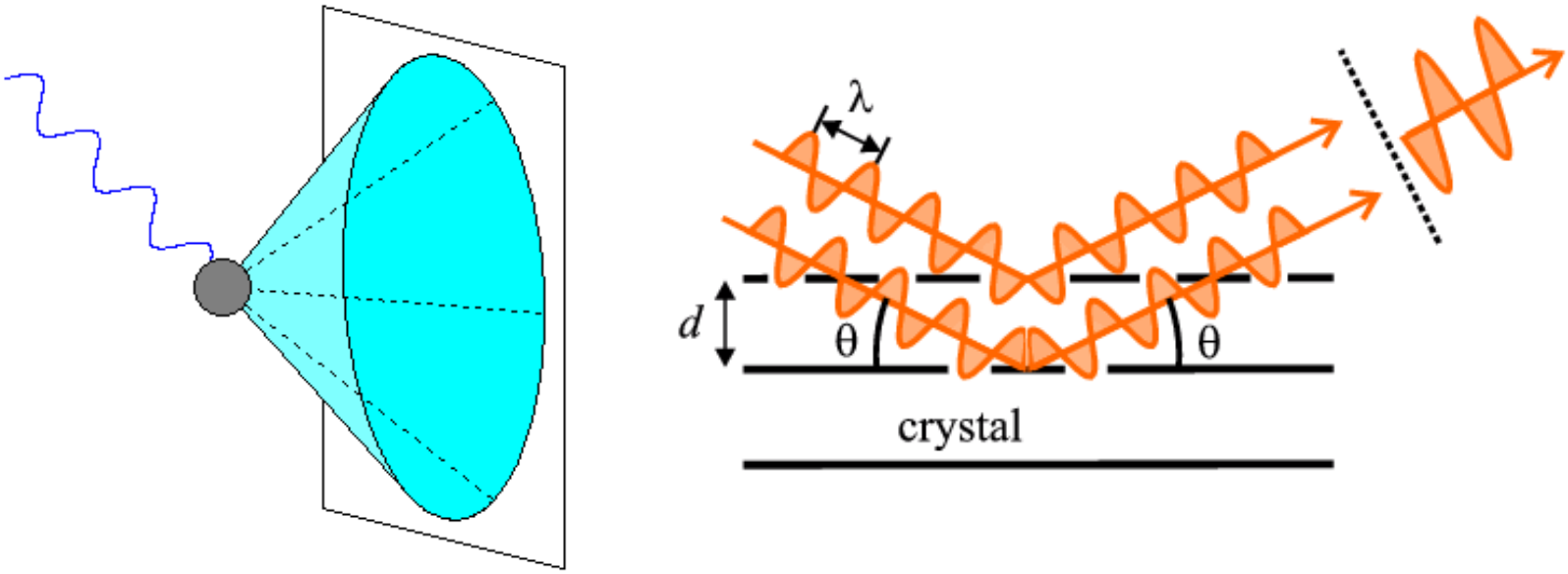

Elements of Modern X-ray Physics
Second Edition

Chapter 5
Kinematical scattering II: crystalline order

Jens Als-Nielsen and Des McMorrow

John Wiley & Sons Ltd

Chinese translation by Donglai Feng <dlfeng@fudan.edu.cn>

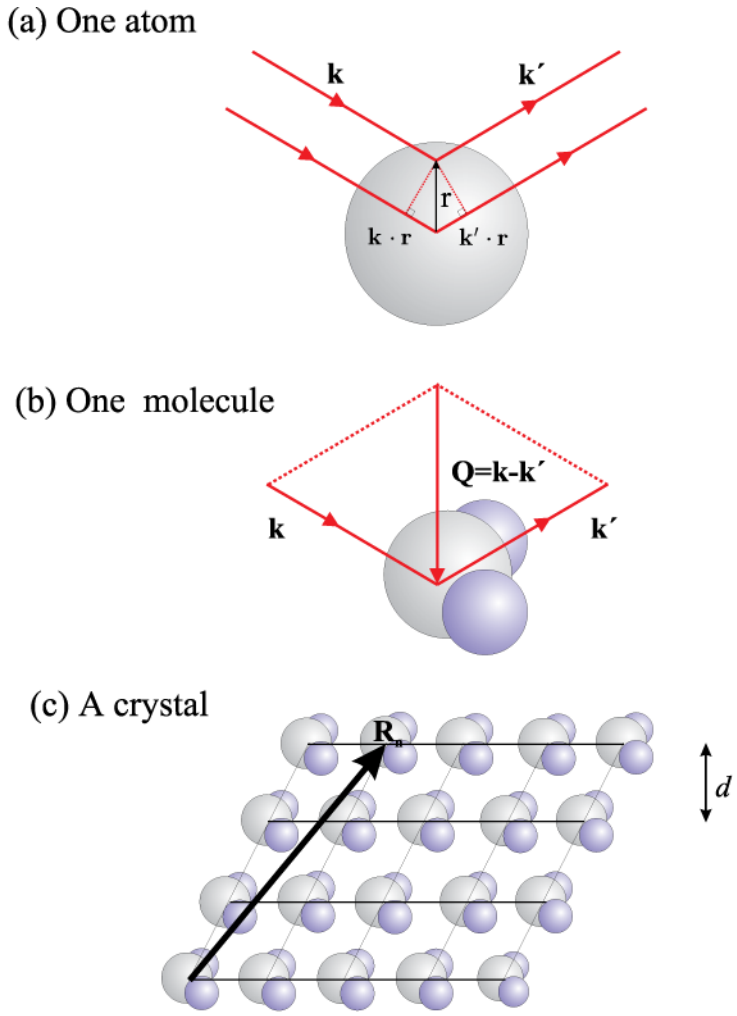

Fig. 1.7 (a) Scattering from an atom. An X-ray with a wavevector **k** scatters from an atom to the direction specified by **k′**. The scattering is assumed to be elastic, i.e. $|\mathbf{k}| = |\mathbf{k}'| = 2\pi/\lambda$. The difference in phase between a wave scattered at the origin and one at a position **r** is $(\mathbf{k} - \mathbf{k}') \cdot \mathbf{r} = \mathbf{Q} \cdot \mathbf{r}$. This defines the wavevector transfer **Q**. (b) The scattering from a molecule. Here the scattering triangle is shown which relates **k**, **k′** and **Q**. (c) Scattering from a molecular crystal. The molecules are organized on a lattice with position vectors $\mathbf{R_n}$, and a lattice plane spacing of d.

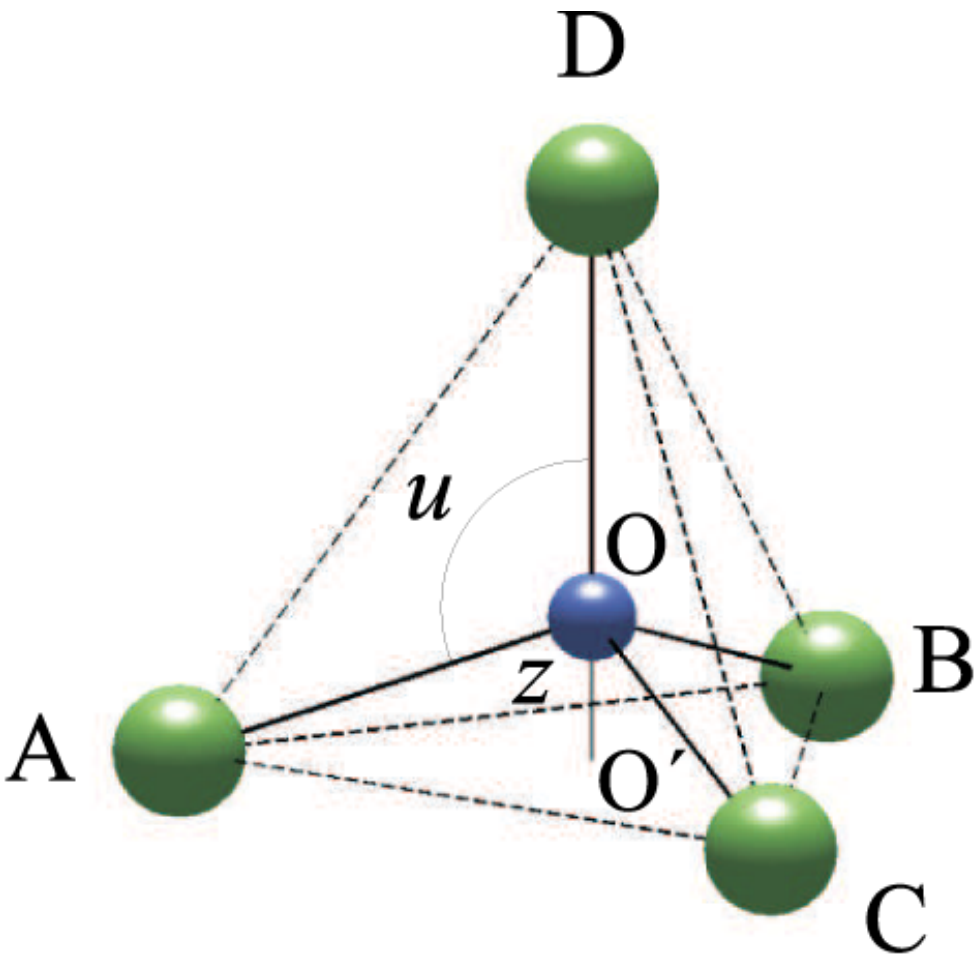

Fig. 4.6 The CF_4 molecule. The C-F bond length is 1.38 Å, and the geometry is such that the ratio of the length of OD to OO′ is 3:1.

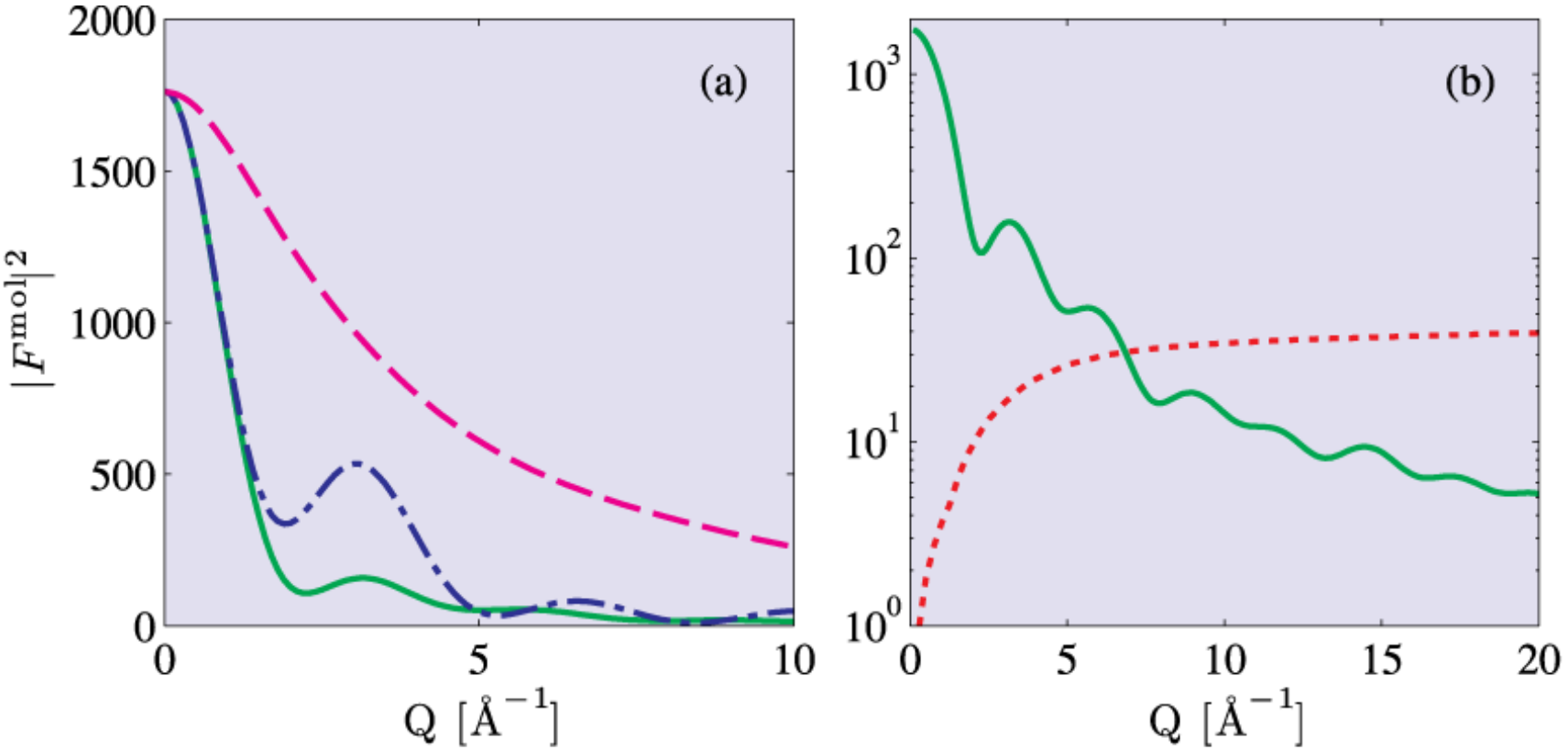

Fig. 4.7 The calculated molecular structure factor squared of the CF_4 molecule. (a) Dashed-dotted blue line is from Eq. (4.13); solid green line is calculated from a spherical average of the structure factor (Eq. (4.14)); magenta line is the square of the form factor of atomic molybdenum which has the same number of electrons as the CF_4 molecule. (b) Solid green line is the spherically averaged structure factor of CF_4; red dashed line is the Compton scattering calculated from the information given in the *International Tables of Crystallography*.

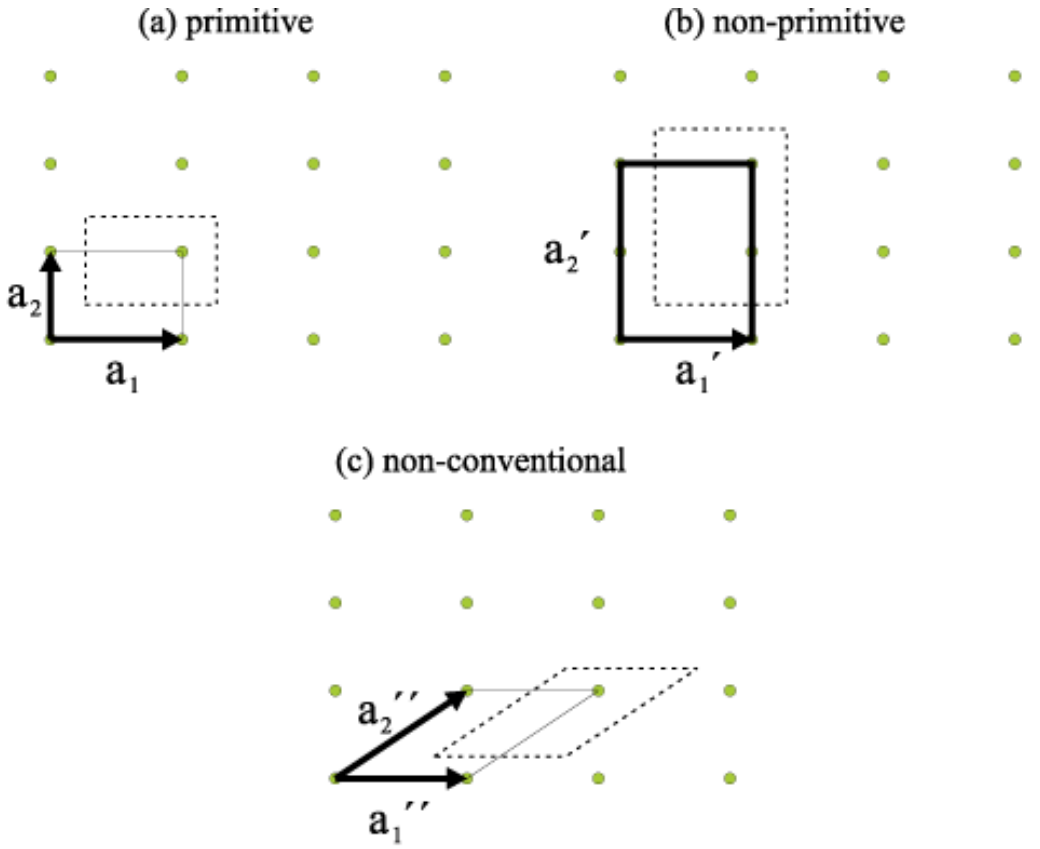
(a) primitive
(b) non-primitive
a2
a1
a2′
a1′
(c) non-conventional
a2′′
a1′′
(d) Crystal=lattice ★ basis
Lattice
Basis
Crystal

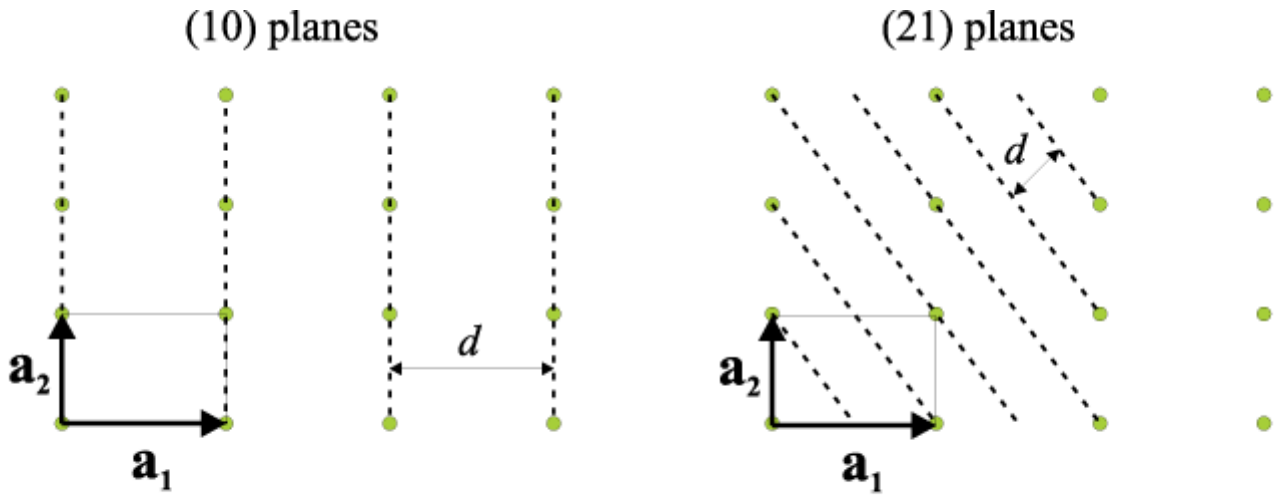

Fig. 5.2 Lattice planes and Miller indices for the 2D rectangular lattice: (a) the (10) planes; (b) the (21) planes. In both cases the *d* spacing of the planes is indicated.

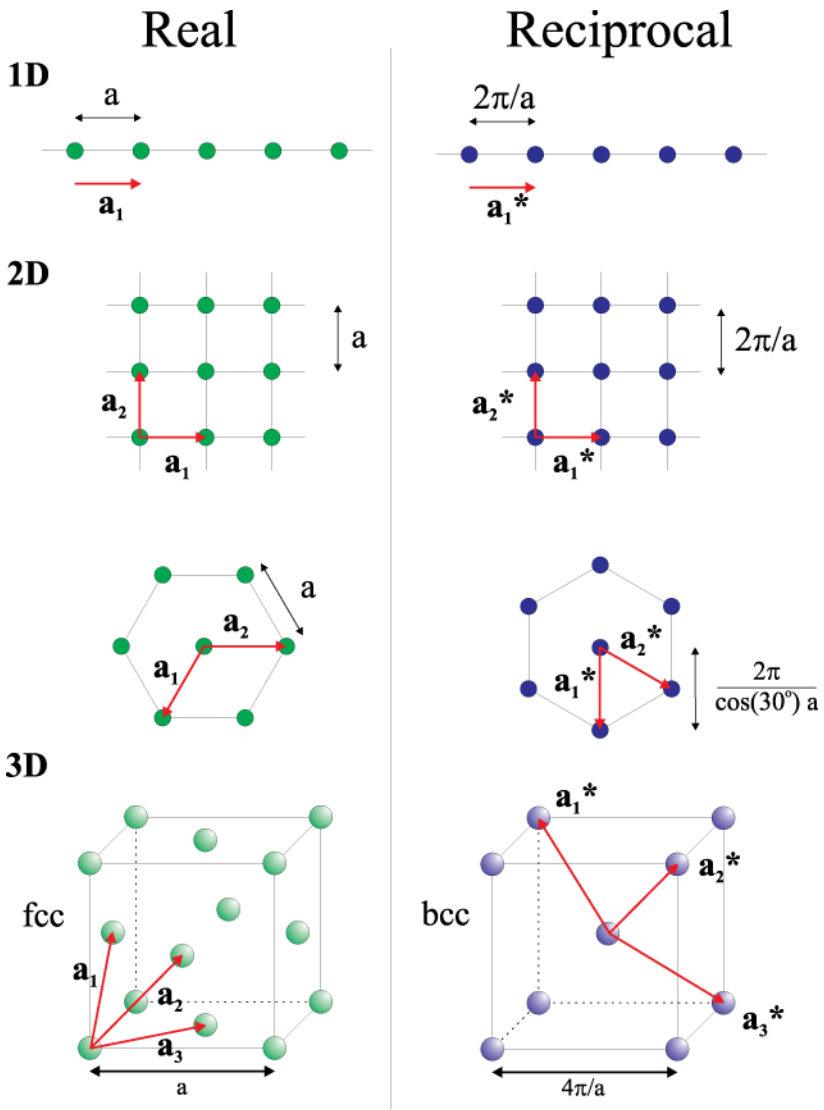

Fig. 5.3 Example of the construction of reciprocal lattices in one, two, and three dimensions.

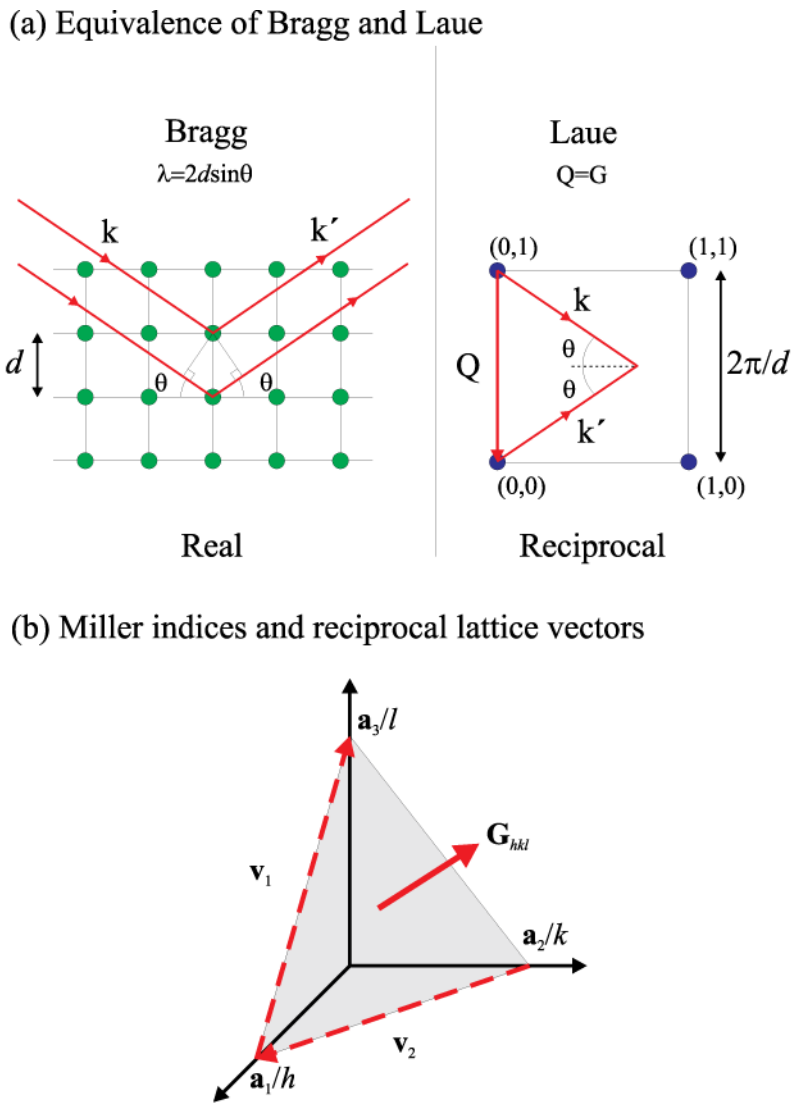

Fig. 5.4 (a) The equivalence of Bragg's Law and the Laue condition for the particular case of the 2D square lattice. (b) Construction to prove that the reciprocal lattice vector $\mathbf{G}_{hkl}$ is perpendicular to the (h, k, l) planes, and has a magnitude equal to $2\pi/d_{hkl}$.

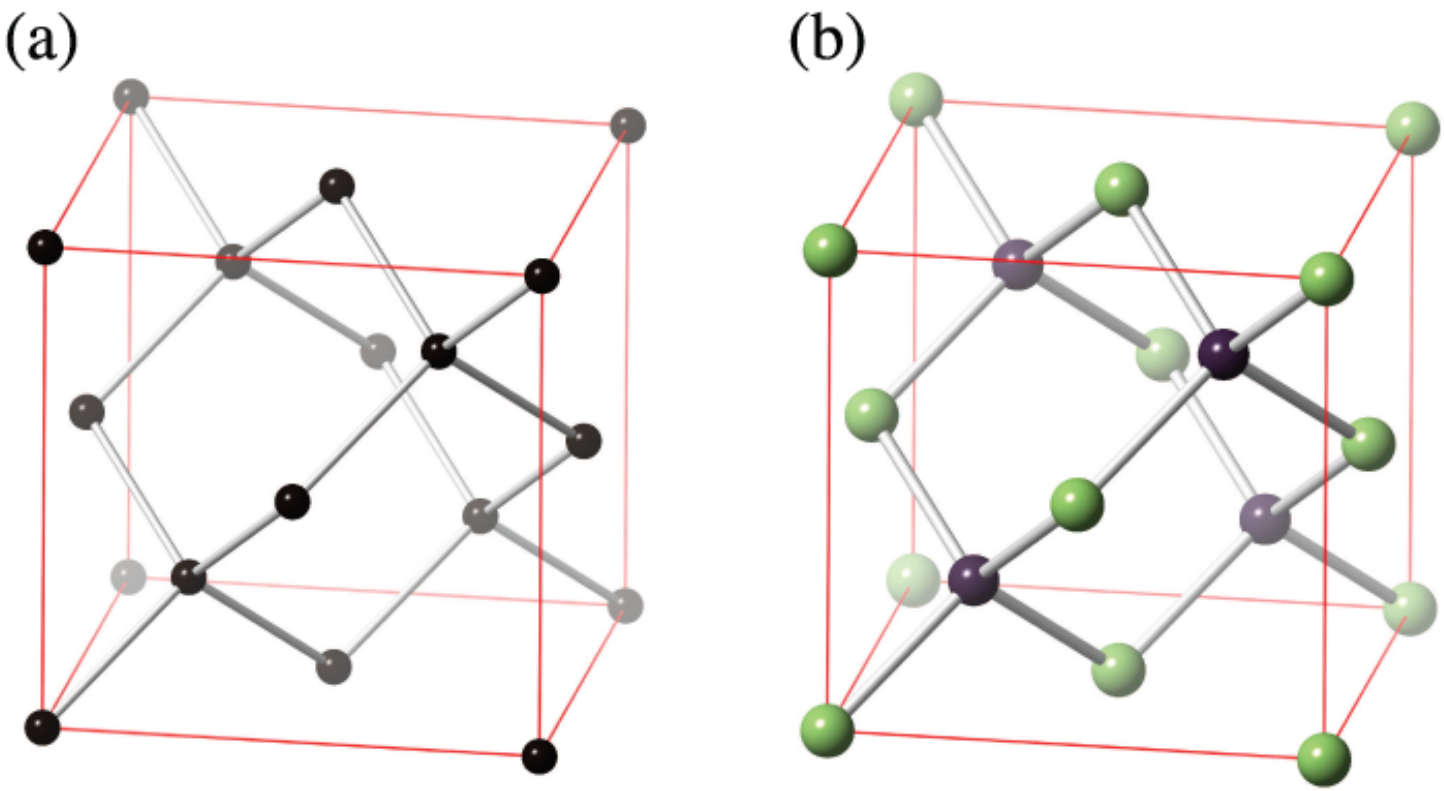

Fig. 5.5 The diamond lattice (a) can be formed from two inter-penetrating *fcc* lattices displaced by $(\frac{1}{4}\,\frac{1}{4}\,\frac{1}{4})$ with respect to each other. For the zinc sulfide (also known as zinc blende) structure (b) the two lattices are occupied by different types of atom.

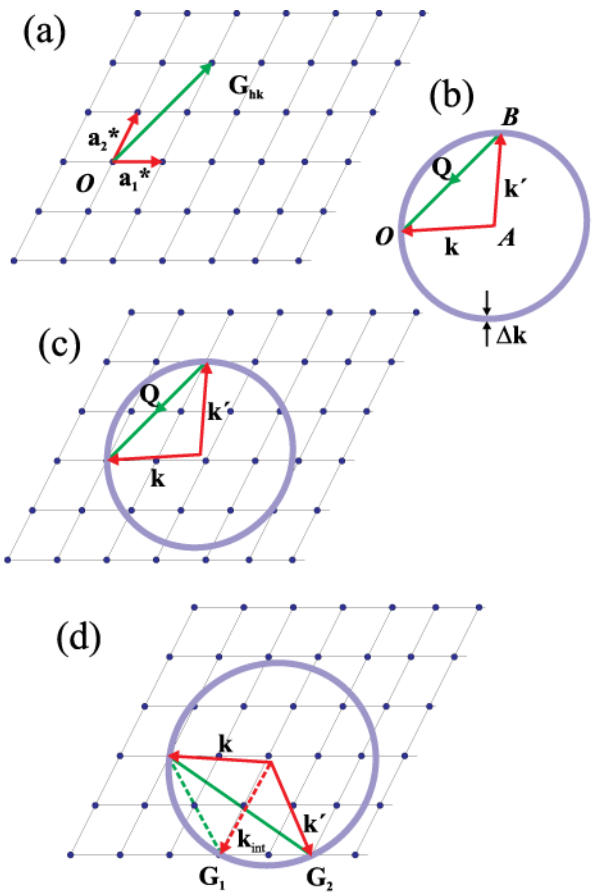

Fig. 5.6 The Ewald circle in two dimensions. (a) In 3D the reciprocal lattice is generated by integer coordinates (h, k, l) of the reciprocal basis vectors $(\mathbf{a}_1^*, \mathbf{a}_2^*, \mathbf{a}_3^*)$. For simplicity a 2D lattice at points given by $\mathbf{G} = h\mathbf{a}_1^* + k\mathbf{a}_2^*$ is shown. (b) The scattering triangle. Monochromatic incident radiation specified by $\mathbf{k} = \mathbf{AO}$ can be scattered to any wavevector $\mathbf{k}' = \mathbf{AB}$ terminating on the sphere of radius k. The bandwidth of the incident radiation Δk is indicated by the thickness of the circle. The scattering vector is defined as the vector $\mathbf{Q} = \mathbf{BO}$. (c) The Ewald circle (or Ewald sphere in 3D) is a superposition of (a) and (b) with $\mathbf{k}$ terminating on the origin of the reciprocal lattice. (d) Multiple scattering occurs if two or more reciprocal lattice points fall on the Ewald sphere. The rotation of the crystal and detector are set to record the $\mathbf{G}_2$ reflection, but as $\mathbf{G}_1$ is on the circle, the incident wave will also be scattered to $\mathbf{k}_{int}$. *Inside* the crystal $\mathbf{k}_{int}$ is scattered to $\mathbf{k}'$ by the reflection $\mathbf{G}_2 - \mathbf{G}_1$, and intensity may appear in the direction of $\mathbf{k}'$, even if the unit cell structure factor for this reflection vanishes.

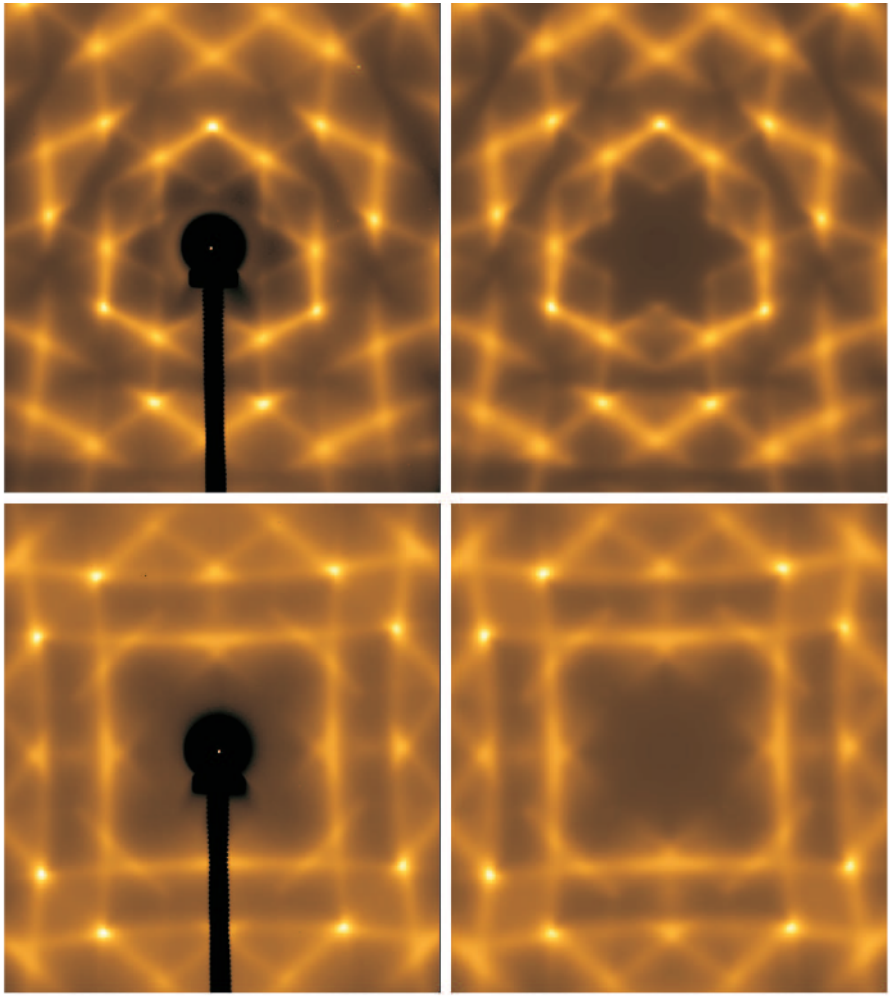

Fig. 5.14 Thermal diffuse scattering (TDS) from Si. The data were collected in a transmission geometry (photon energy 28 keV) using an image plate detector. The data were collected on the UNI-CAT beamline at the Advanced Photon Source in an exposure time of ~10 s. The top and bottom left panels show the data taken with a (111) and a (100) axis parallel to the incident beam respectively. The data are plotted on a logarithmic scale. The brighter spots are not Bragg peaks, as the Laue condition is never exactly fulfilled, but are due to the build up of TDS close to the position of where the Bragg peaks would occur. The right panels show the corresponding calculated images based on a simultaneous pixel-by-pixel fit to the data [Holt et al., 1999].

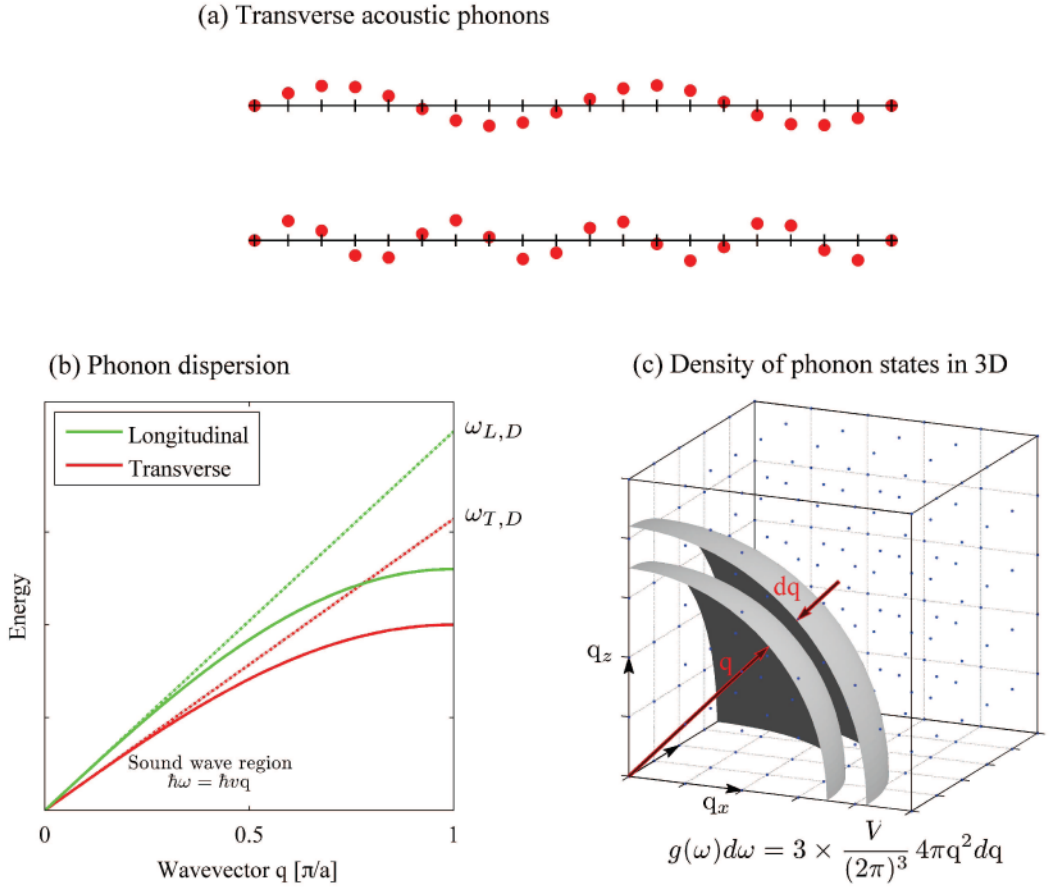

Fig. 5.15 (a) Representative snap shots of the atomic displacements associated with transverse acoustic phonons calculated for two different wavevectors. (b) Phonon dispersion relation for a monoatomic crystal. The phonons can have either a longitudinal or one of two transverse polarizations. In the Debye model the dispersion relation is assumed to be linear, $\omega = vq$, up to some cut off frequency ω_D. In three dimensions the cut off frequency is defined by $\int_0^{\omega_D} g(\omega)d\omega = 3N$, where $g(\omega)$ is the density of states and N is the number of atoms. (c) Periodic boundary conditions produce quantization of the allowed wavevectors, $\mathbf{q} = (2\pi/L)(l, m, n)$ with l, m and n integer, illustrated here in the positive octant. In general, the density of states taking into account the three possible polarizations is $g(\omega)d\omega = 3V/(2\pi)^3 4\pi q^2 dq$. For the Debye model $g(\omega) = 9N\omega^2/\omega_D^3$ with $\omega_D^3 = 6N\pi^2 v^3/V$.

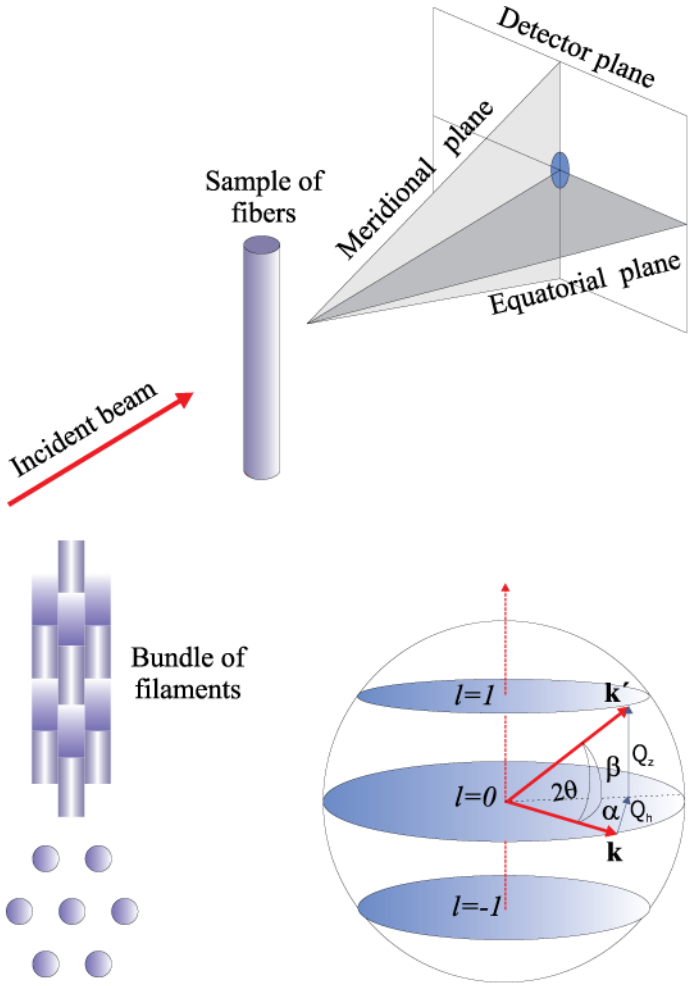

Fig. 5.25 Top: geometry of fibre diffraction. The fibre sample is perpendicular to the incident monochromatic beam. Bottom left: the fibre sample comprises a large number of filaments, randomly orientated in the azimuthal angle. Bottom right: periodicity along the fibre implies that Bragg reflections are restricted to layers.

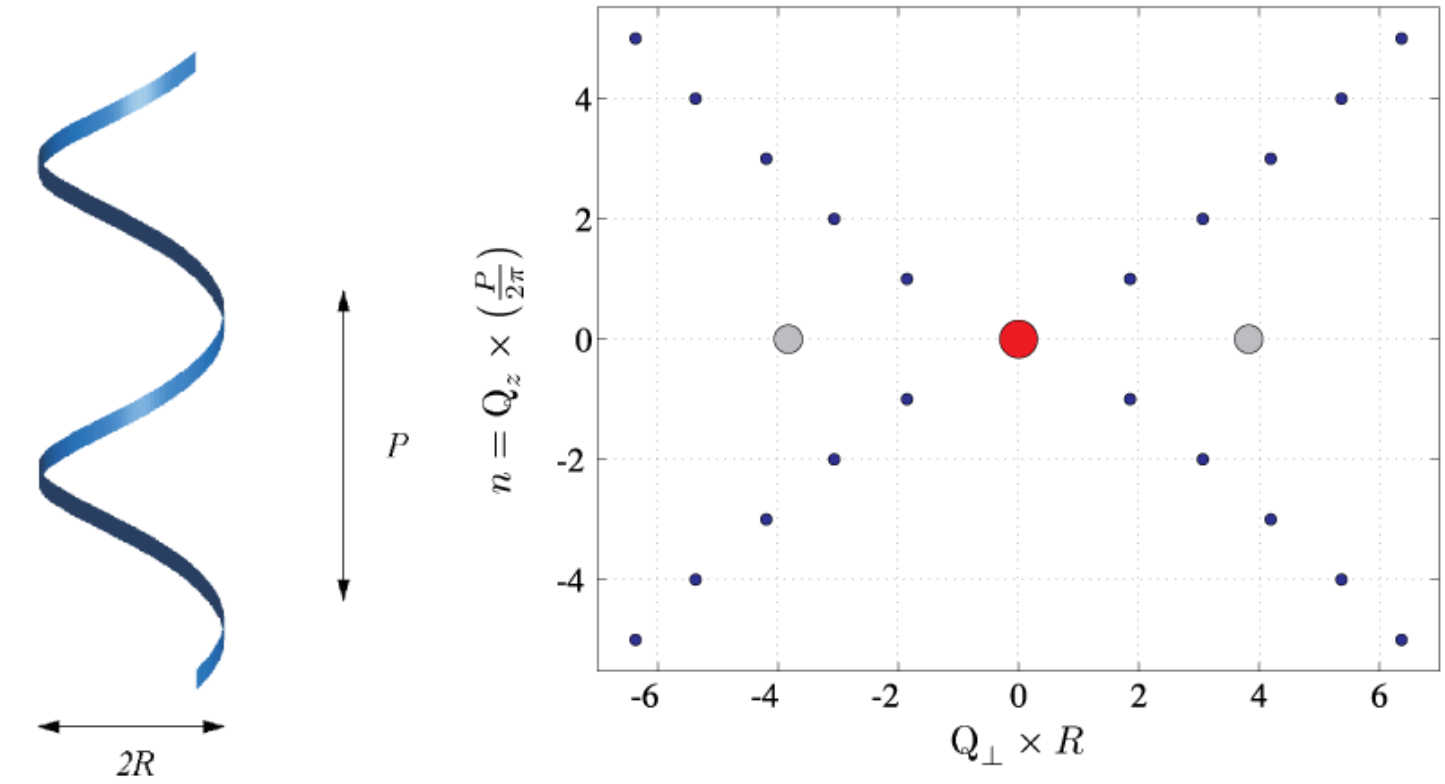

Fig. 5.27 Scattering from a single, infinitely long helix of radius R and period P. The structure factor squared has principle maxima arising from the peaks in the Bessel functions, and form a cross in reciprocal space as indicated by the blue circles. The grey circles on the equatorial axis are the secondary maxima from the zeroth-order Bessel function. Here Q_z and $Q_\perp$ are the components of the scattering vector parallel and perpendicular to the axis of the helix respectively.

Rosalind Franklin
Francis Crick
James Watson
1953

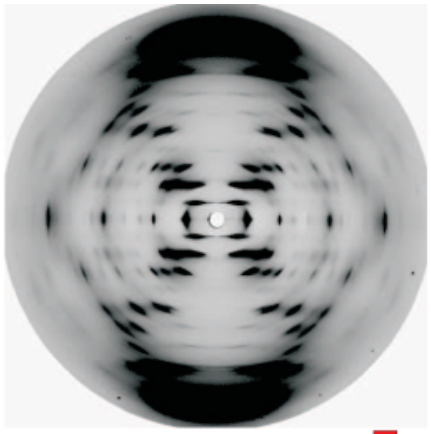

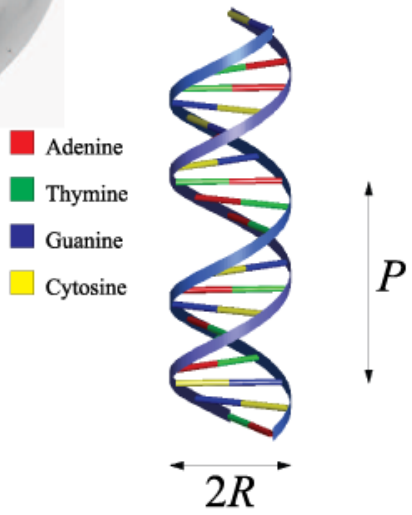

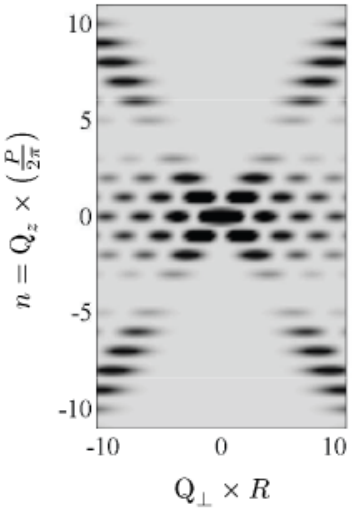

I. K. Robinson X-ray diffraction 2017

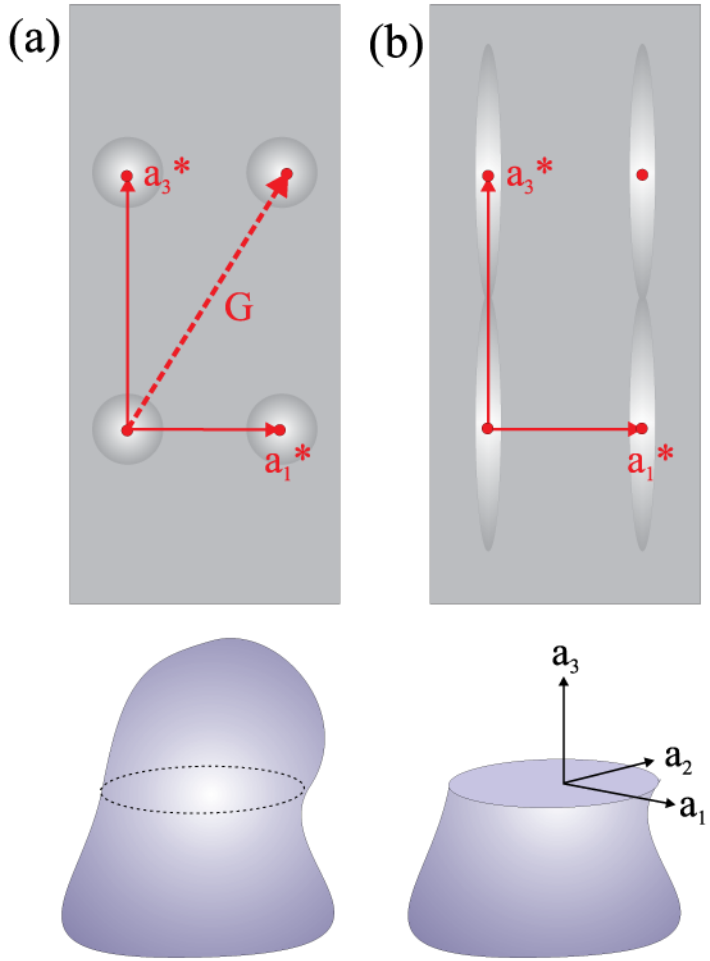

Fig. 5.12 (a) Top: a map of reciprocal space in the plane spanned by $\mathbf{a}_1^*$ and $\mathbf{a}_3^*$ for the crystal shown in the bottom part of the figure. (b) Same as (a) except that the crystal has been cleaved to produce a surface perpendicular to the $\mathbf{a}_3$ axis. This produces streaks of scattering – known as crystal truncation rods – through all Bragg peaks in a direction perpendicular to the surface.

VESTA software: $IrTe_2$

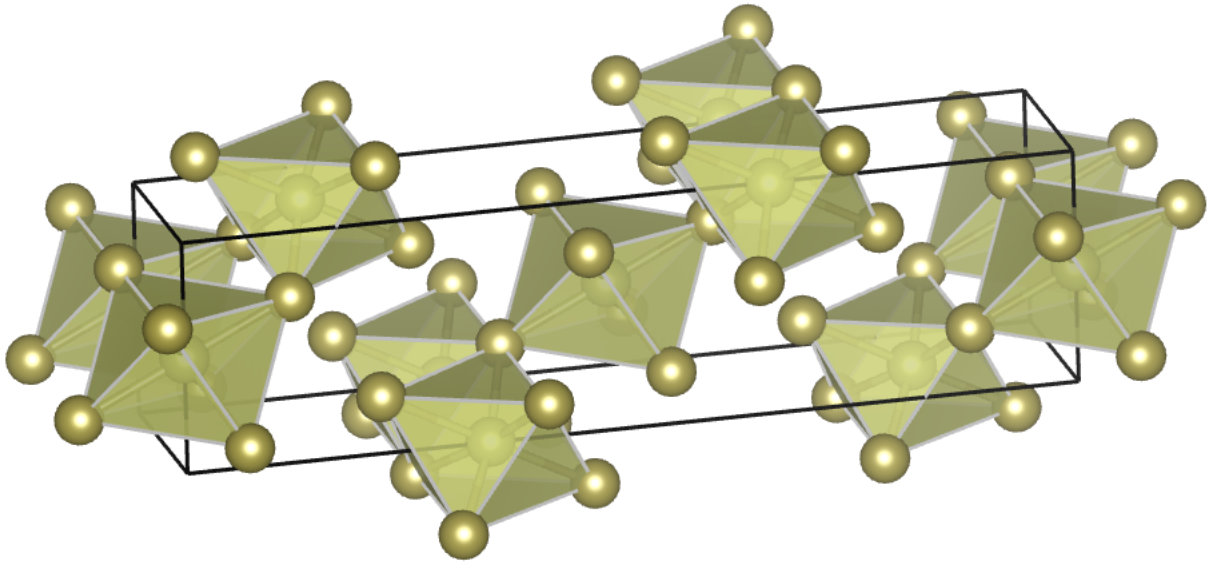

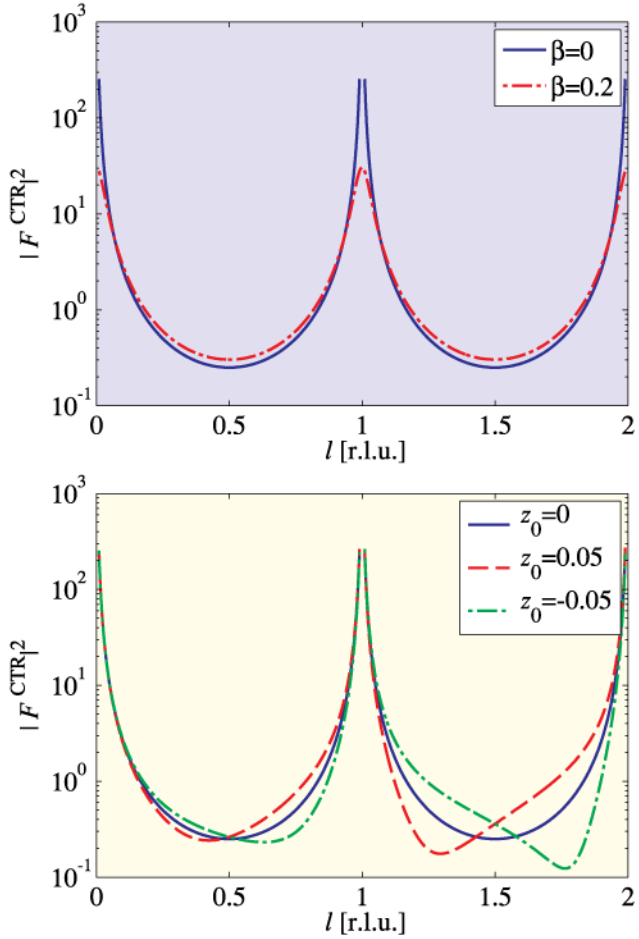

Fig. 5.13 ⋆ Top: Crystal truncation rod from a perfectly flat surface. Solid line, no absorption ($\beta = 0$); dashed-dotted line with absorption. Typically β is of order 10^{-5}, as may be seen from the values of the absorption coefficient μ listed in Table 3.1. Here β has been chosen to be 0.2, an unrealistically high value, but one that serves to illustrate the effects of absorption. For simplicity $A(\mathbf{Q})$ has been chosen to be unity. Bottom: Crystal truncation rod ($\beta = 0$) from a flat surface with an overlayer. The relative displacement of the overlayer from the bulk lattice spacing is given by z_0. The effect of the displacement of the layer is seen to become more pronounced at higher wavevector transfers.

Class Outline

- Crystal structure (using VESTA software)
- Surface diffraction and surface structure
- Powder diffraction methods
- Williamson-Hall analysis of size and strain
- Pair Distribution Function (PDF)

First UHV Experiments (1981)

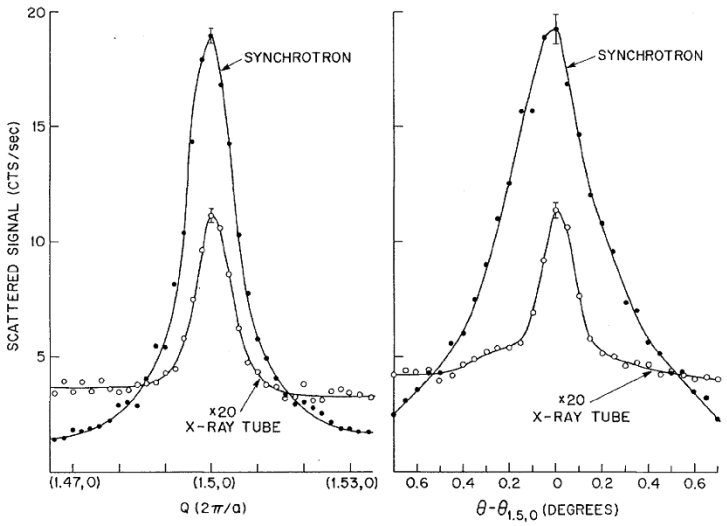

FIG. 1. A plot of the $(\frac{3}{2}, 0)$ Bragg reflection as a function of the momentum transfer $Q(2\pi/a)$ and the crystal's mosaic spread (deg).

P. Eisenberger and W. C. Marra,
PRL **46** 1081 (1981)
experiments done at SSRL

Diffuse Scattering from Si Wafer

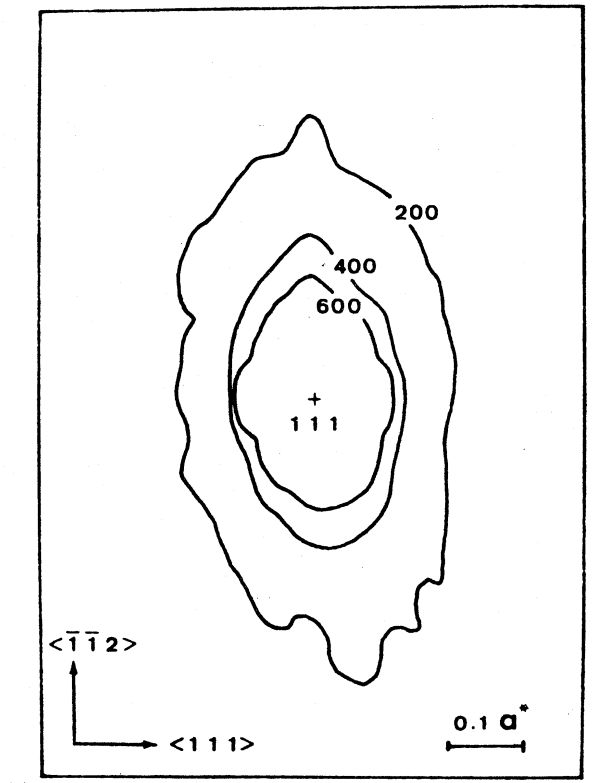

Unpolished wafer

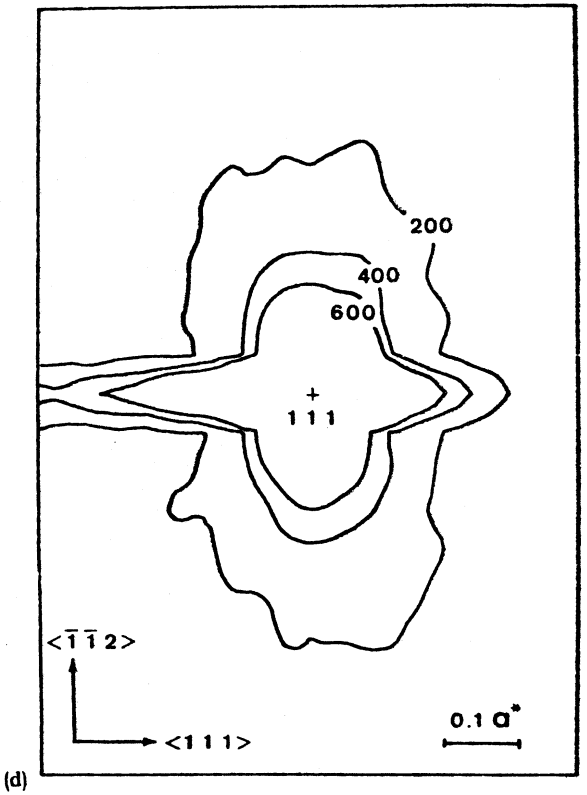

40 microns removed

N. Kashiwagara, J. Harada and M. Ogino, J. Appl. Phys 54 2706 (1983)

Surfaces in Dynamical Diffraction

A. M. Afanas'ev *et. al.*, Acta Cryst **A40** 352 (1984)

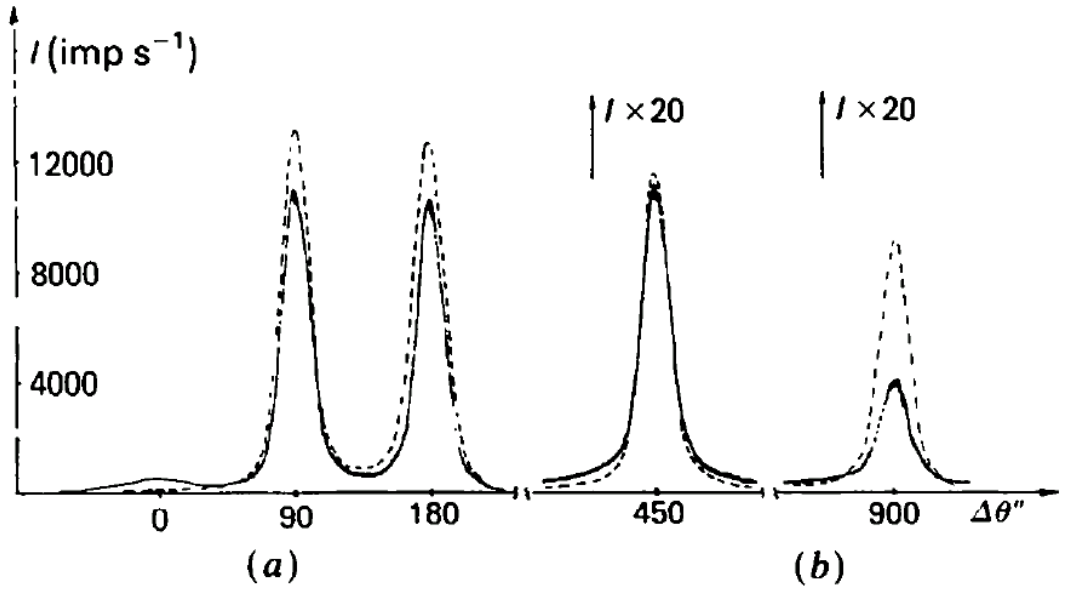

Fig. 2. TDC spectra from Ge(111) crystals, $(n, -n, n)$ arrangement, symmetric Bragg diffraction for (a) $\alpha = 90''$, (b) $\alpha = 450''$. Dashed line for ideal crystal, solid line for crystal first polished with diamond paste and then partially etched.

Effect of etching seen in triple-axis measurement of rocking curve

Scattering of X-rays From Crystal Surfaces

S.R.Andrews & R.A.Cowley JPCM **18** 6427 (1985)

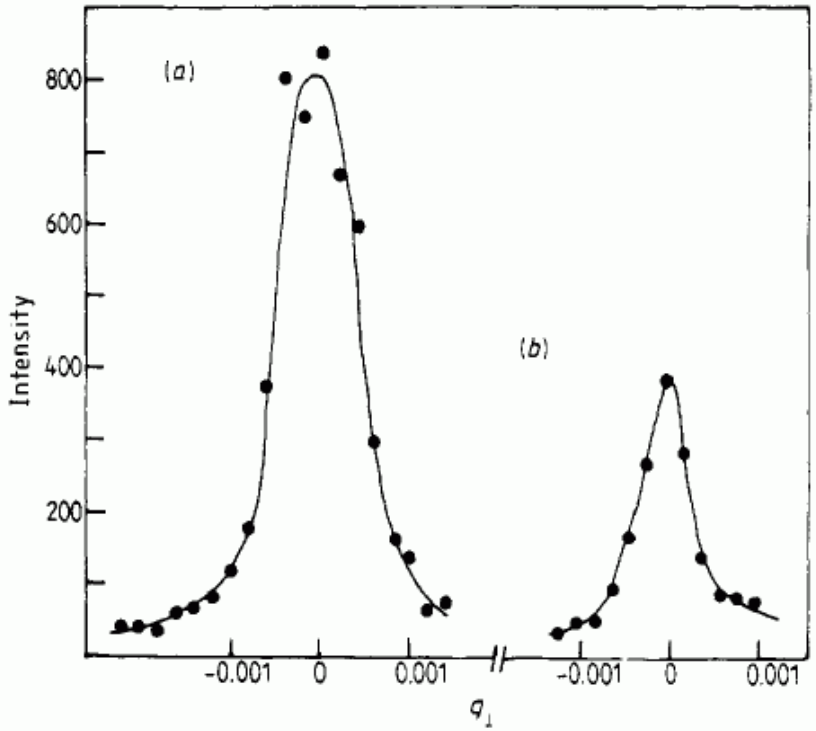

Figure 1. The intensity of scattering, as a function of q , (*a*) for $\boldsymbol{Q}$ = (0, 0, 4.005) (vertical scale in counts per 2 s) and (*b*) $\boldsymbol{Q}$ = (0, 0, 4.025) (vertical scale in counts per 300 s) in the GaAs sample with an (001) surface corresponding to figure 2, curve B.

Diffraction as a Surface Integral

Die äußere Form der Kristalle
in ihrem Einfluß auf die Interferenzerscheinungen
an Raumgittern
Von M. v. Laue

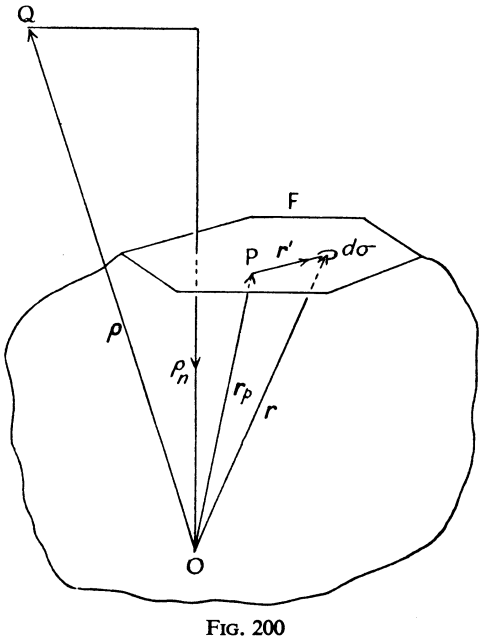

FIG. 200

Annalen der Physik [5] 26 55 (1936)

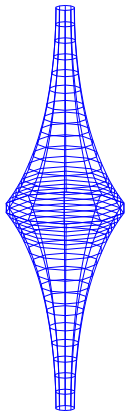

"Stacheln"

Crystal Truncation Rods (1986)

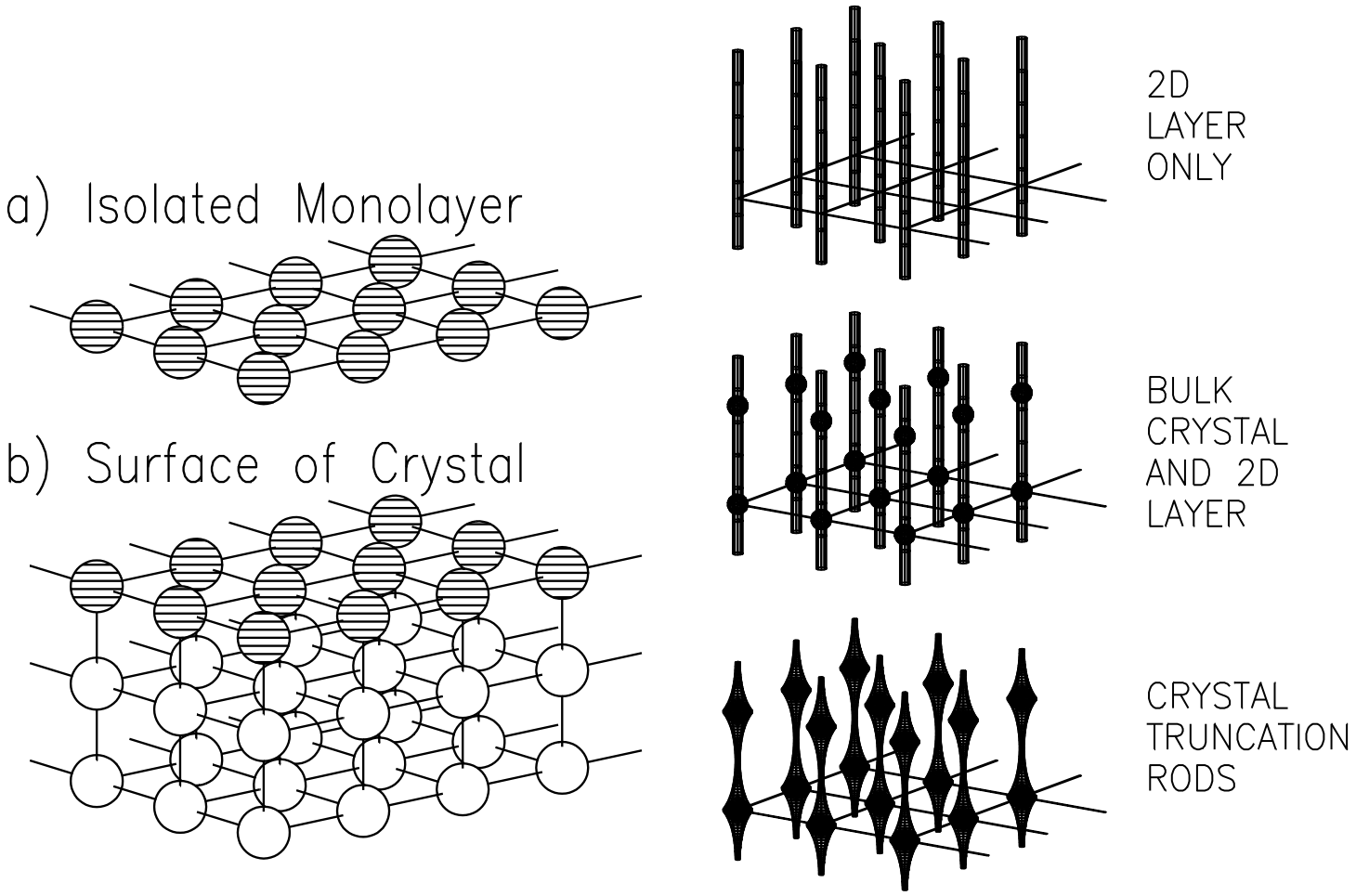

CRYSTAL TRUNCATION RODS AND SURFACE ROUGHNESS

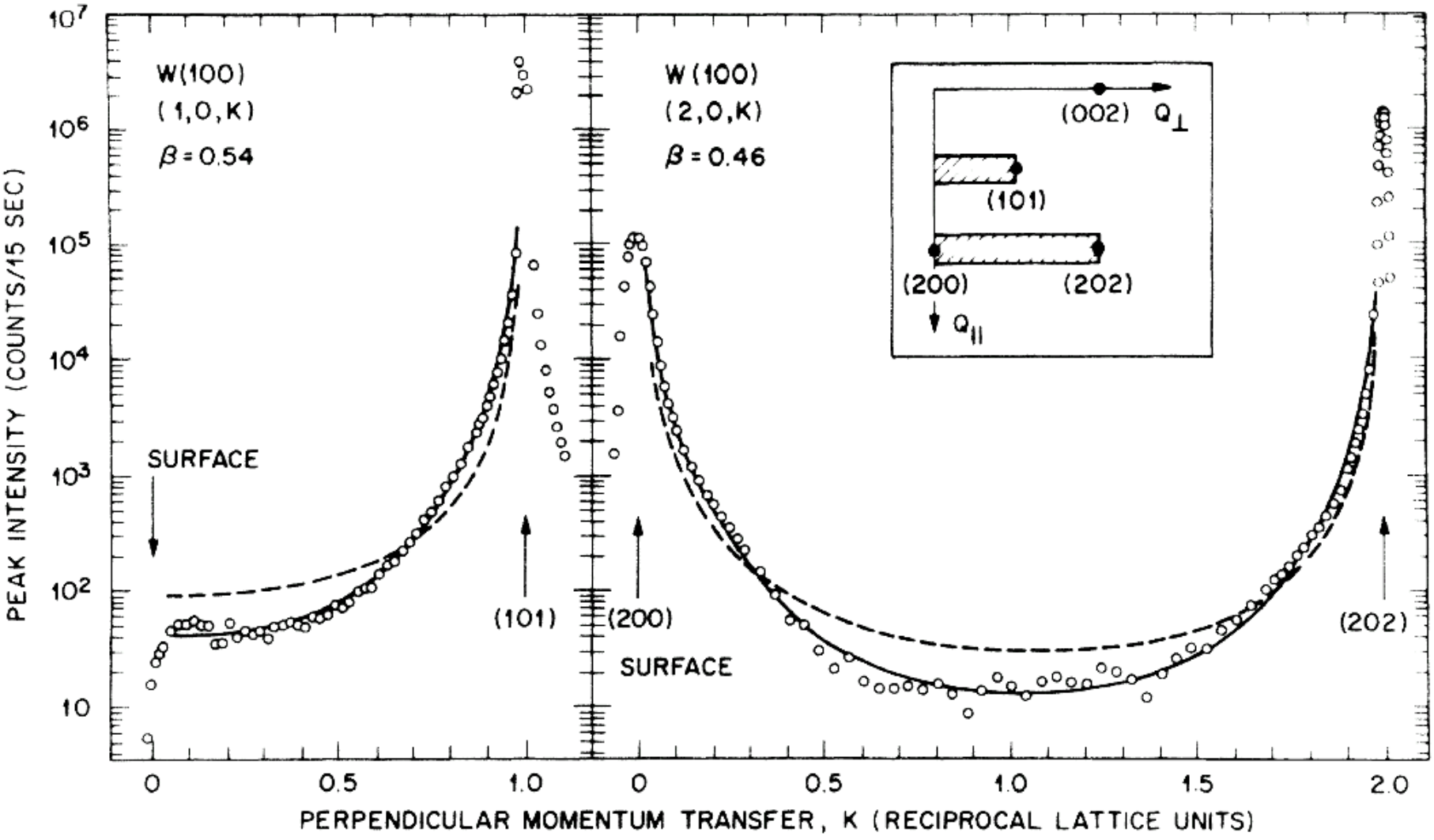

I. K. Robinson X-ray diffraction 2017

CTR as Convolution

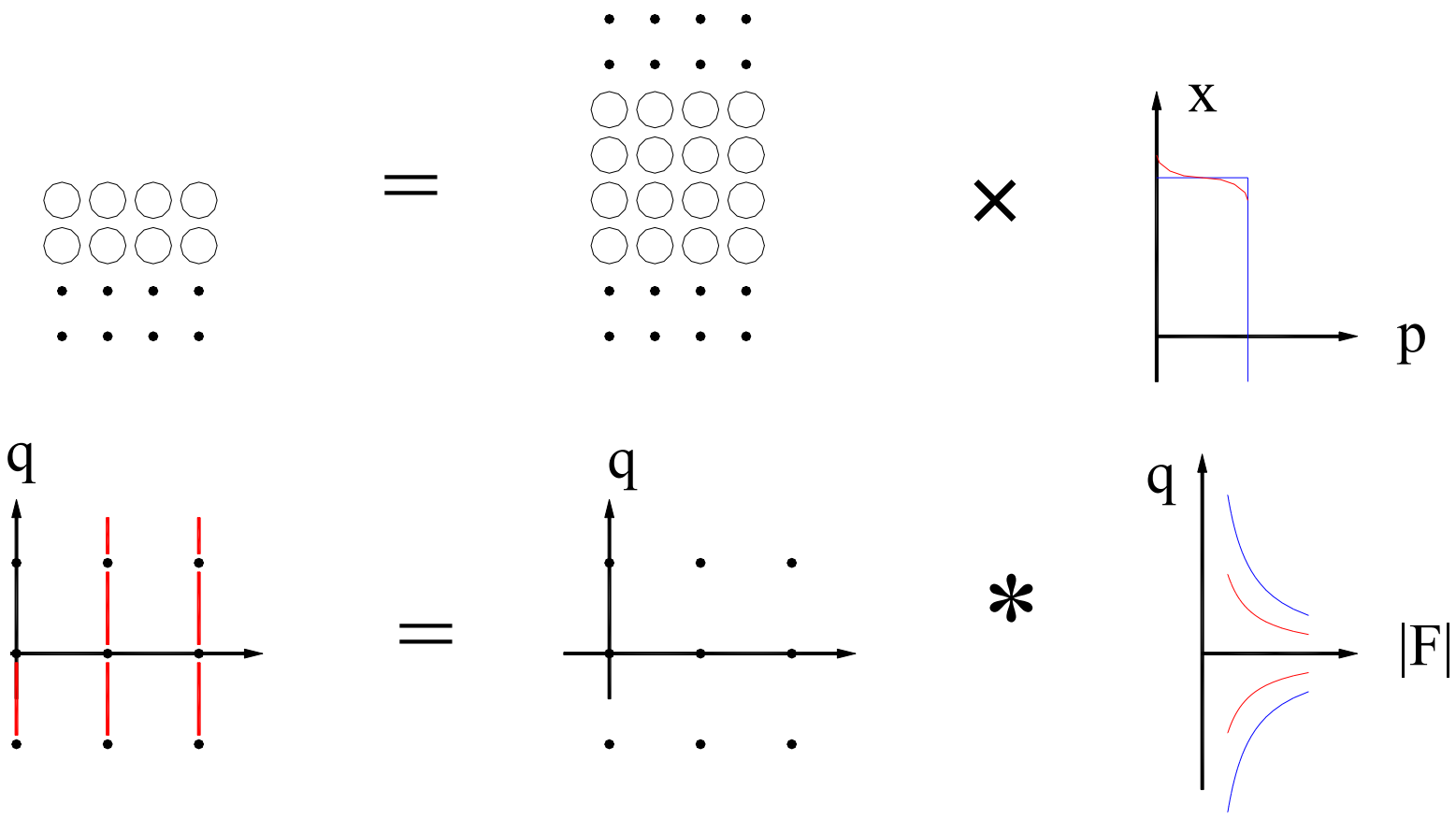

CTR is Sensitive to Surface Structure

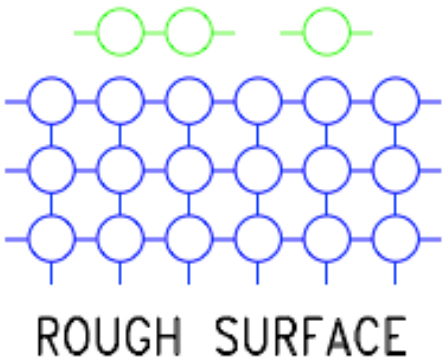

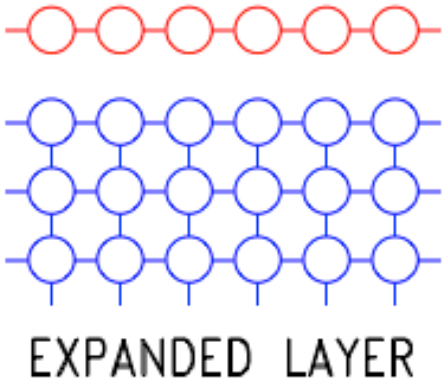

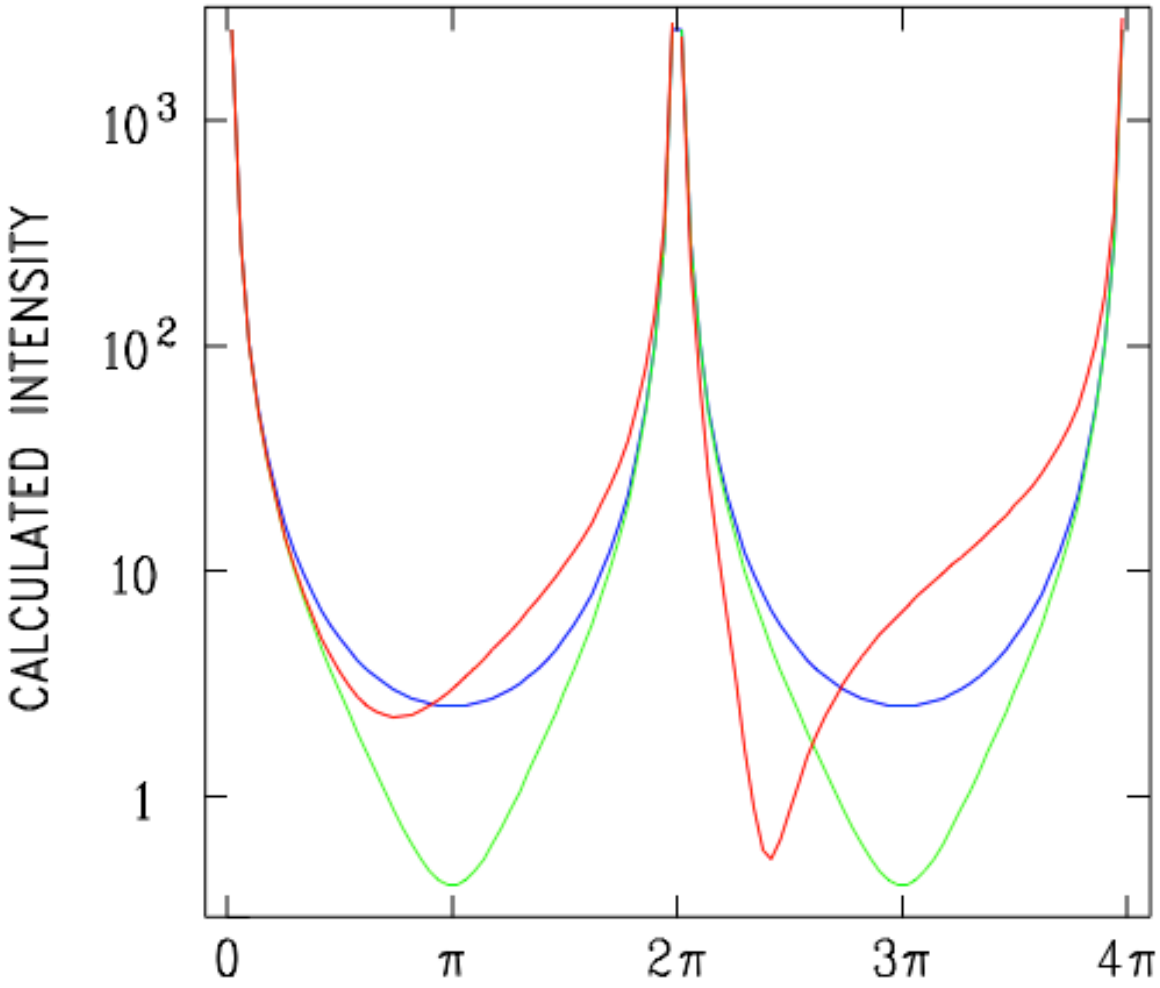

I. K. Robinson X-ray diffraction 2017

CTR is Sensitive to Surface Structure

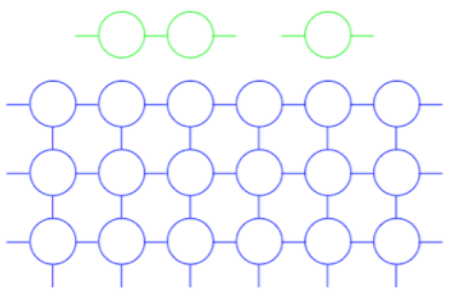

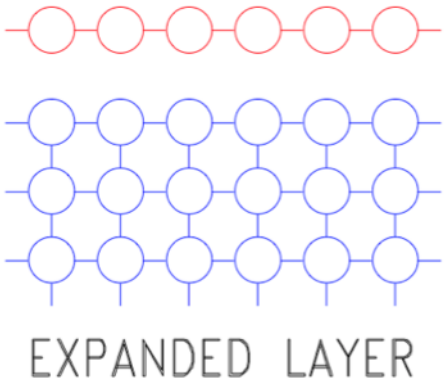

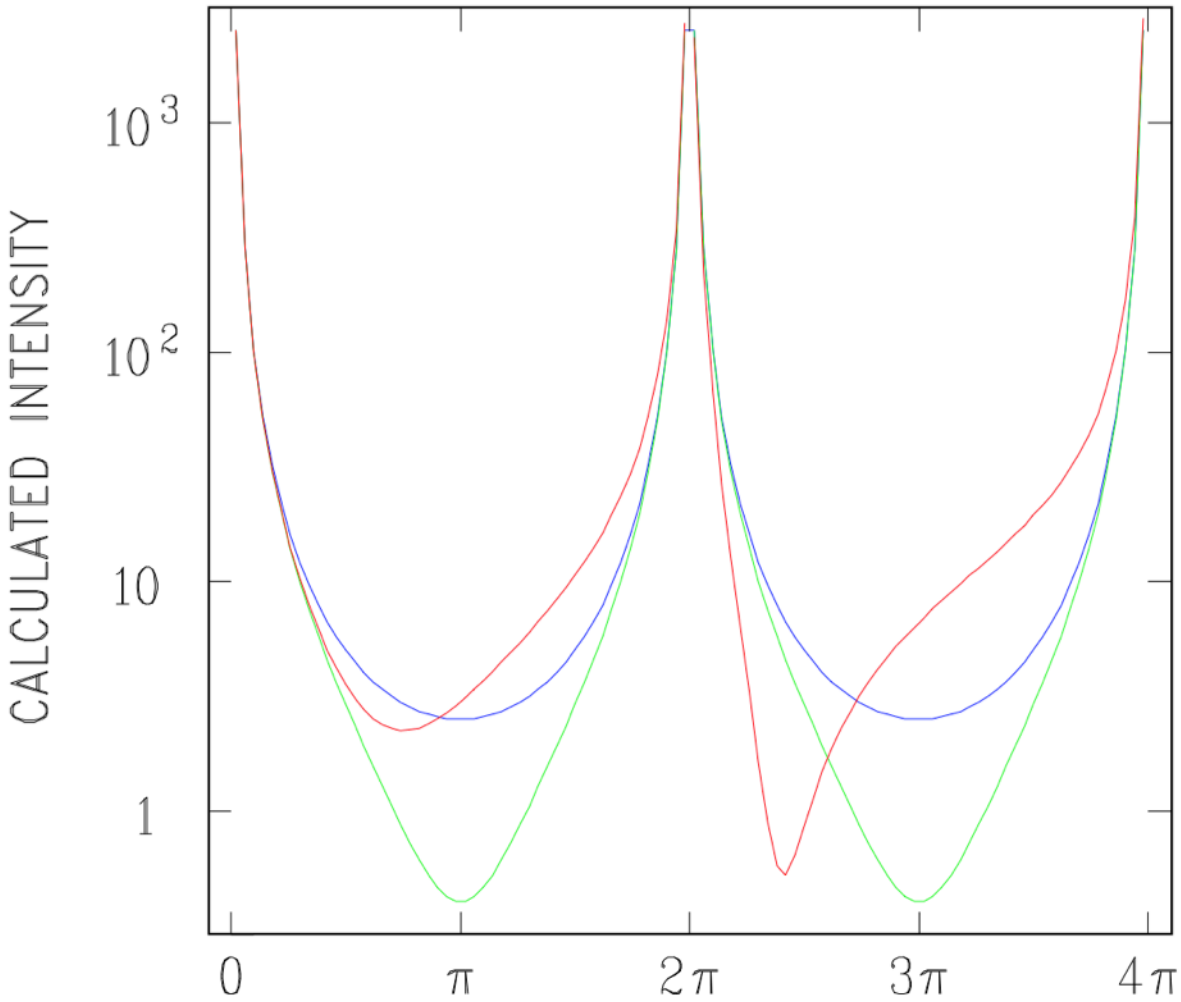

I. K. Robinson X-ray diffraction 2017

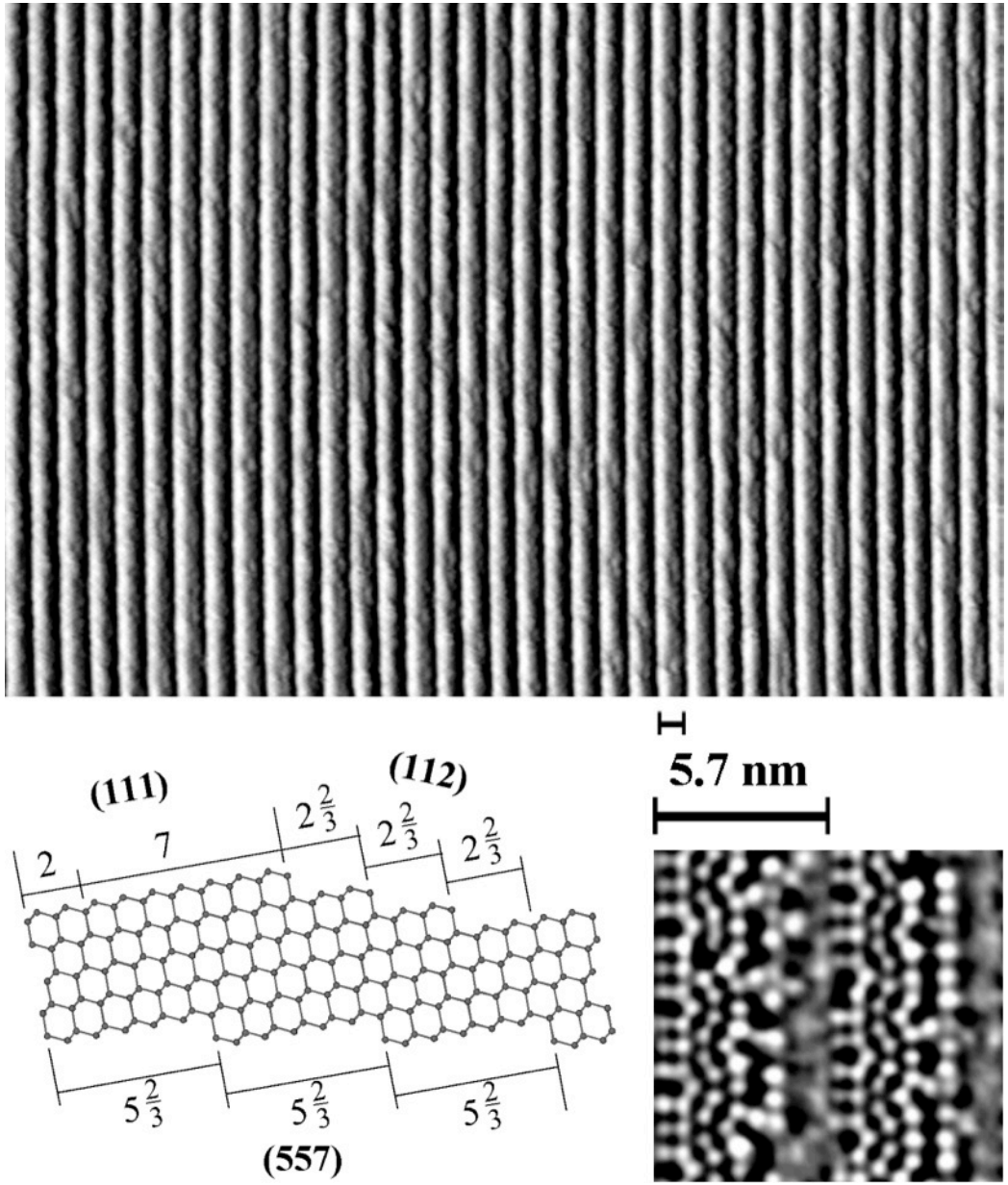

I. K. Robinson X-ray diffraction 2017

Crystallography of Stepped Surfaces

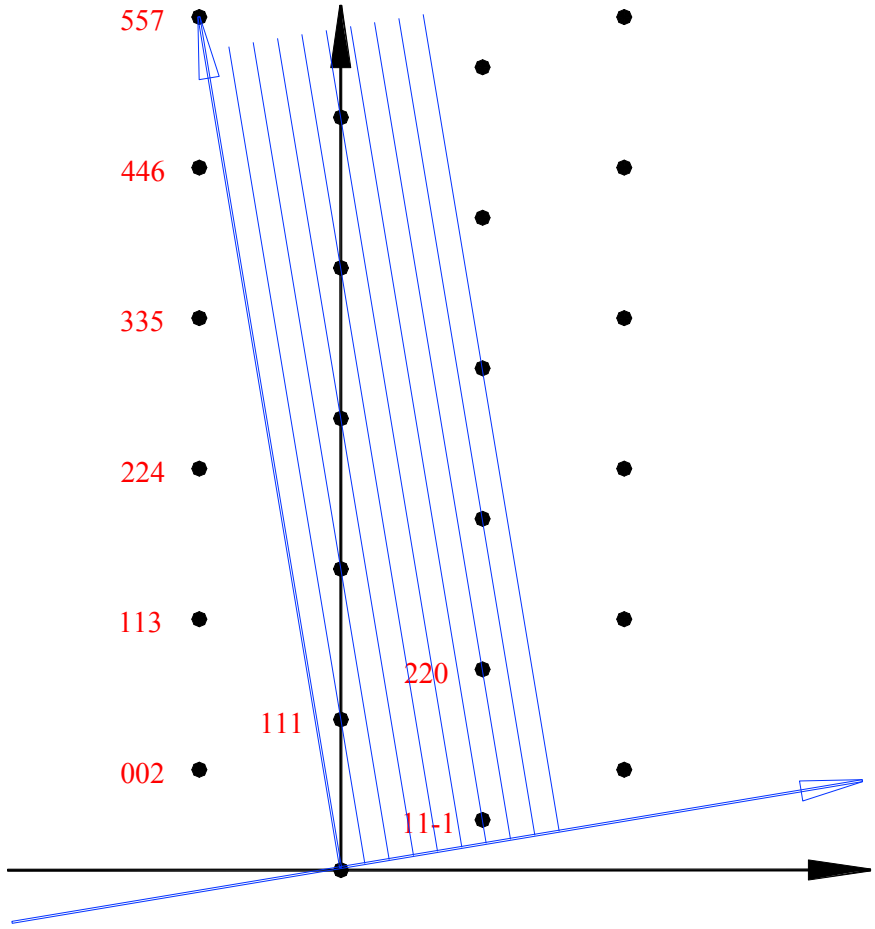

Silicon (111)

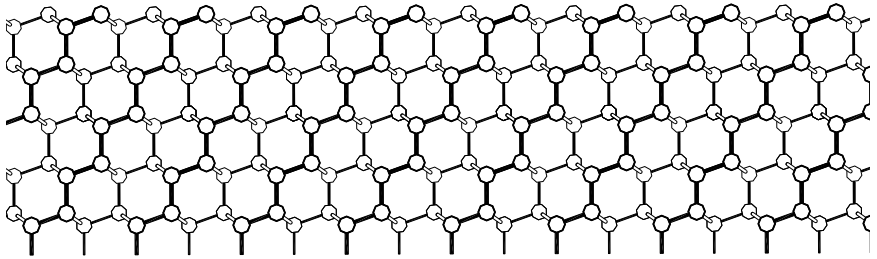

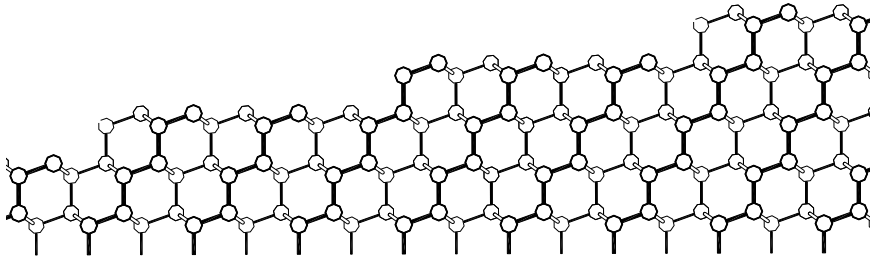

Si(557) surface

Si(557) coated with Au

R. Losio, et. al., Phys. Rev. Lett. 86 4632 (2001)

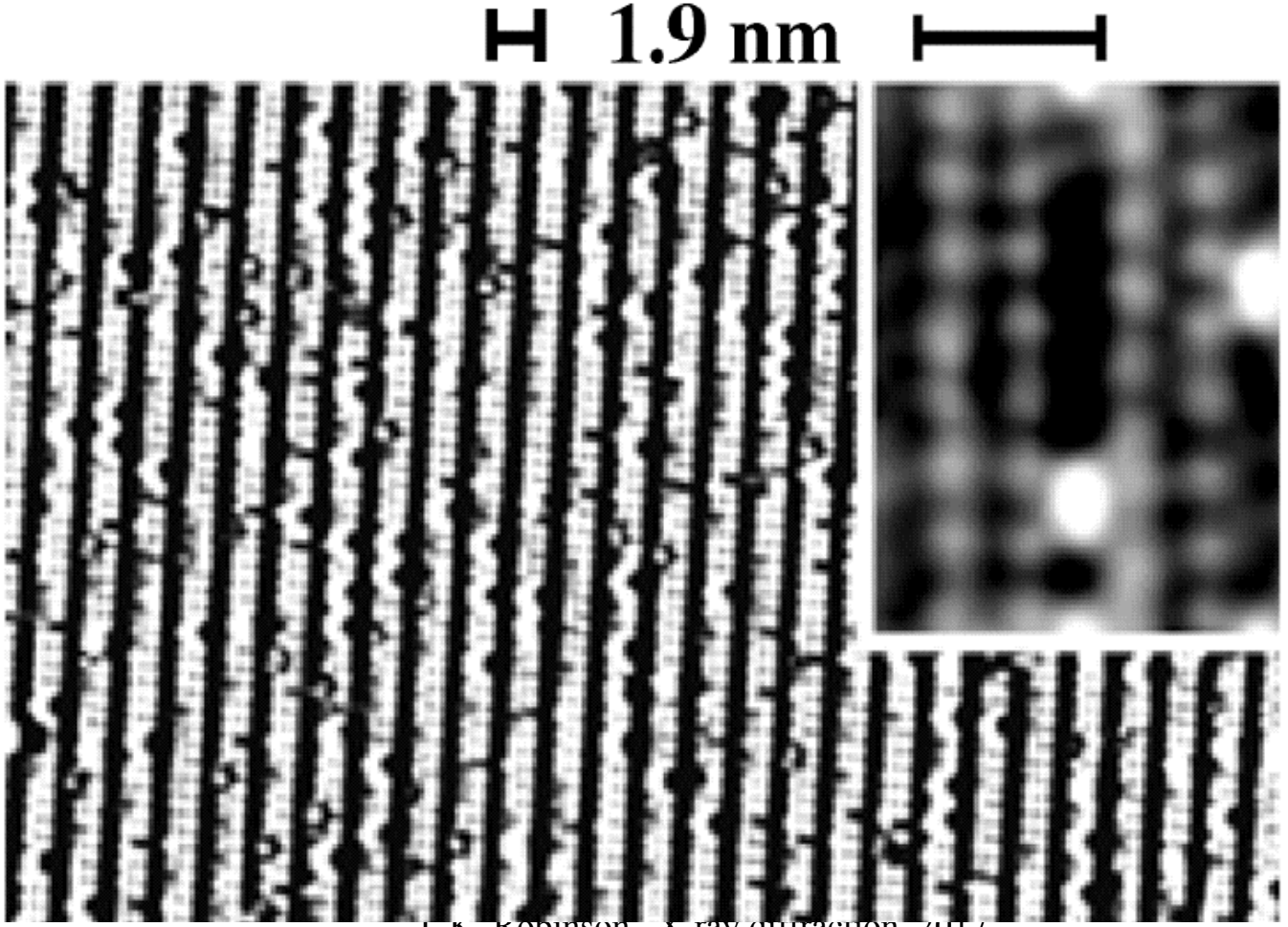

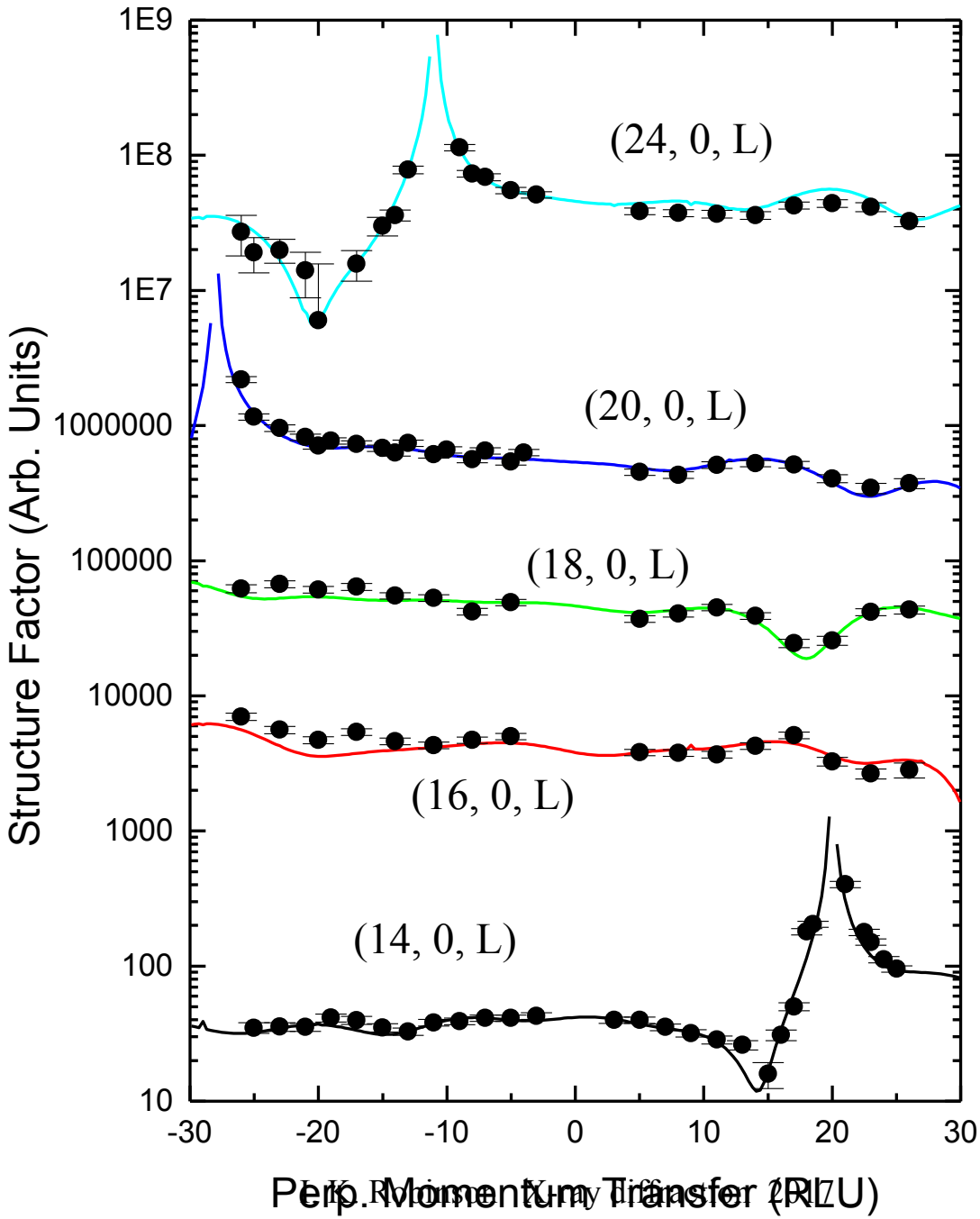
1E9
1E8
1E7
1000000
100000
10000
1000
100
10
-30
-20
-10
0
10
20
30
(24, 0, L)
(20, 0, L)
(18, 0, L)
(16, 0, L)
(14, 0, L)
Structure Factor (Arb. Units)
Perp. Momentum Transfer (RLU)

Phasing by a Single Heavy Atom

H. B. Dyer, Acta Cryst. 4 42 (1951)

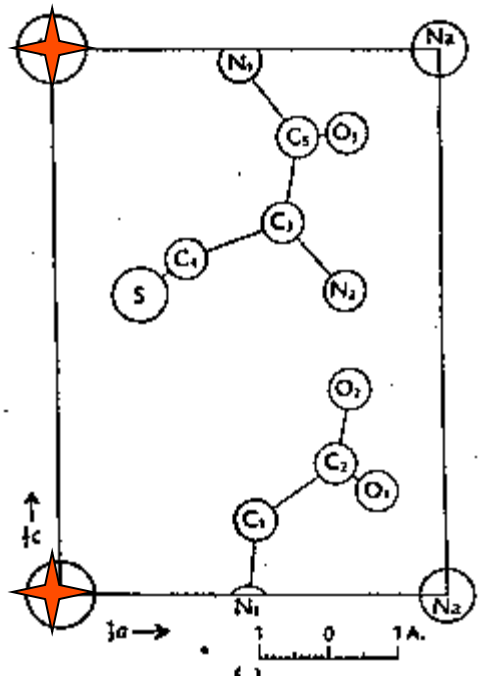

Cysteinylglycine sodium iodide

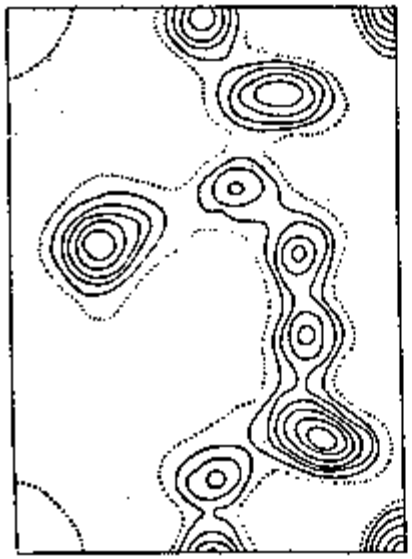

Patterson

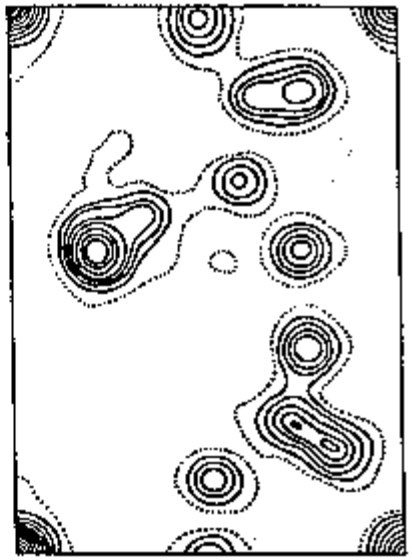

Electron density

X-Z Patterson of Au/Si(557)

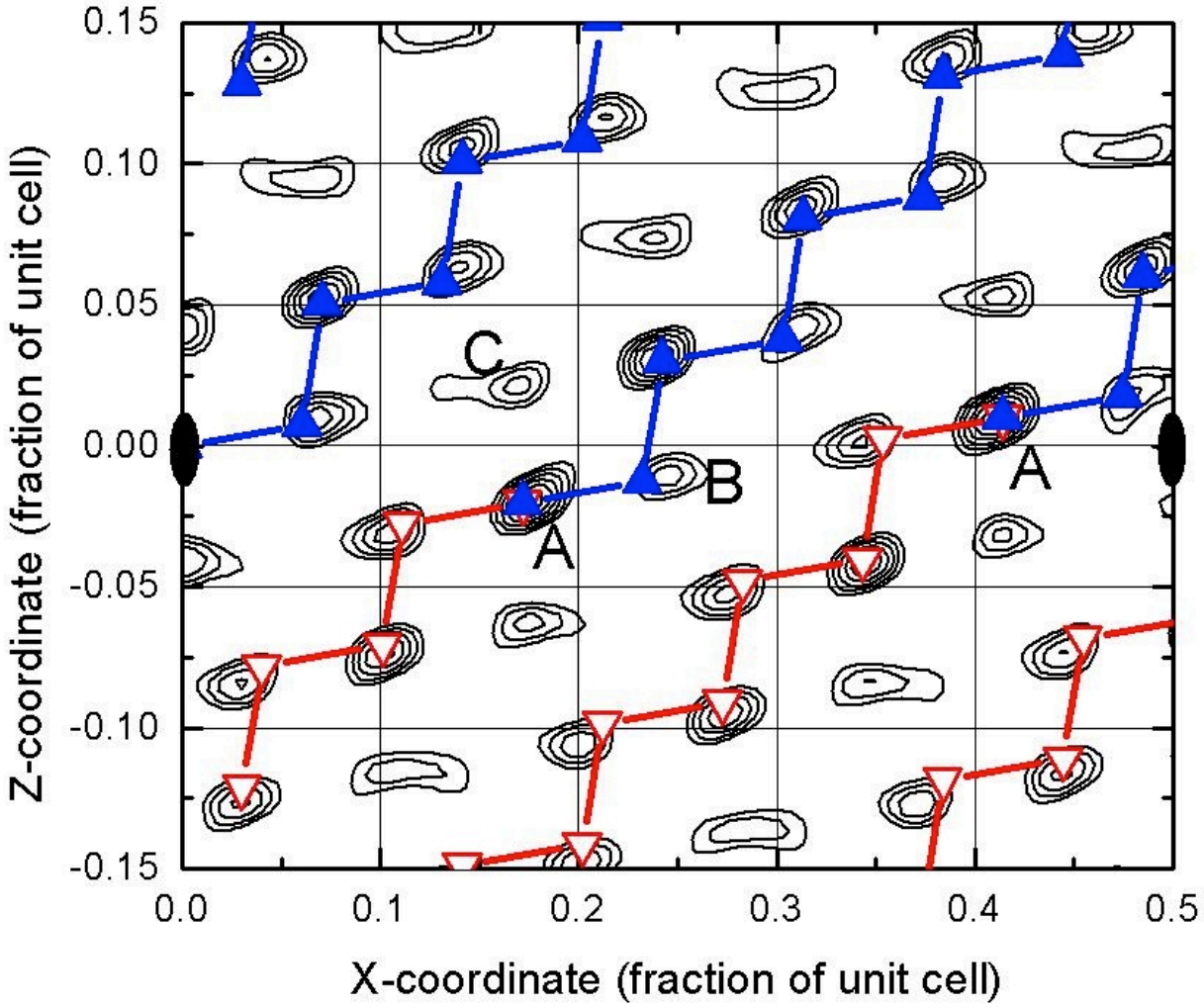

I. K. Robinson X-ray diffraction 2017

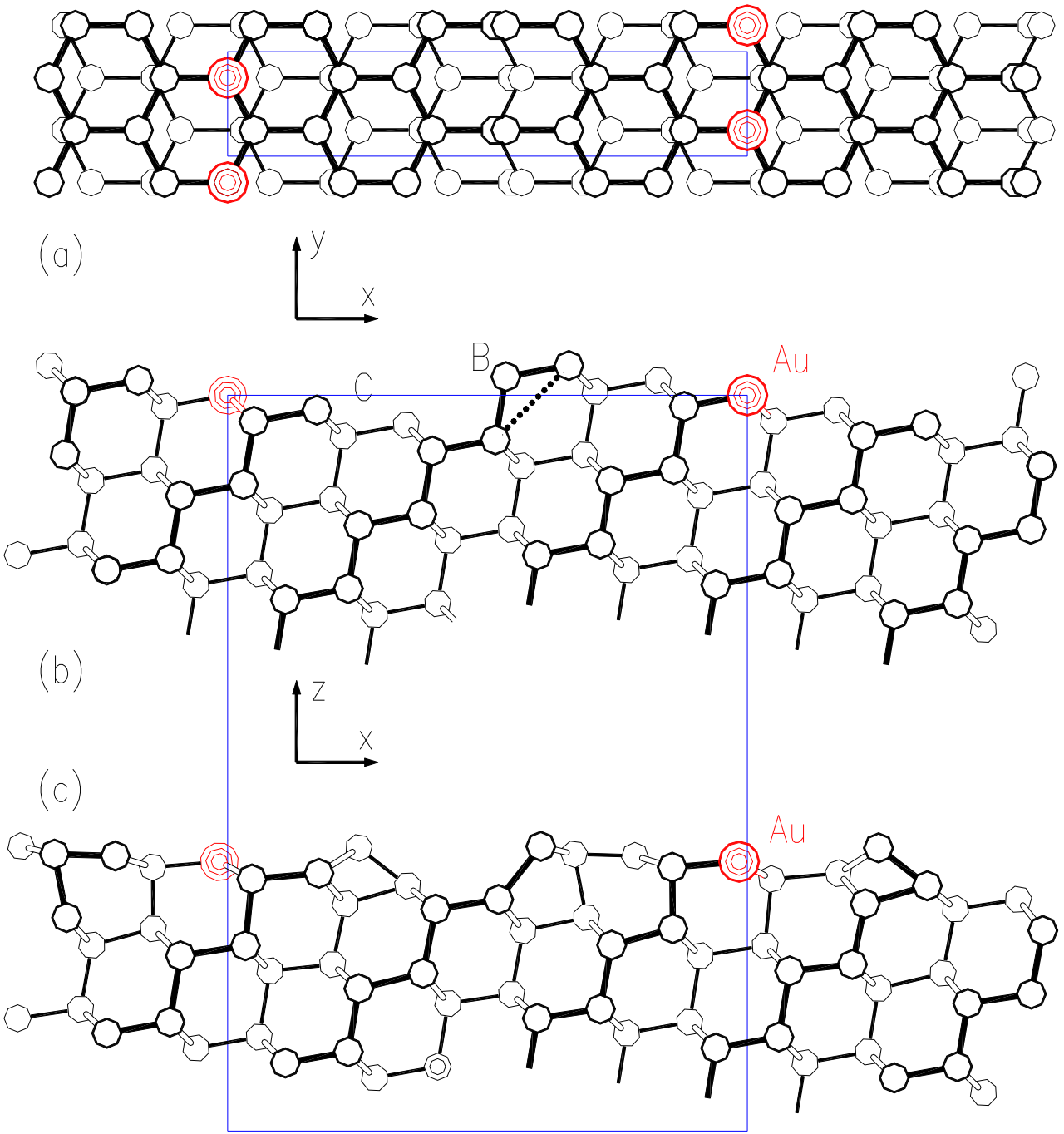
(a)
y
x
B
C
Au
(b)
z
x
(c)
Au

Comparison with STM

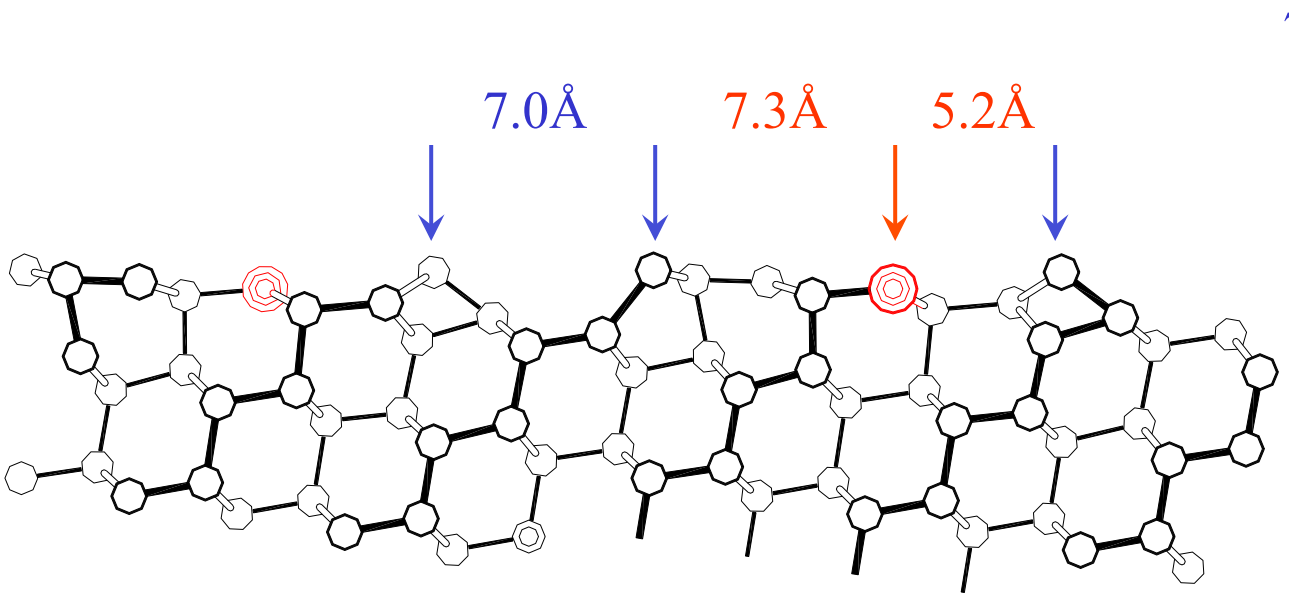

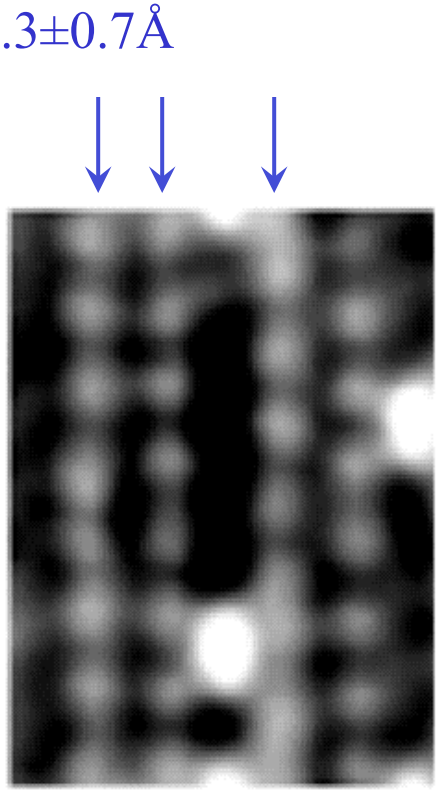

Cu(115) after Oxidation: STM

S. Reiter and E. Taglauer, Surf. Sci. **367** 33 (1996)

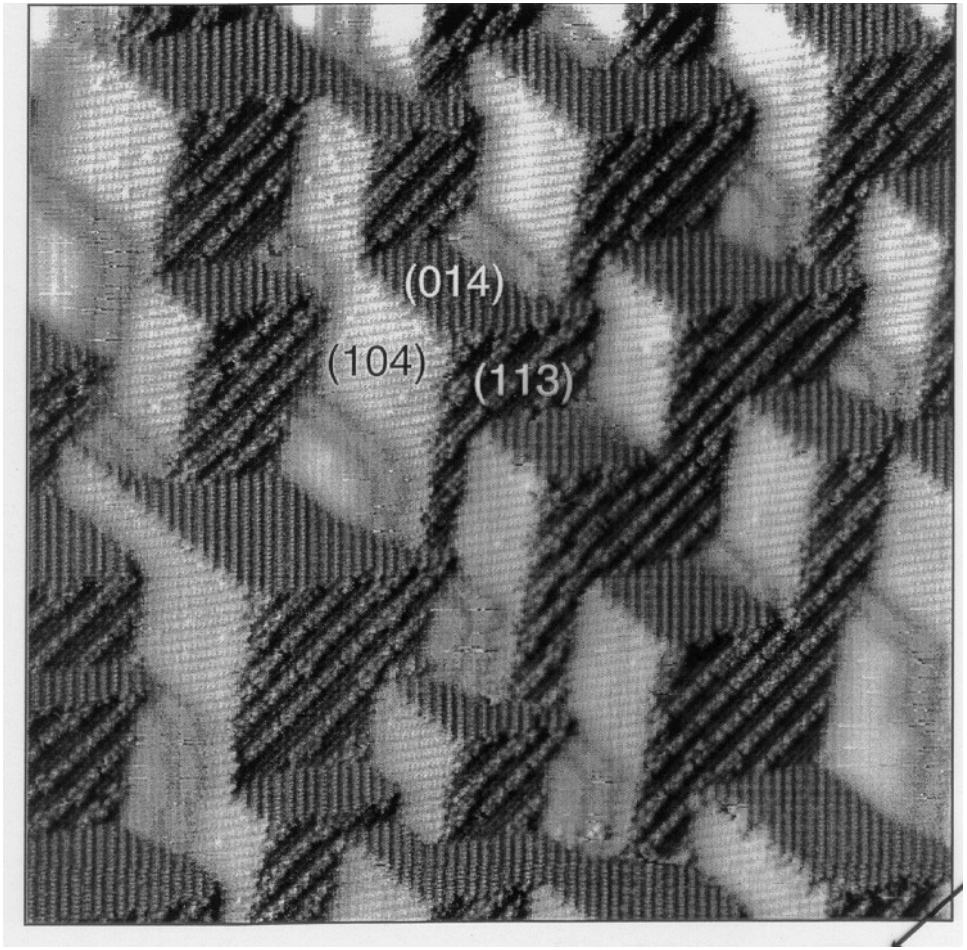

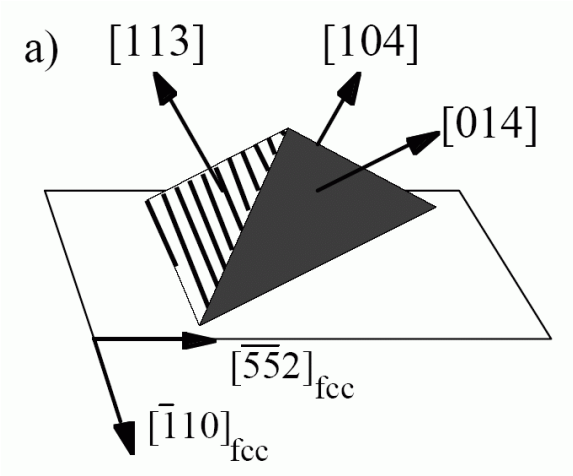

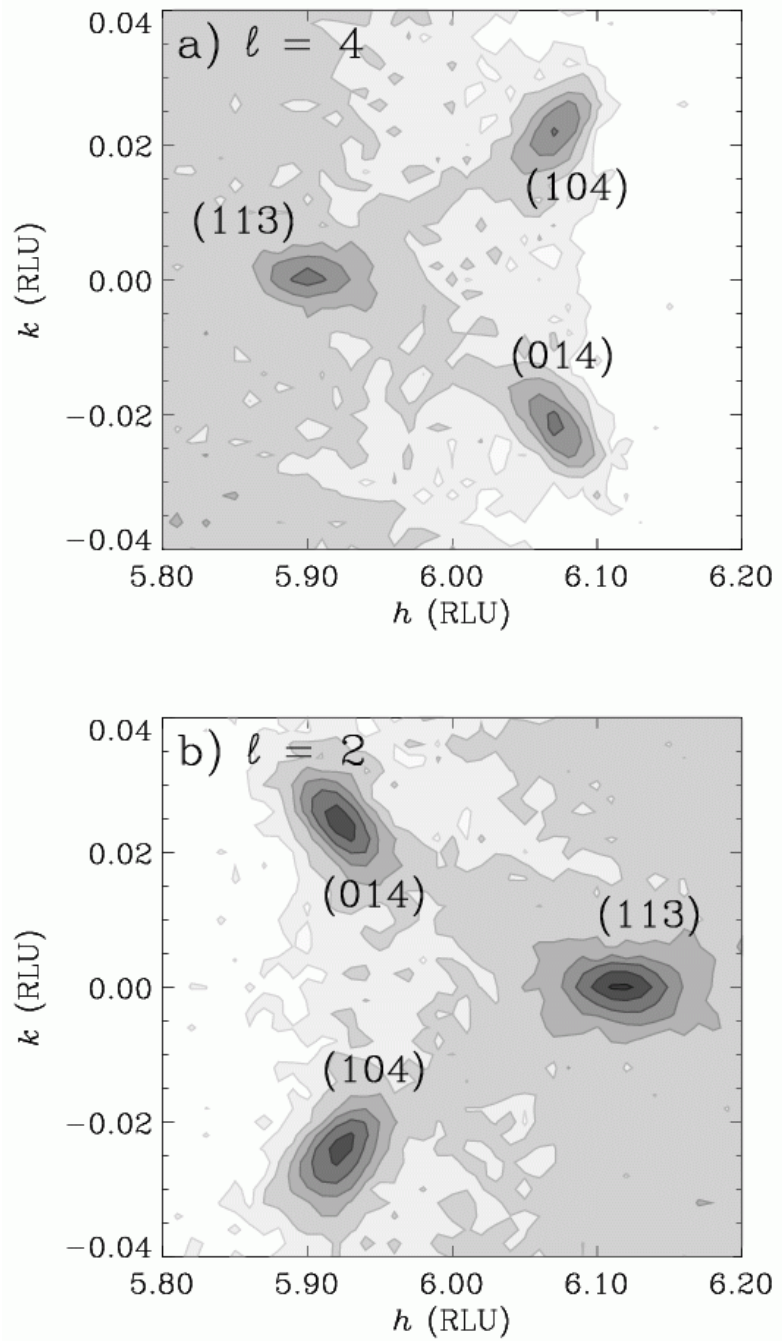

Cu(115) after Oxidation: X16A

Don Walko, UIUC PhD Dissertation (2000)

on X-ray diffraction 2017

(111) Surface of Diamond Lattice

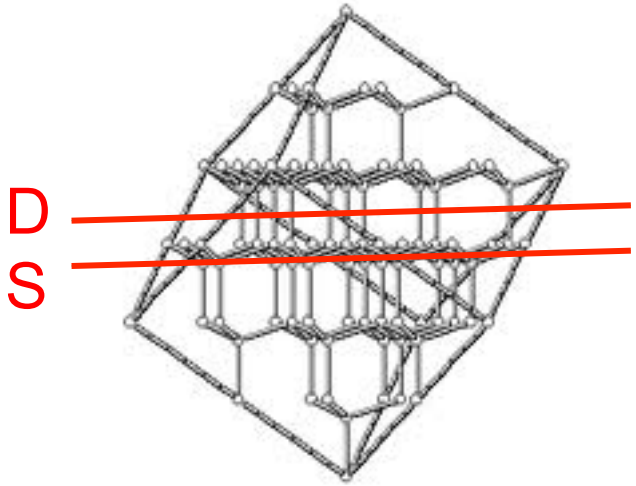

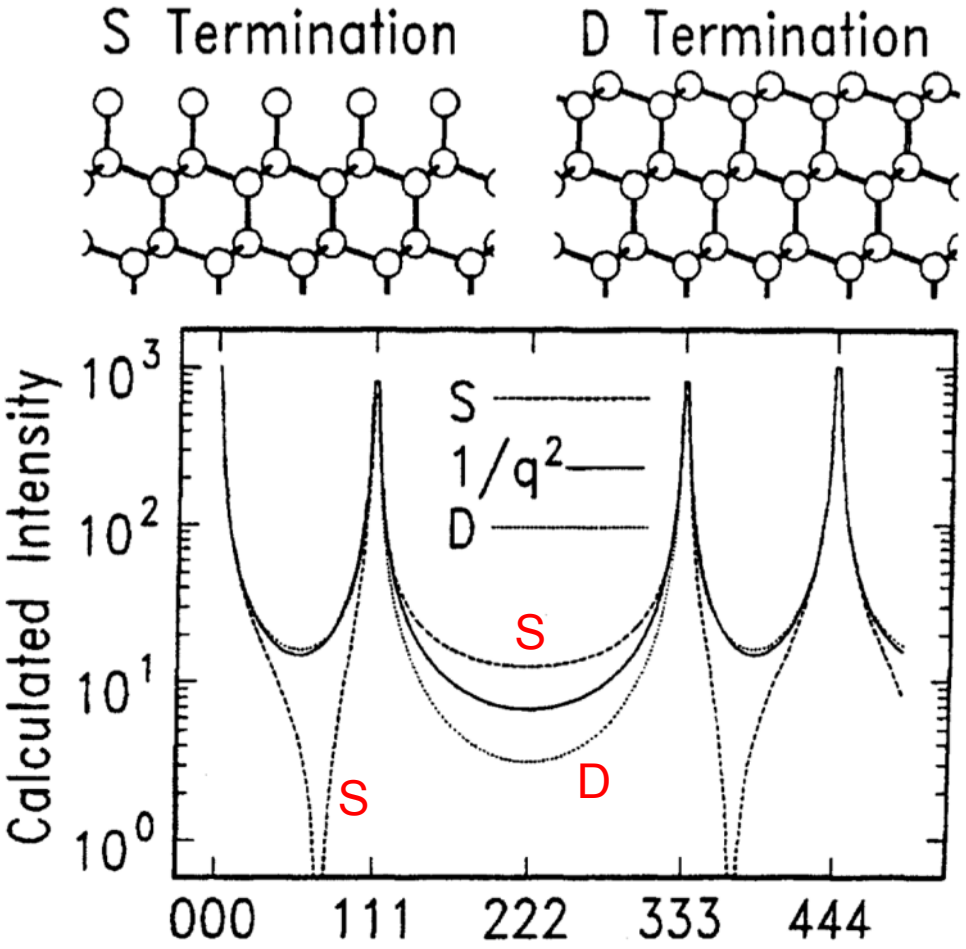

(111) Surface of Diamond Lattice

Si(111) 7x7 buried under a-Si
PRL 57 2714 (1986)

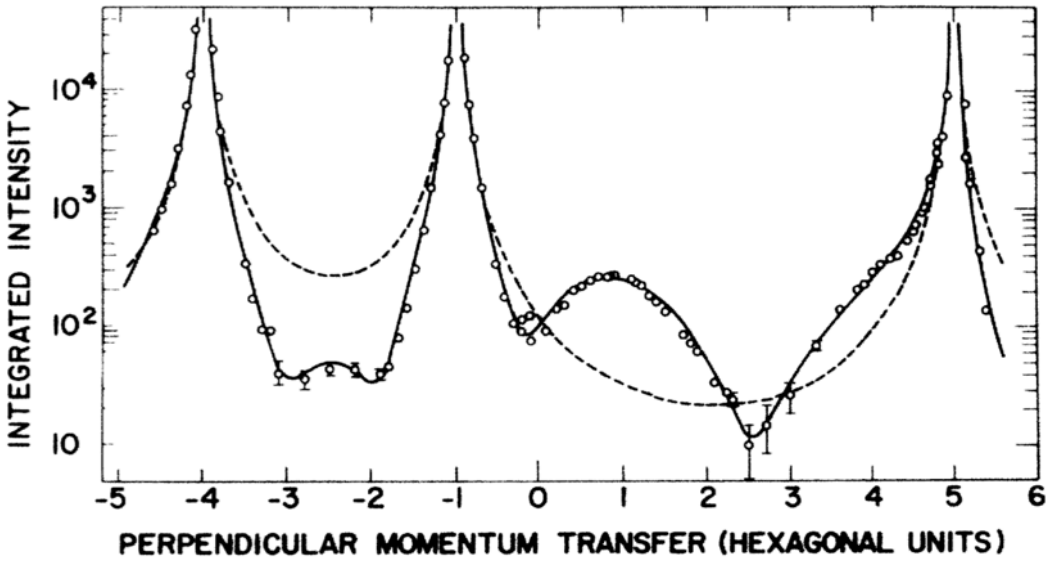

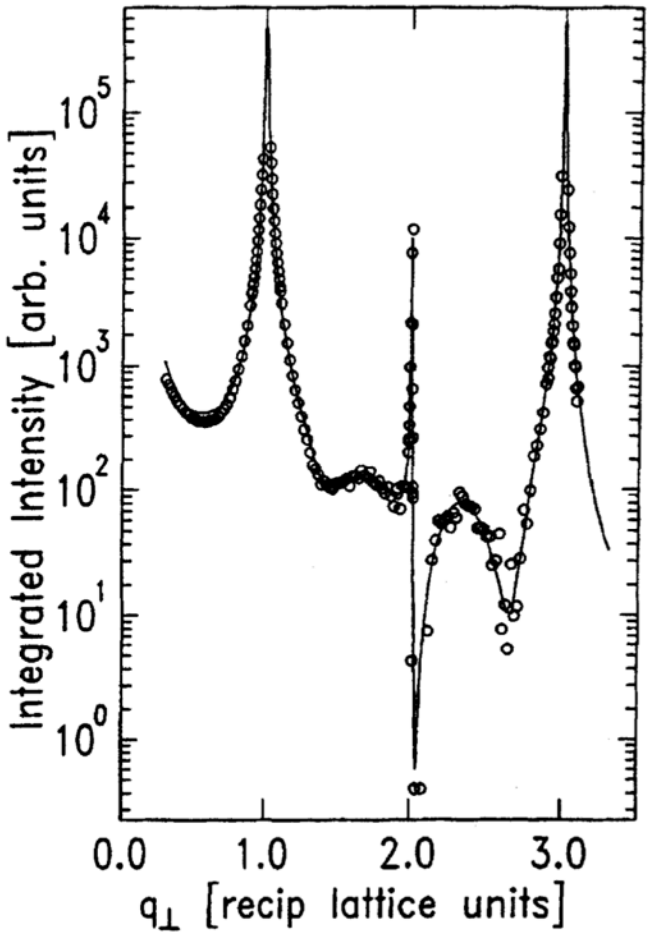

Patterson: Dimer-Adatom-Stacking-Fault

K. Takayanagi et al, Surf. Sci. 164 367 (1985)

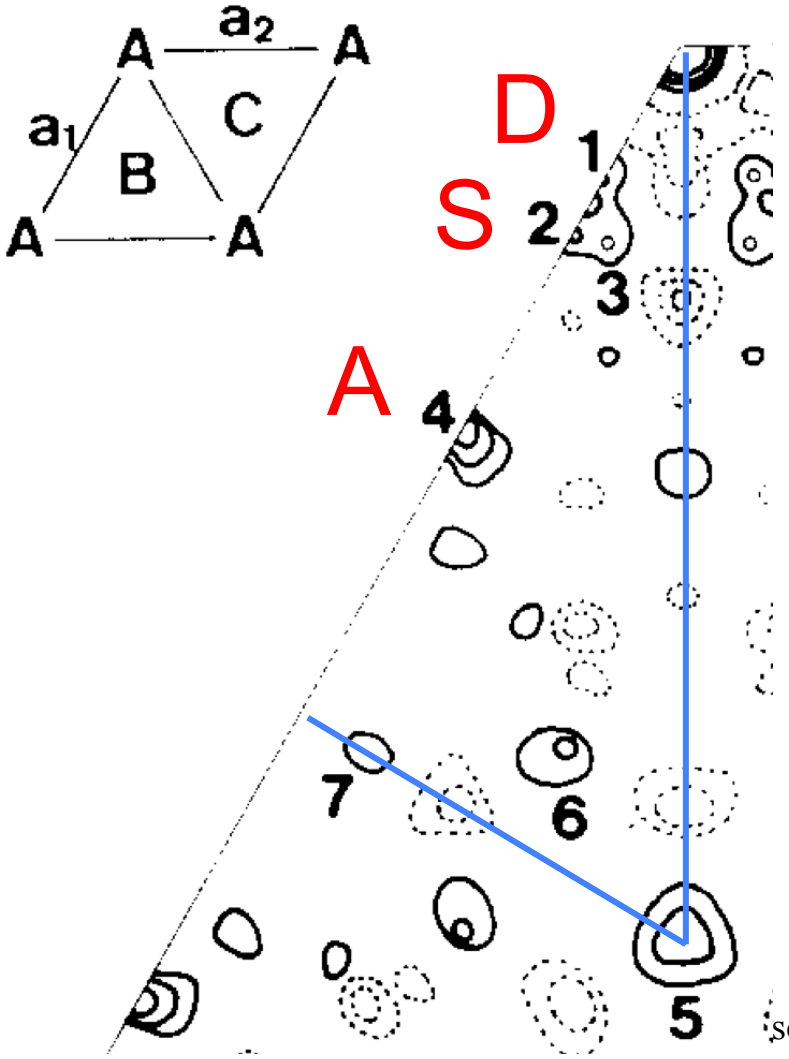

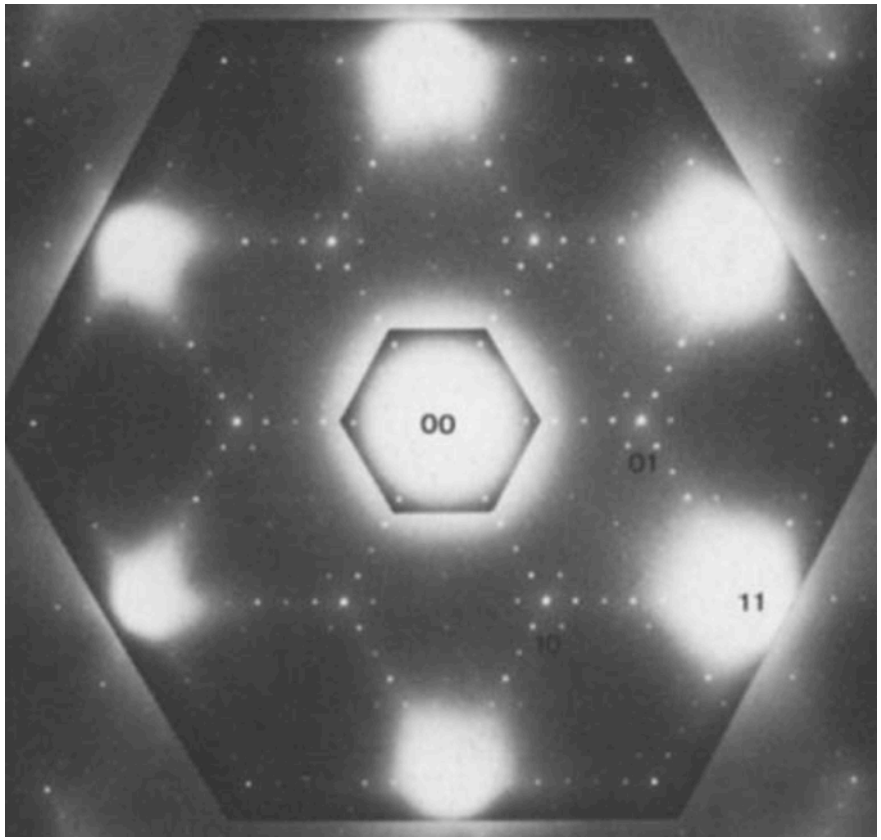

DAS Model
Si(111) 7x7

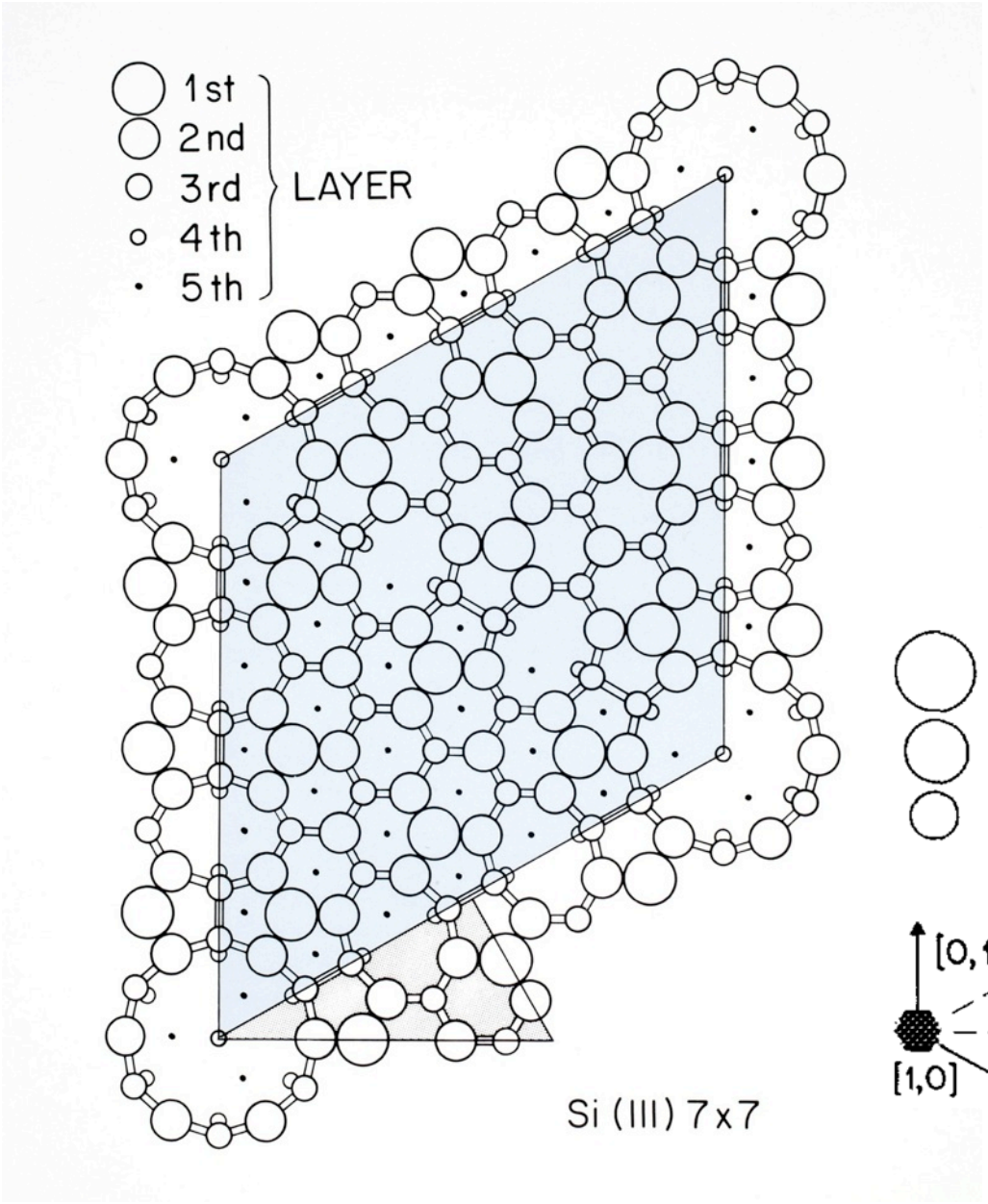

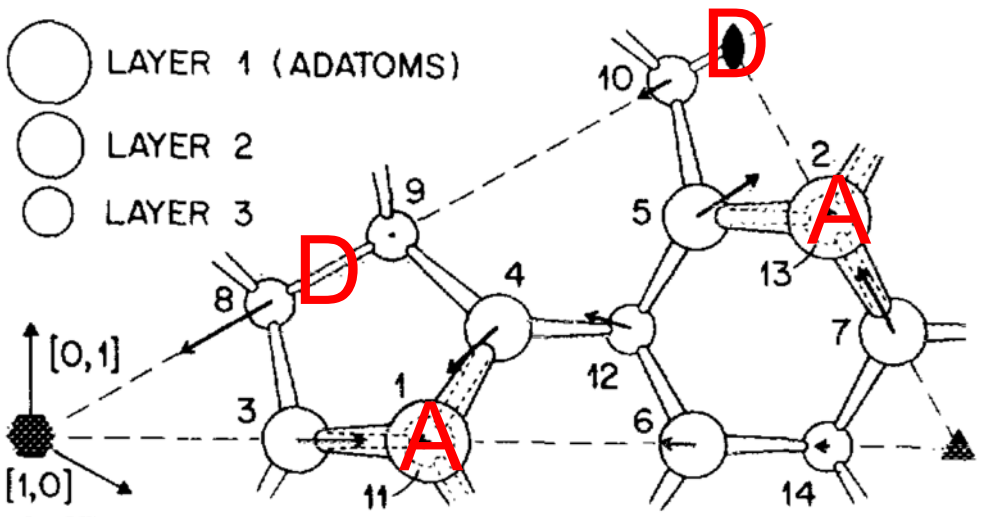

Si(111)7x7 1999 data
Arunabha Ghose

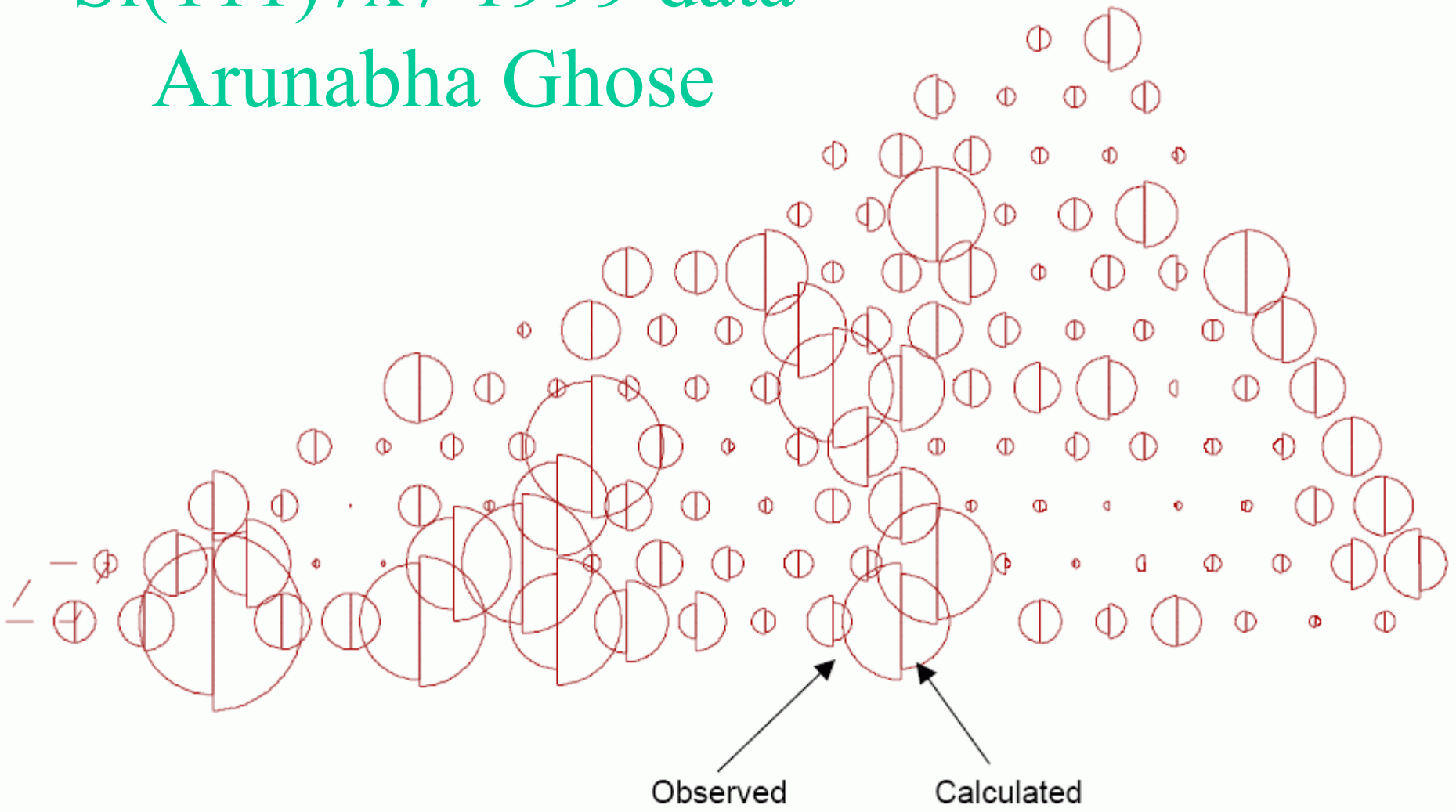

Adatom Geometry

Jim Ciston and Laurie Marks, Northwestern U

J. Ciston et al, Phys. Rev. B 79 193302 (2009)

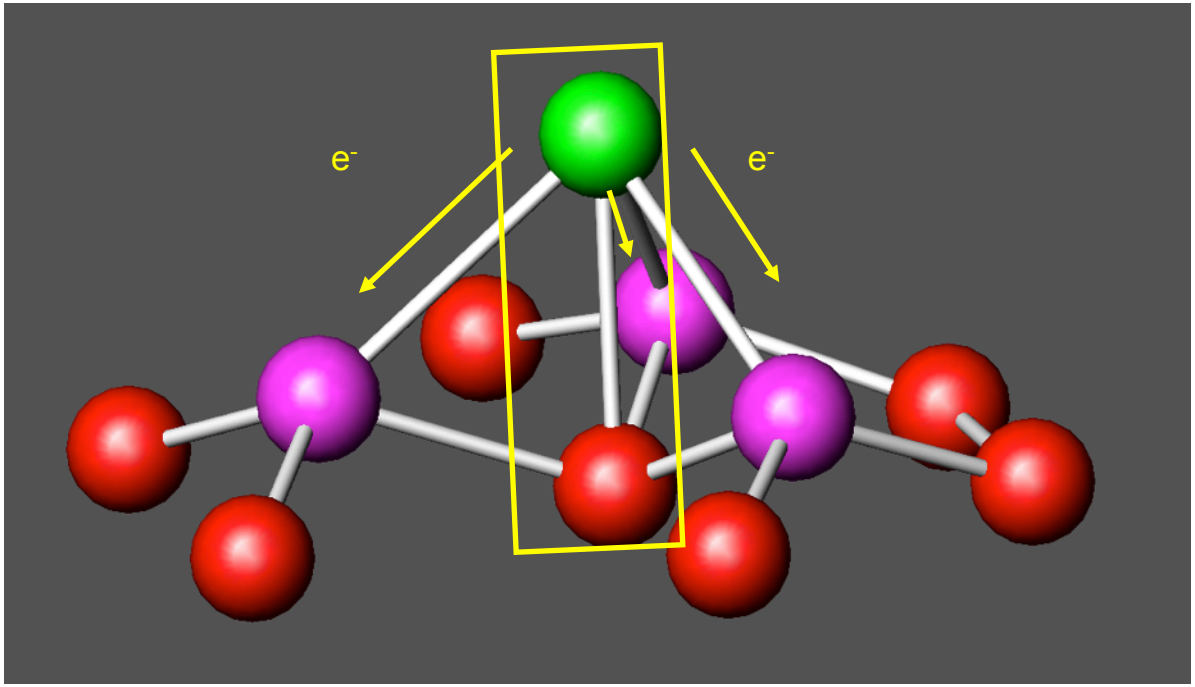

a) IAM-BCPA Anti-Bond feature difference map for an isolated Si-Si pair
b) (110) slice through an unfaulted central adatom (DFT difference map)

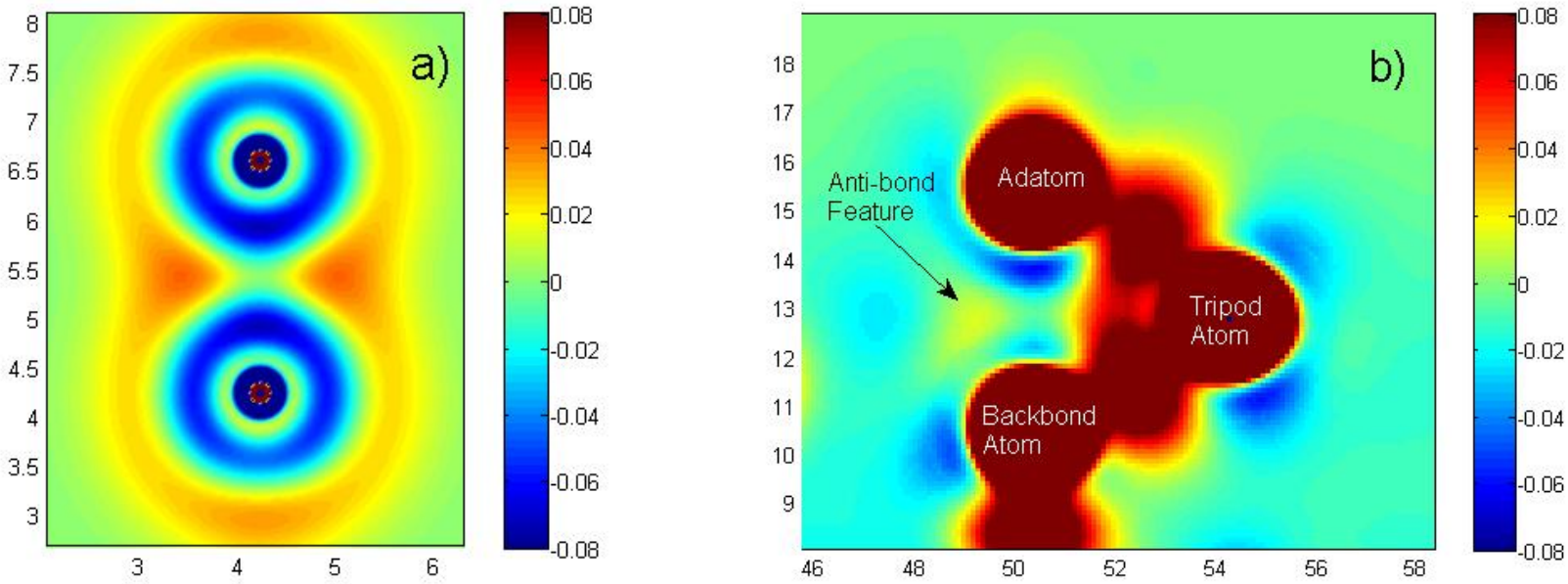

Class Outline

- Crystal structure (using VESTA software)
- Surface diffraction and surface structure
- Powder diffraction methods
- Williamson-Hall analysis of size and strain
- Pair Distribution Function (PDF)

Powder diffraction

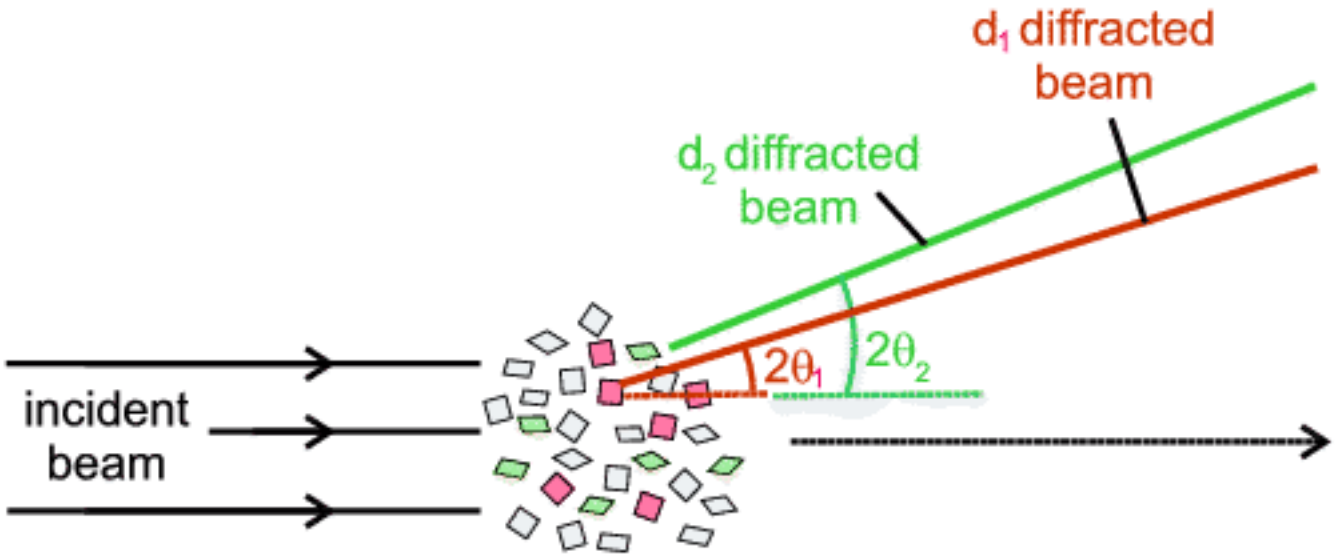

Quartz powder pattern

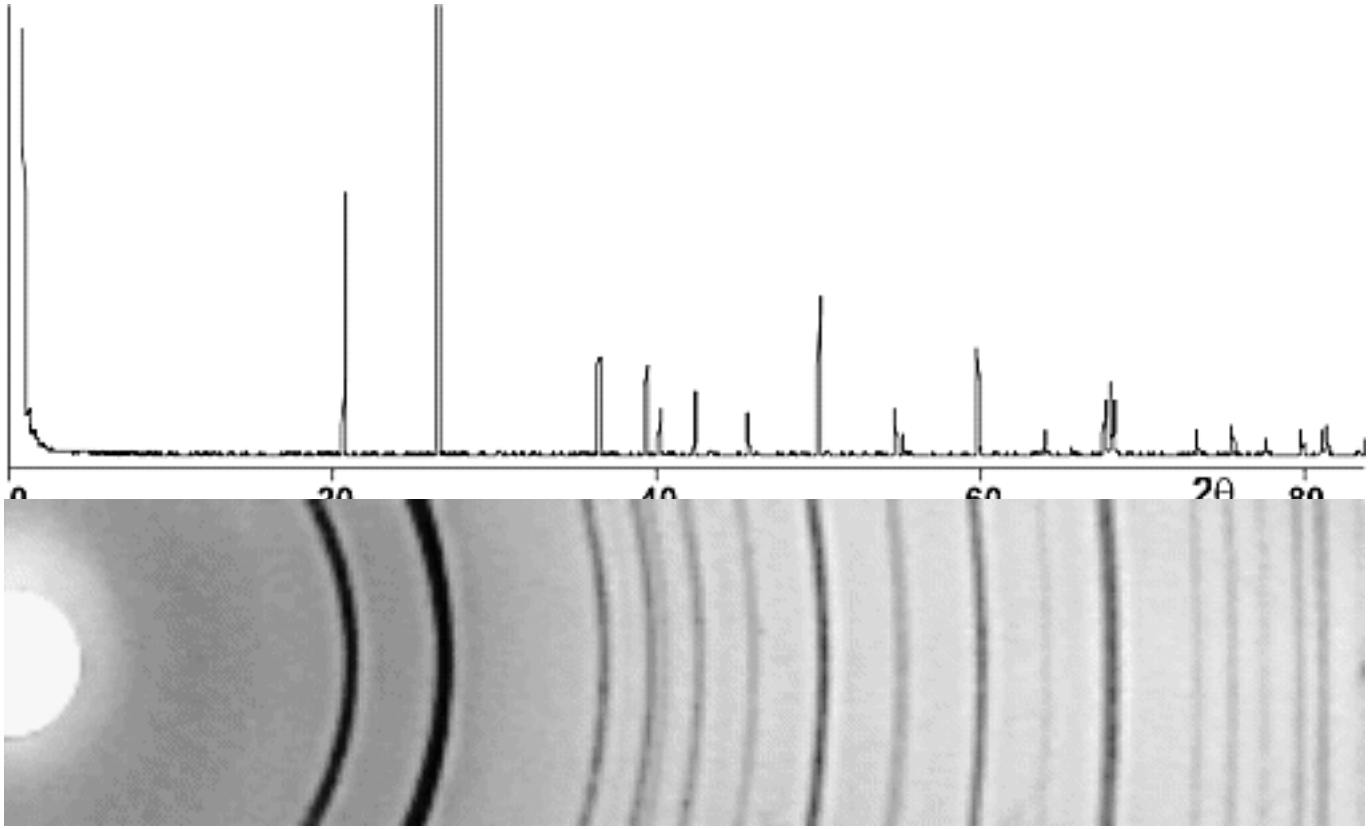

Bragg-Brentano geometry

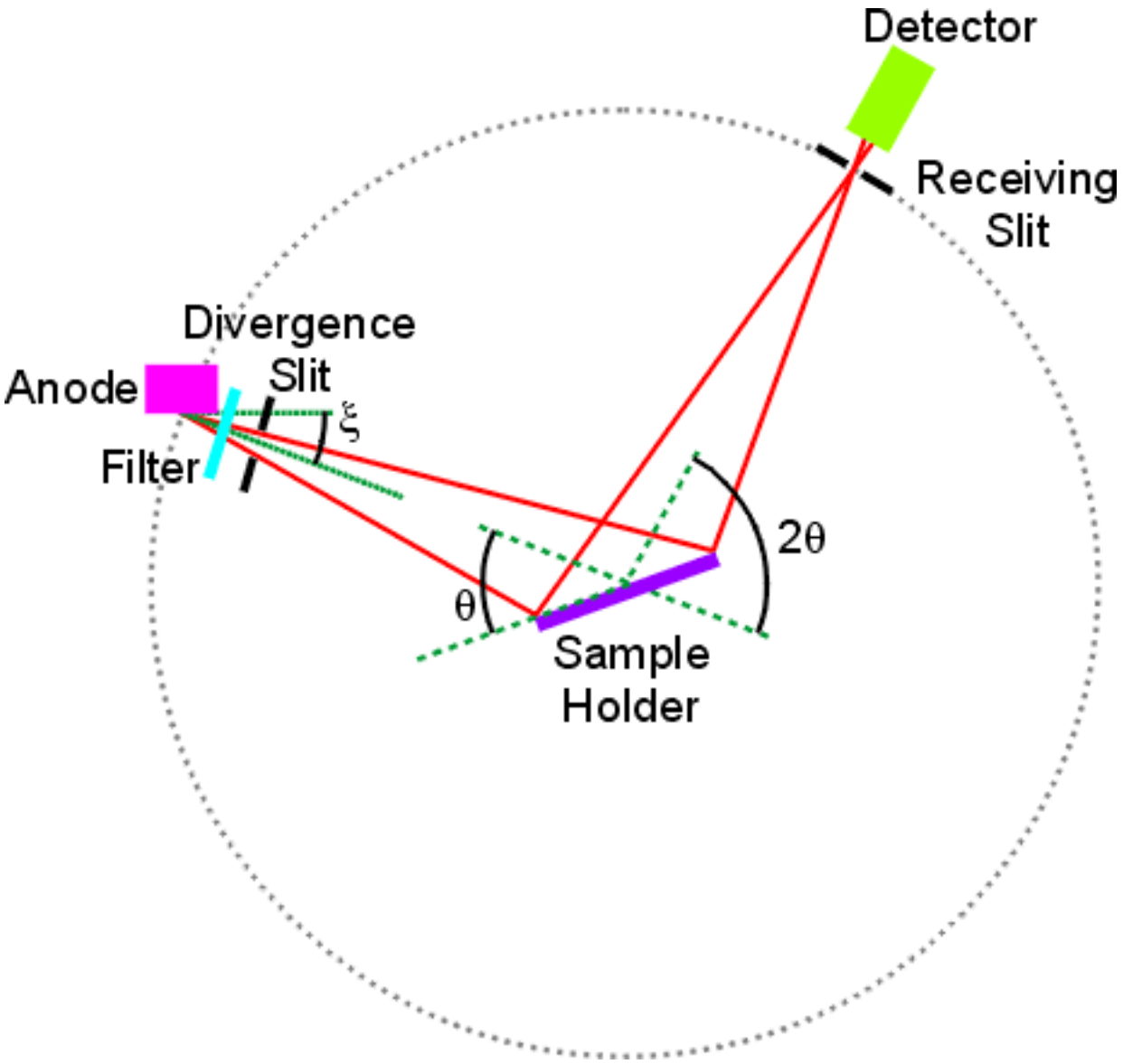

Powder instrument (JKC)

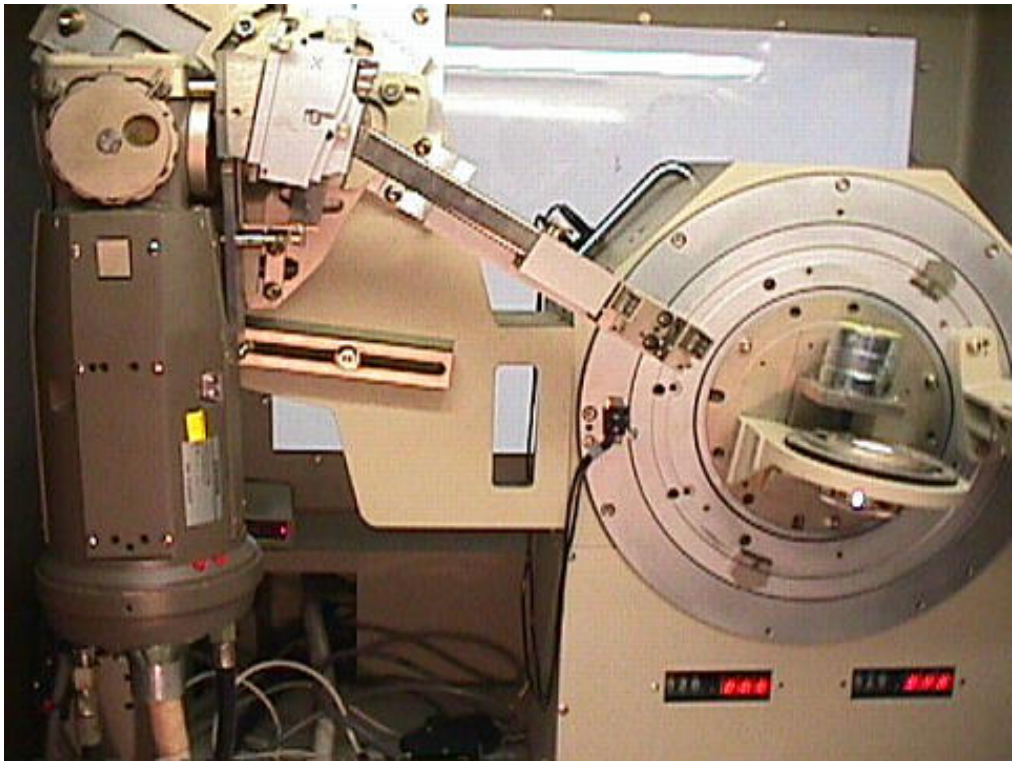

Bragg-Brentano Variations

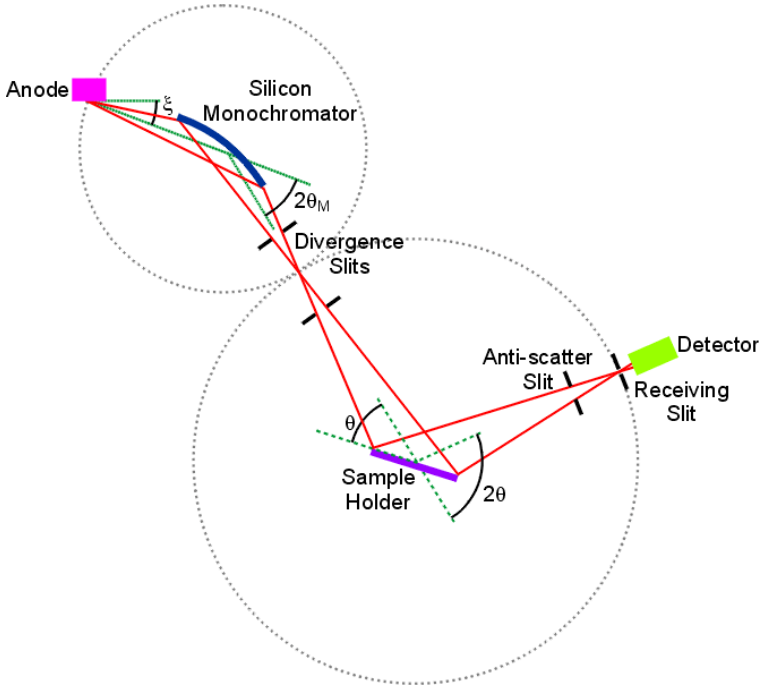

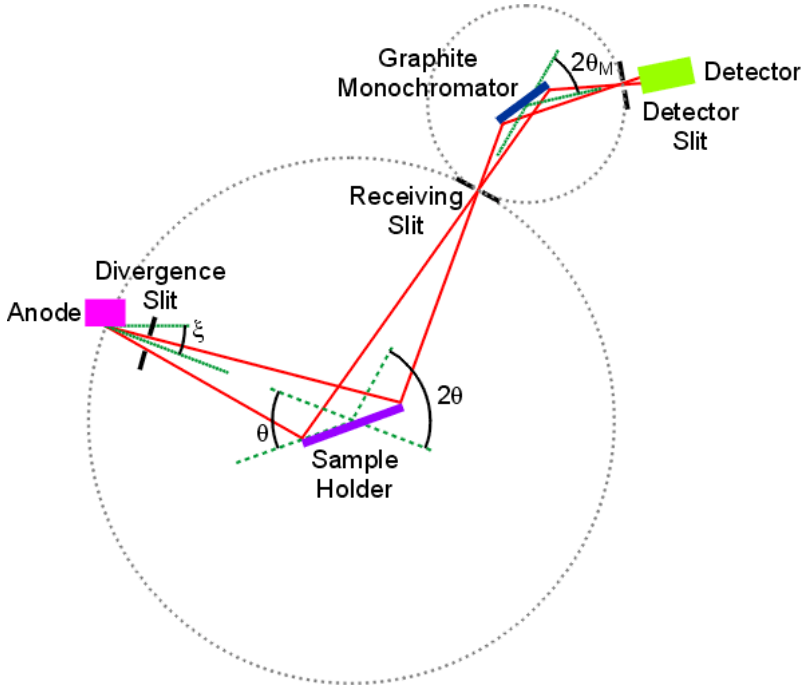

Debye Scherrer method

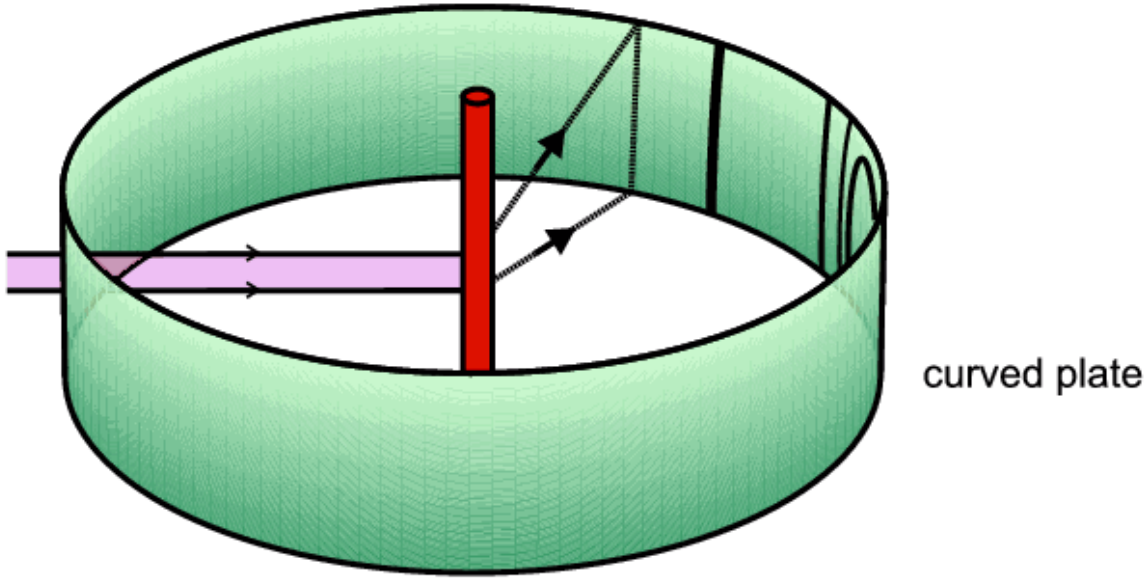

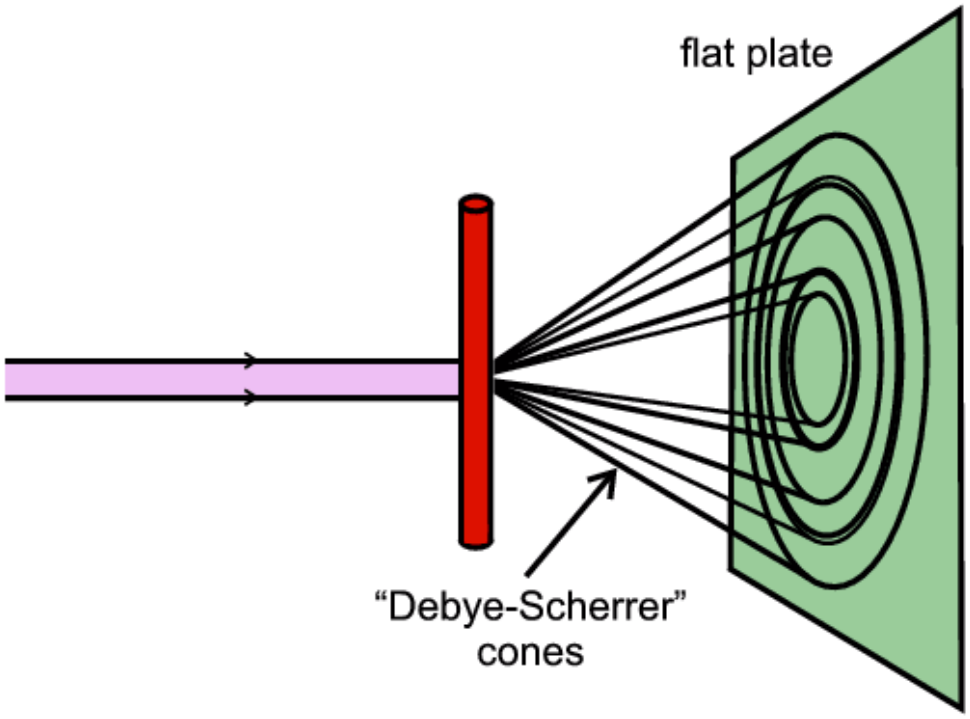

Mortar and Sieves: 30-micron size

Size effect on lineshape

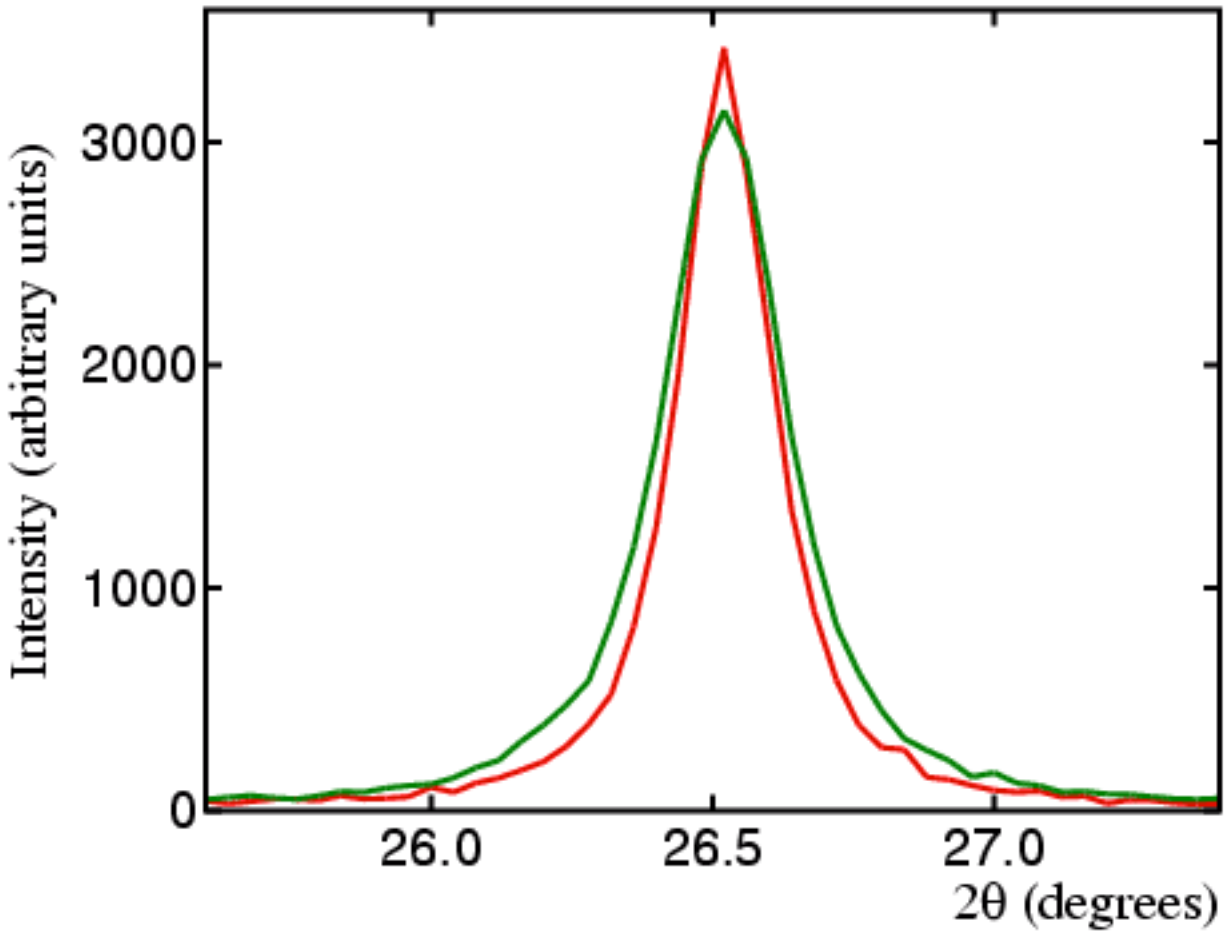

I. K. Robinson X-ray diffraction 2017

Flat Plate Sample Holders

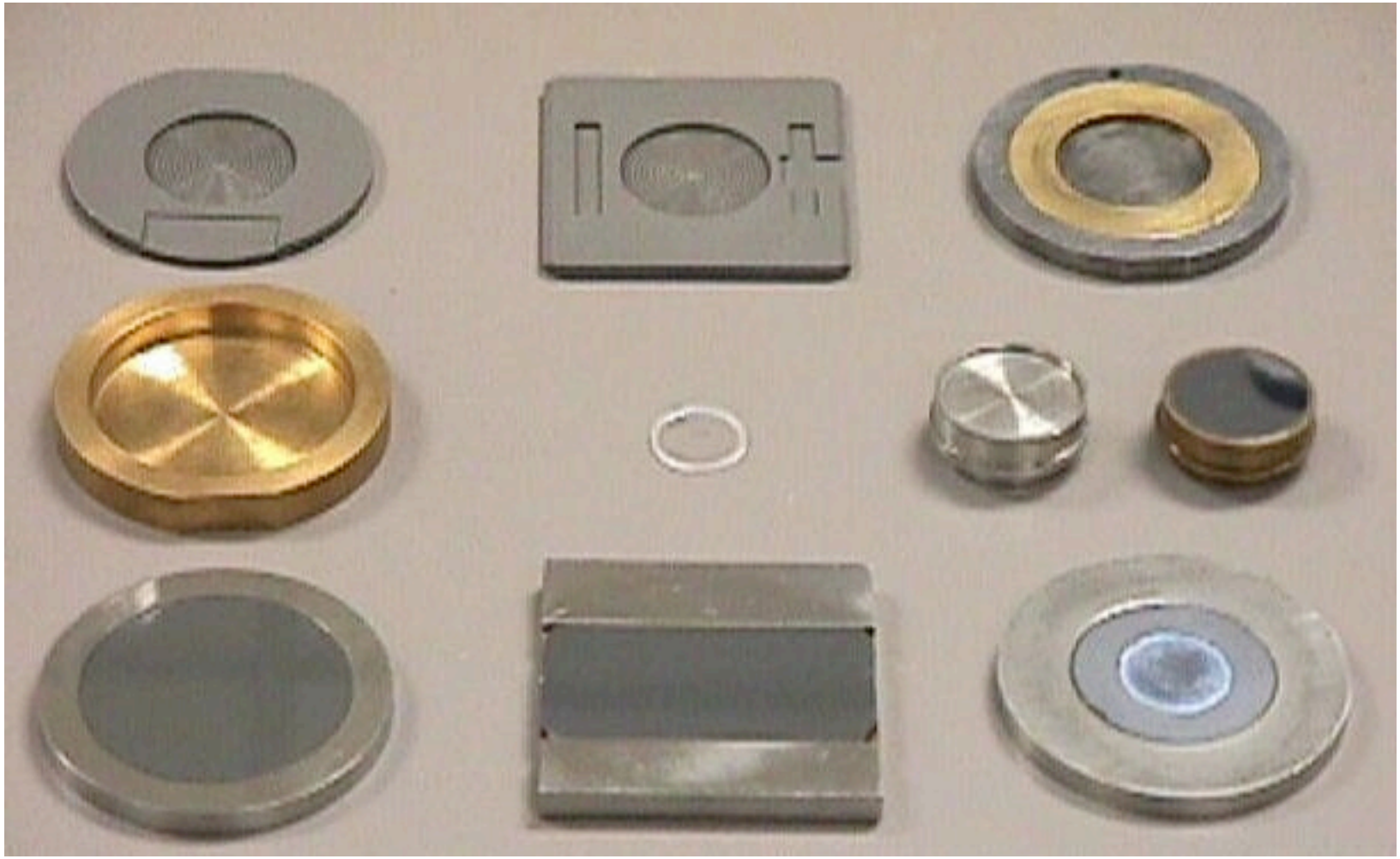

Preferred orientation = texture

hydrated cement phase $Ca_4Al_2(SO_4)O_6.16H_2O$

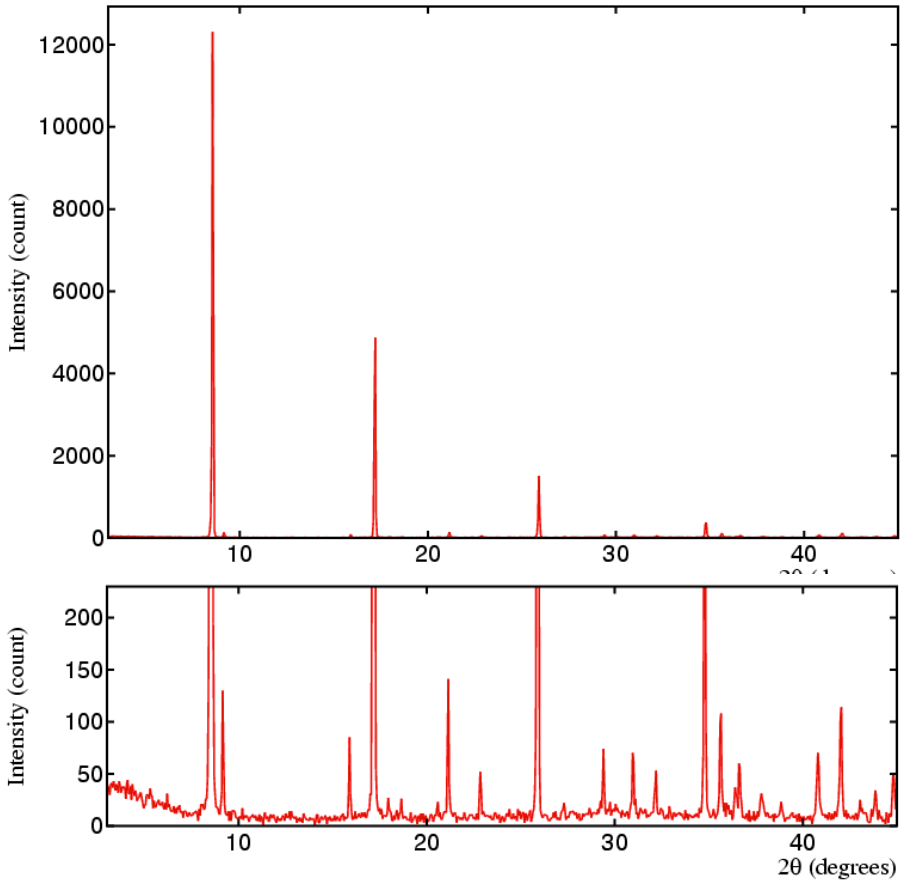

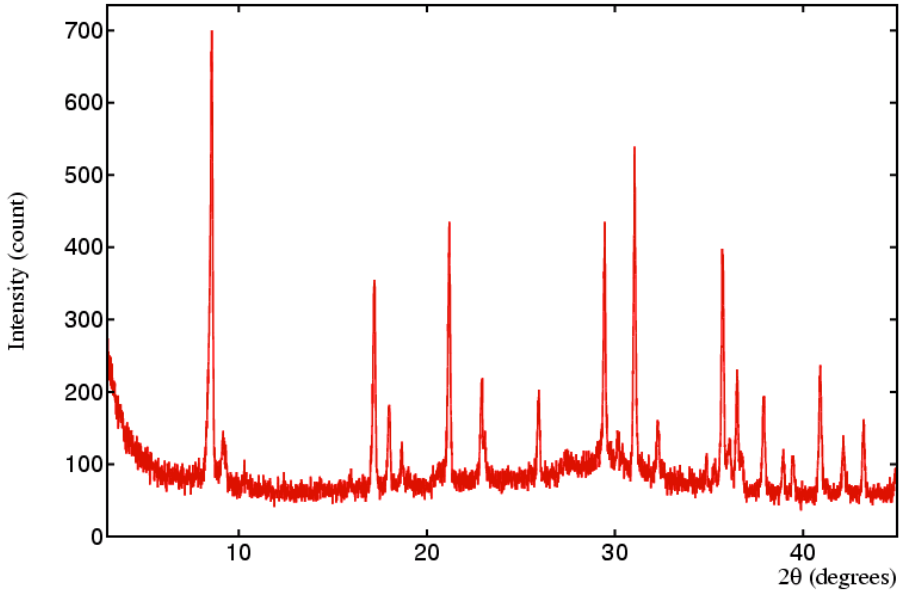

left: flat plate holder
right: capillary holder

Tranparency: glucose example

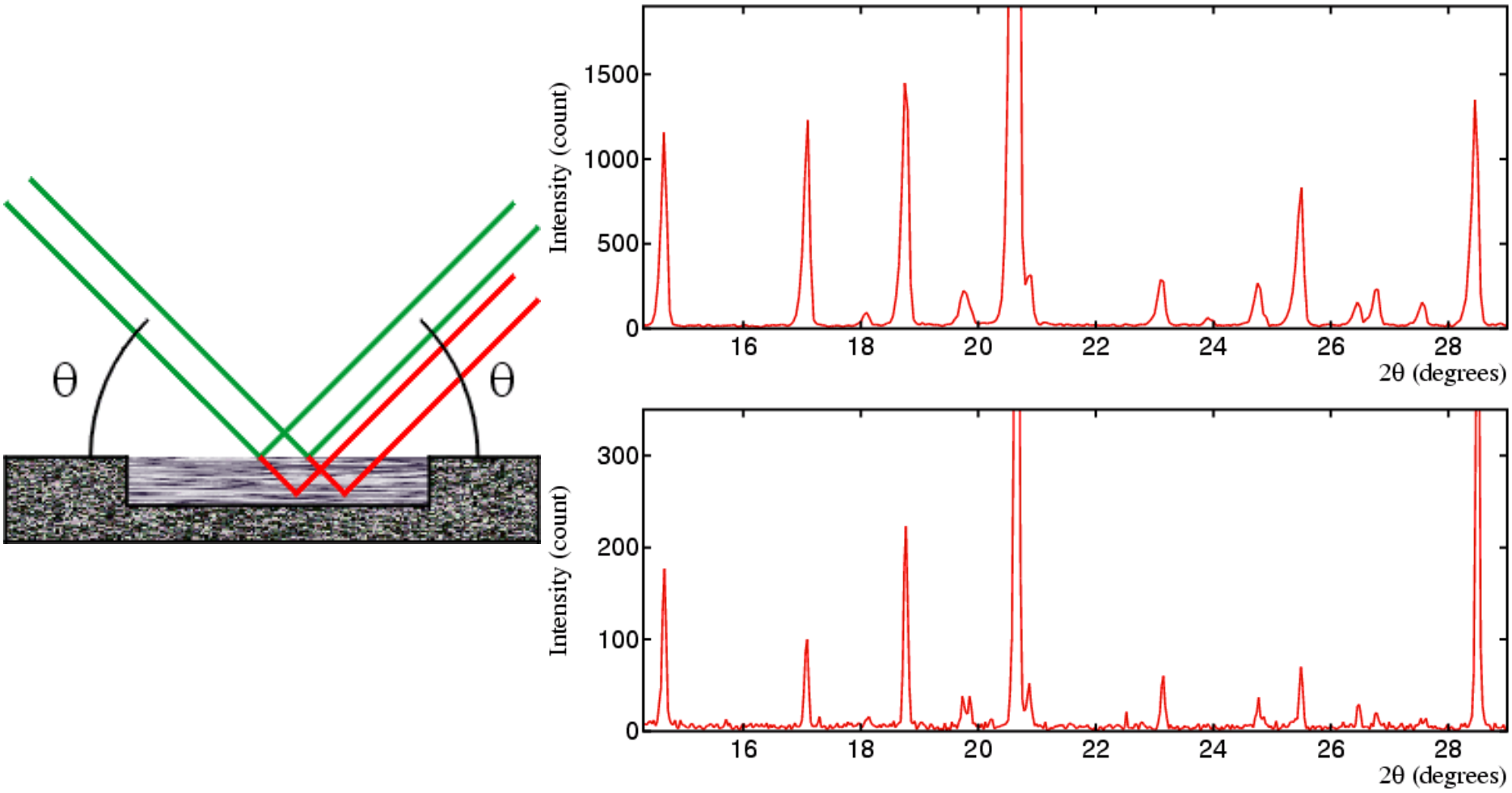

Ideally imperfect crystal

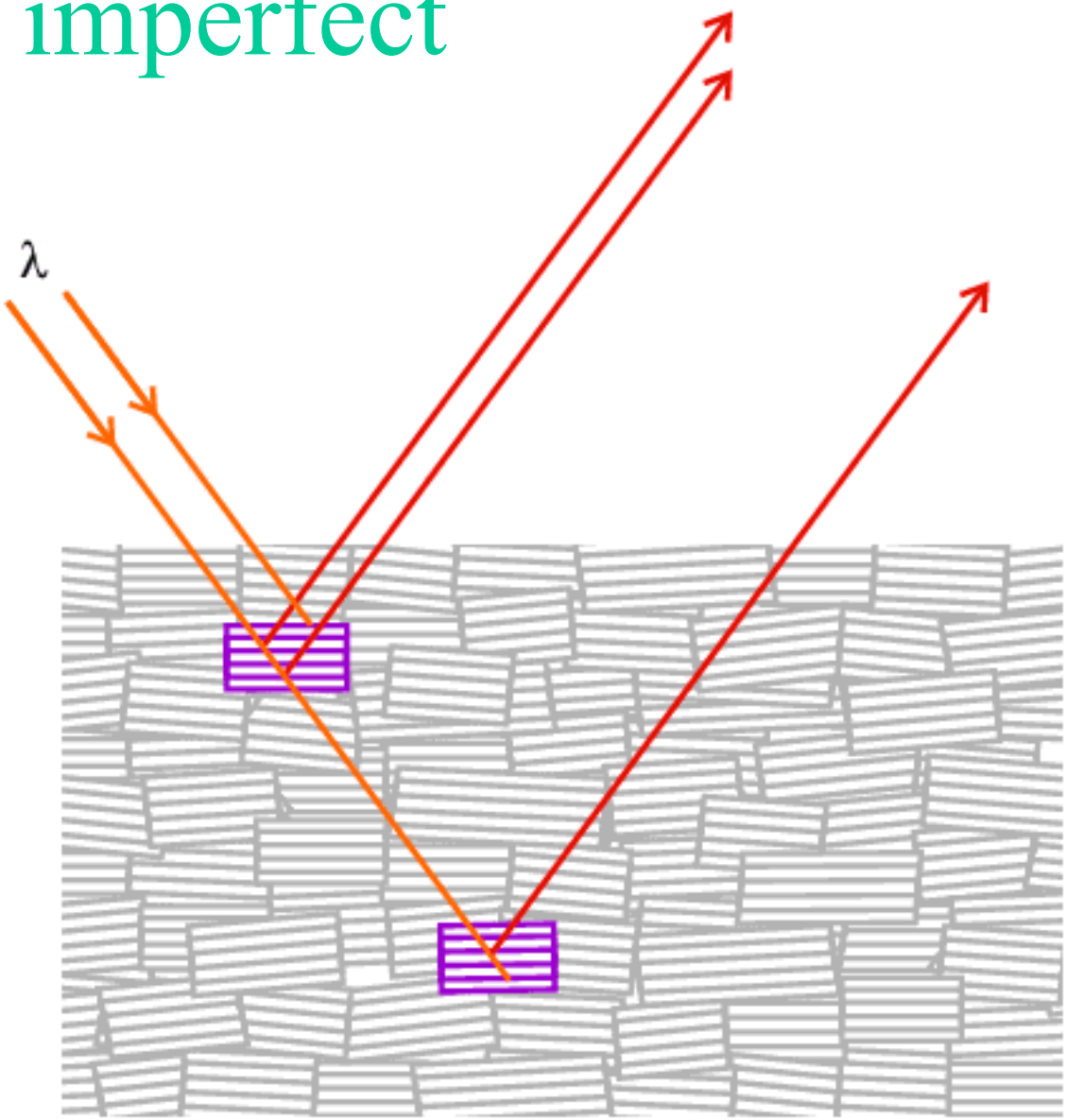

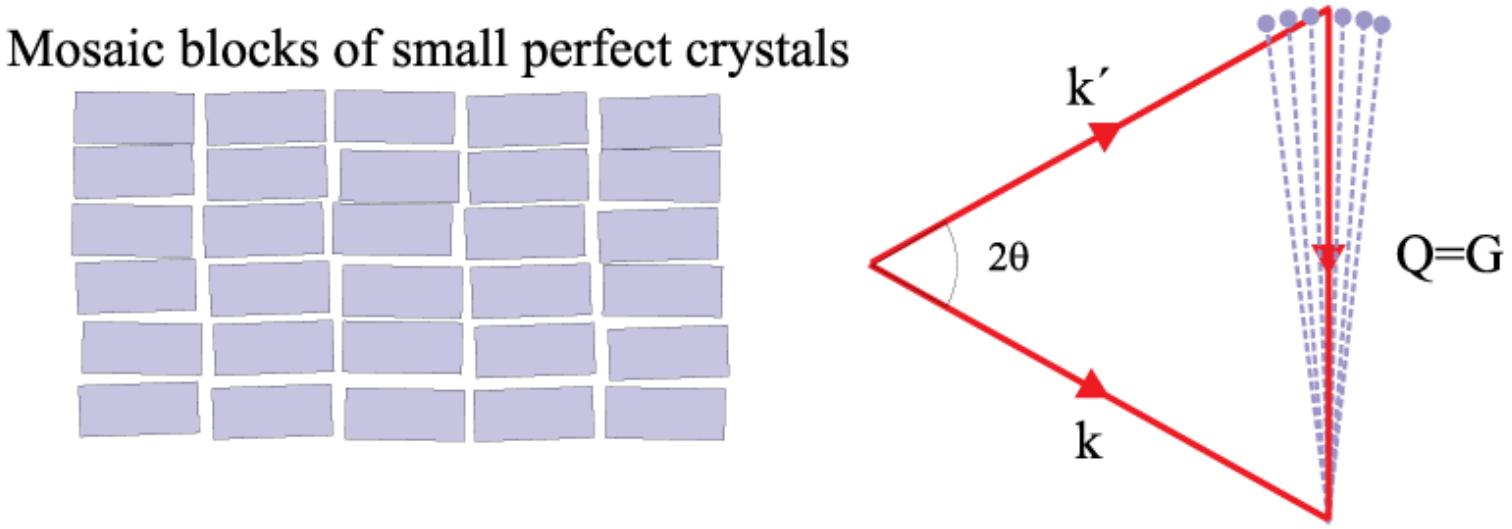

Fig. 5.19 Left: Real single crystals are often composed of small, ideal crystal grains, also called mosaic blocks which have a narrow distribution of orientations, the so-call mosaic distribution. Right: For a given (*h, k, l*) reflection the crystal is rotated, corresponding to rotating **G** about the origin. In this way the integrated intensity from each mosaic block is accumulated.

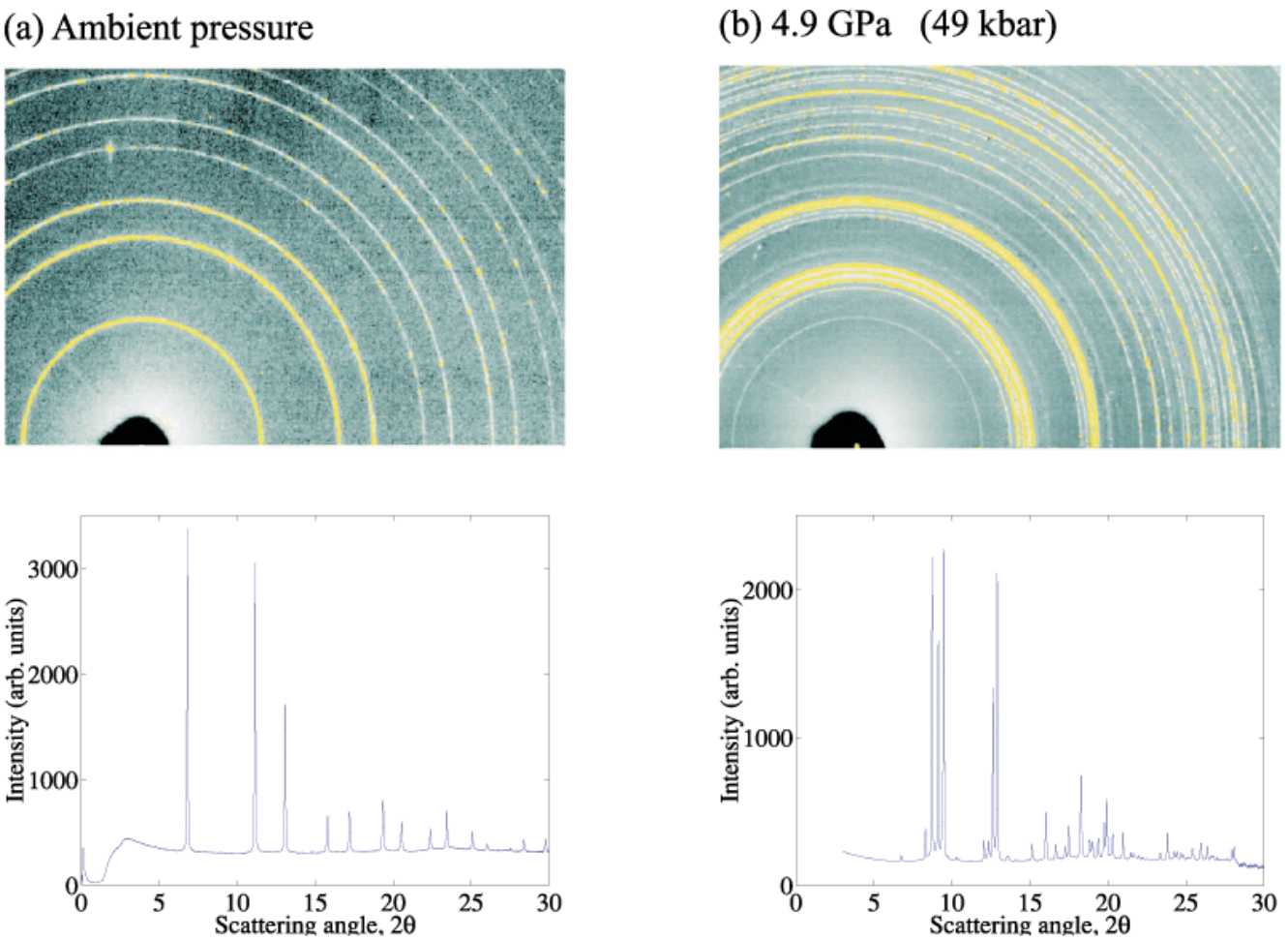

Fig. 5.24 Powder diffraction patterns from InSb at (a) ambient pressure, and (b) at a pressure of 4.9 GPa. The patterns recorded on an image plate detector are shown in the top row, and display rings where the detector intercepts the Debye-Scherrer cones. The data were recorded with an incident wavelength of $\lambda = 0.447$ Å. In the bottom row the radially averaged patterns as a function of 2θ are displayed. The results show that InSb undergoes a phase transition from the zinc sulfide structure to a phase with an orthorhombic structure at pressures above 4.9 GPa. (Data courtesy of Malcolm McMahon, University of Edinburgh.)

Crystal systems

Crystal System	Characteristic Symmetry	Syngony	Unit-Cell Parameters	Independent Parameters
Triclinic	1× 1-fold	-1	$a \neq b \neq c$; $\alpha \neq \beta \neq \gamma$	6
Monoclinic	1× 2-fold	2/*m*	$a \neq b \neq c$; $\alpha = \gamma = 90°$; $\beta \neq 90°$	4
Orthorhombic	3× 2-fold	*mmm*	$a \neq b \neq c$; $\alpha = \beta = \gamma = 90°$	3
Tetragonal	1× 4-fold	4/*mmm*	$a = b \neq c$; $\alpha = \beta = \gamma = 90°$	2
Trigonal (see note)	1× 3-fold	6/*mmm* (P) -3*m* (R)	$a = b \neq c$; $\alpha = \beta = 90°$; $\gamma = 120°$	2
Hexagonal	1× 6-fold	6/*mmm*	$a = b \neq c$; $\alpha = \beta = 90°$; $\gamma = 120°$	2
Cubic	4× 3-fold	*m*-3*m*	$a = b = c$; $\alpha = \beta = \gamma = 90°$	1

Systematic absences determine space group

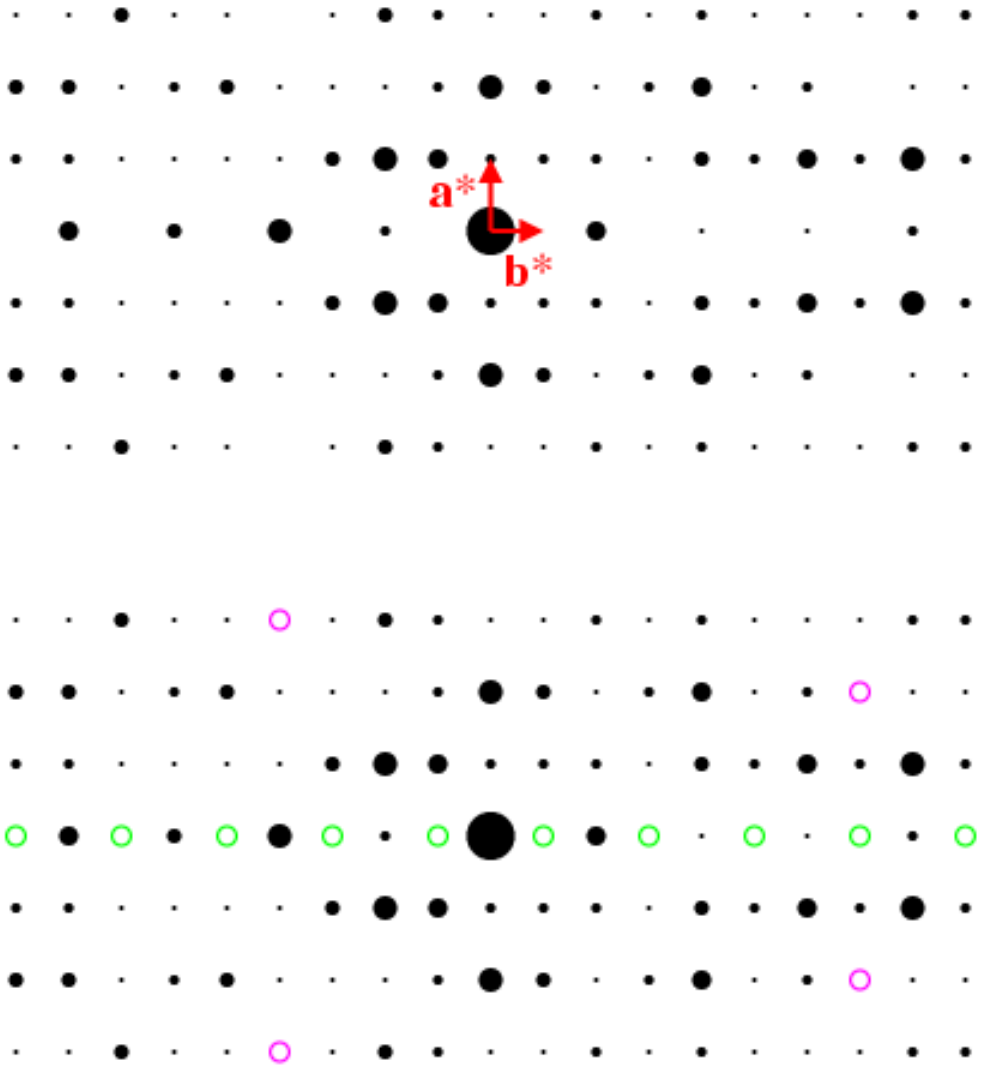

Anisotropic Debye-Waller factors
Tyrosine example

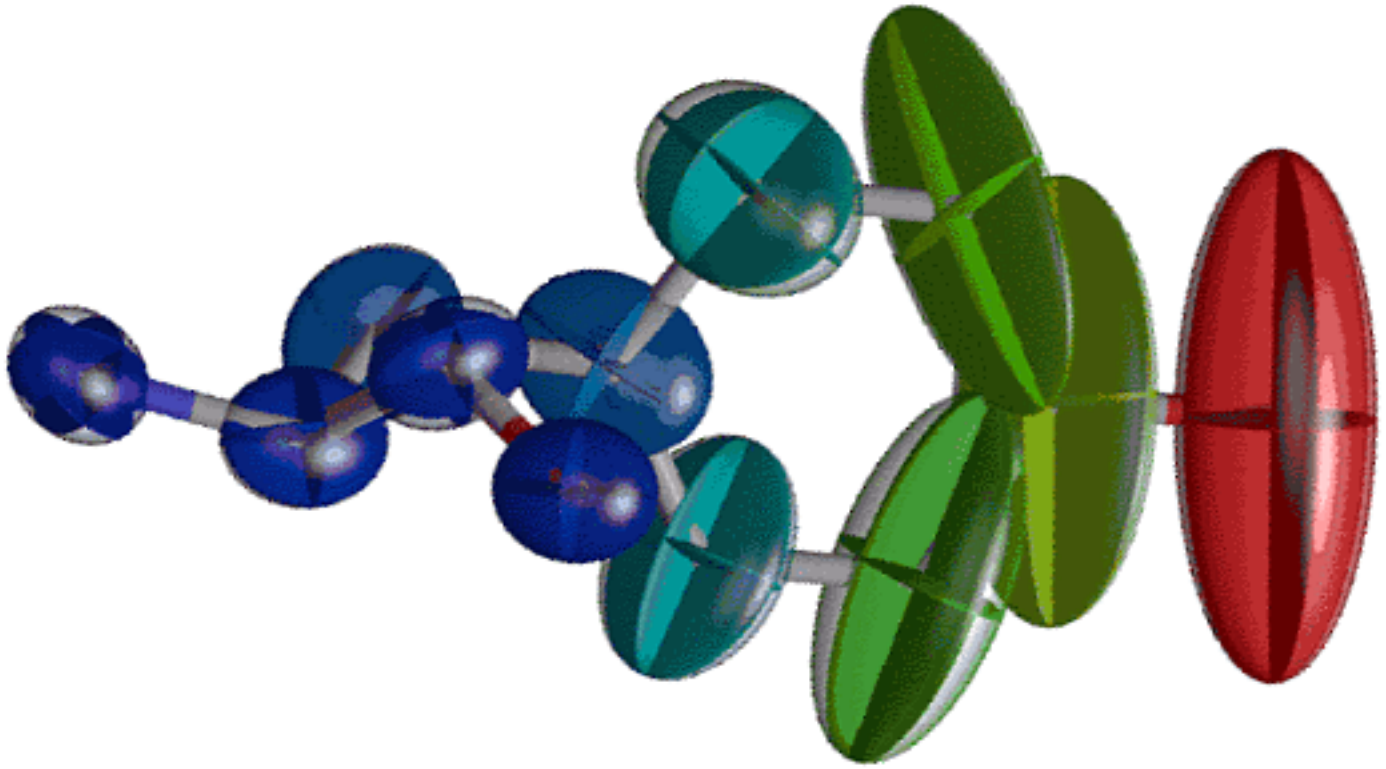

Class Outline

- Crystal structure (using VESTA software)
- Surface diffraction and surface structure
- Powder diffraction methods
- Williamson-Hall analysis of size and strain
- Pair Distribution Function (PDF)

Scattering from array of unit cells

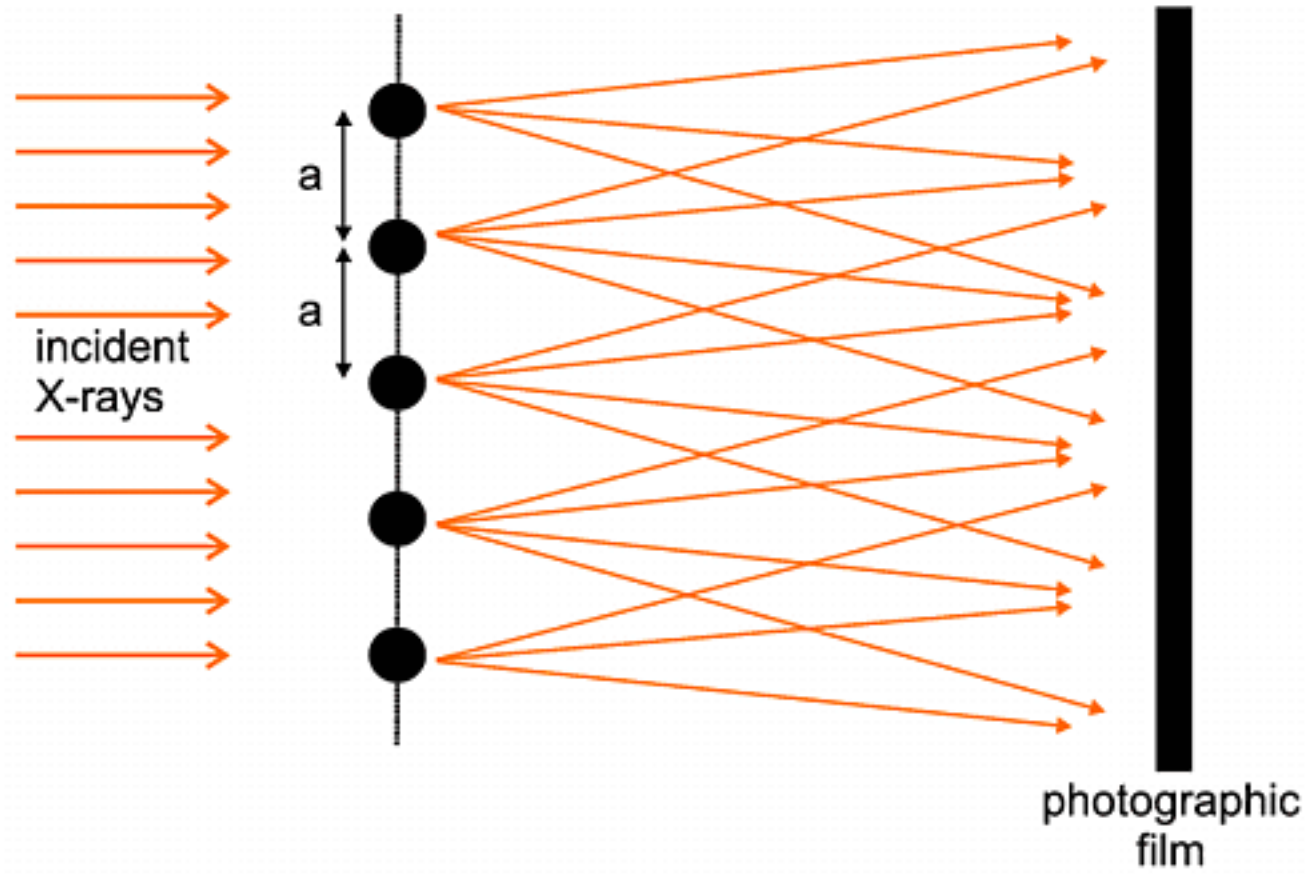

Interference sum over unit cells

$$R_N(Q) = A\sum_{j=0}^{N-1} e^{iQdj}$$

$$= A\frac{1-e^{iQdN}}{1-e^{iQd}}$$

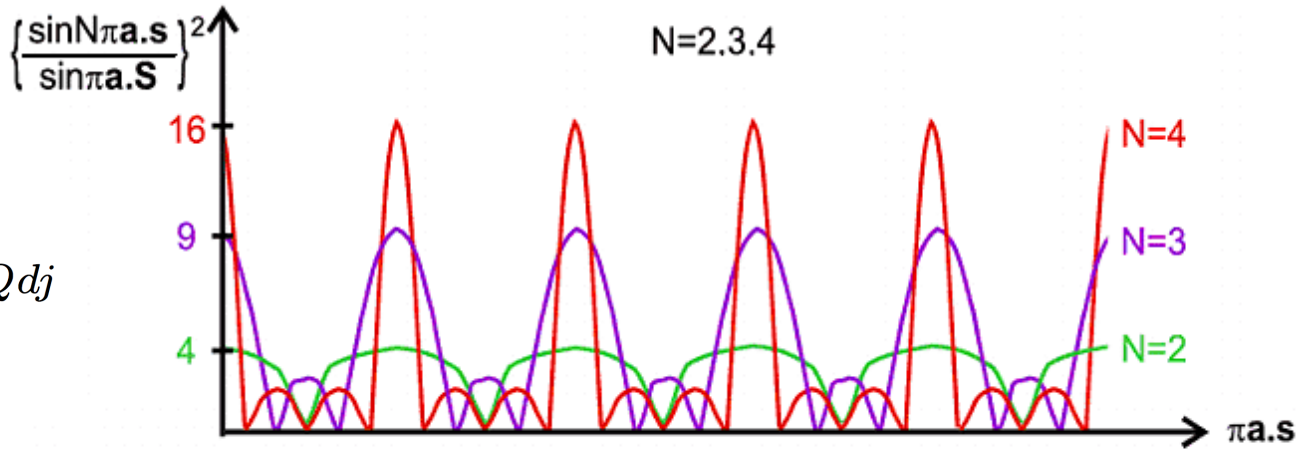

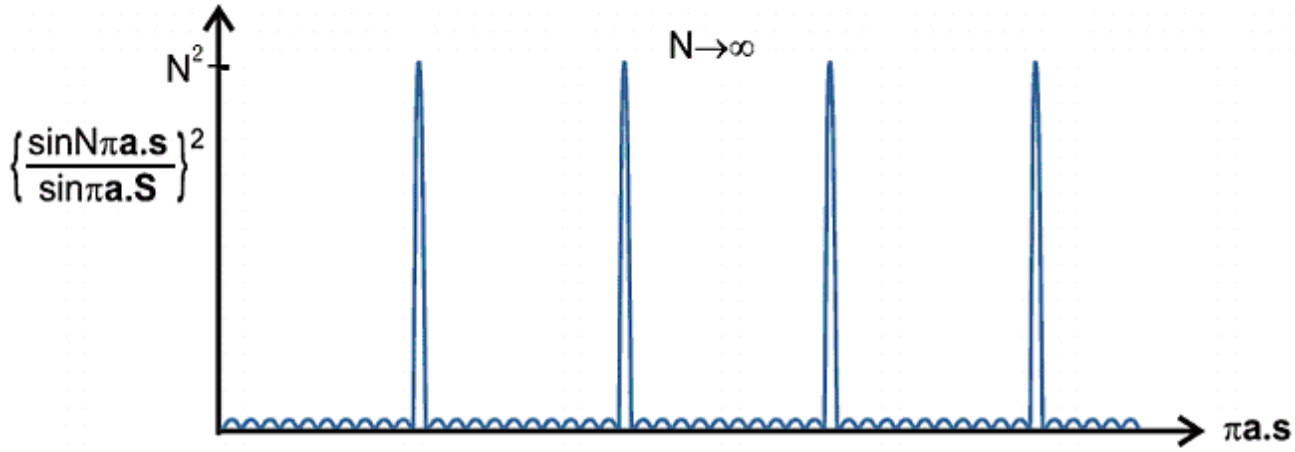

Effect of Strain on Diffraction

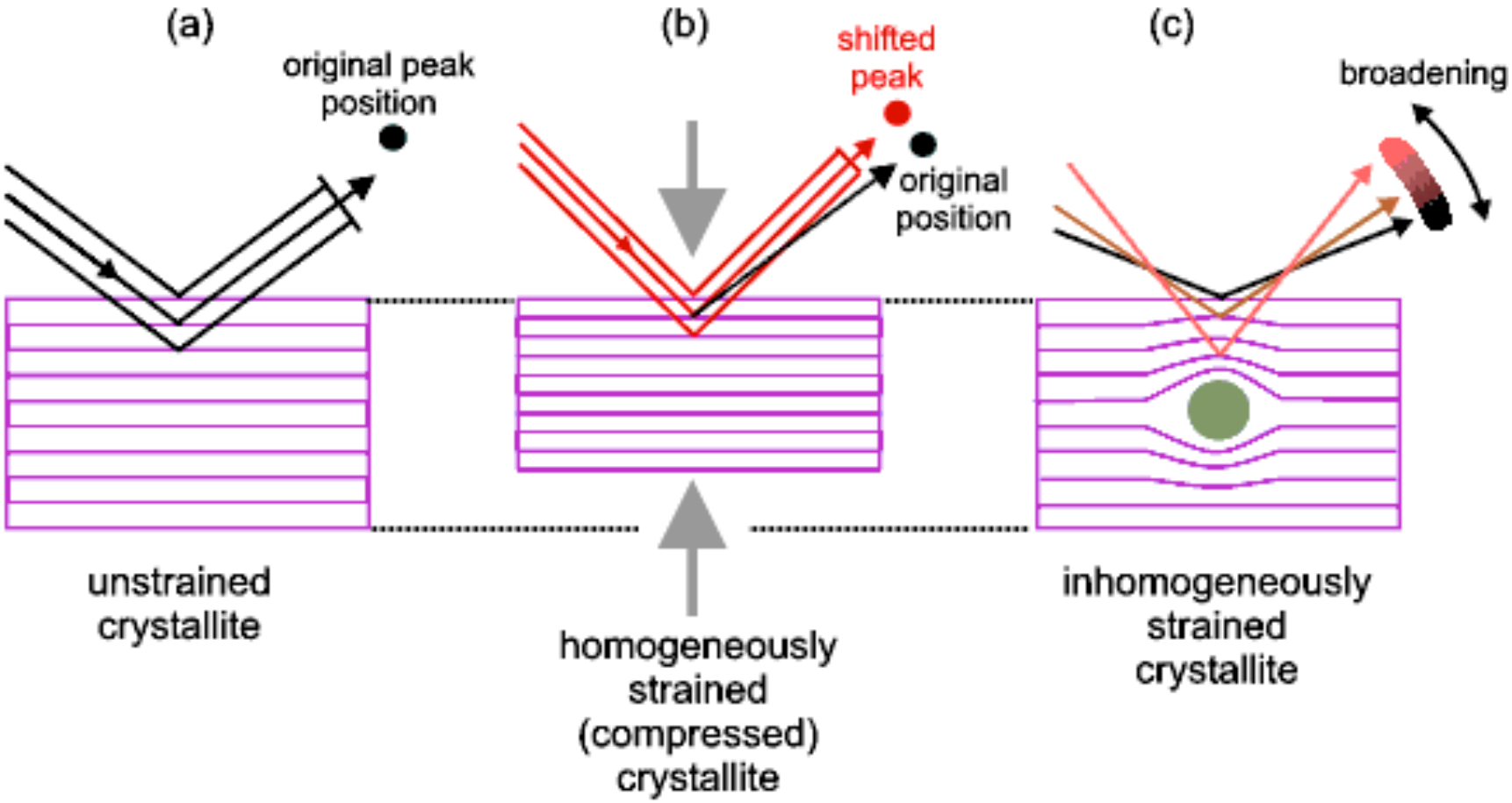

I. K. Robinson X-ray diffraction 2017

G.K.Williamson and W.H.Hall Acta Metall. 1, 22-31 (1953)

Scherrer equation

$$\beta_L = \frac{\mathbf{K}\lambda}{L\cos\theta}$$

$$\beta_e = \mathbf{C}\varepsilon\tan\theta$$

$$\beta_{tot} = \beta_e + \beta_L = \mathbf{C}\varepsilon\tan\theta + \frac{\mathbf{K}\lambda}{L\cos\theta}$$

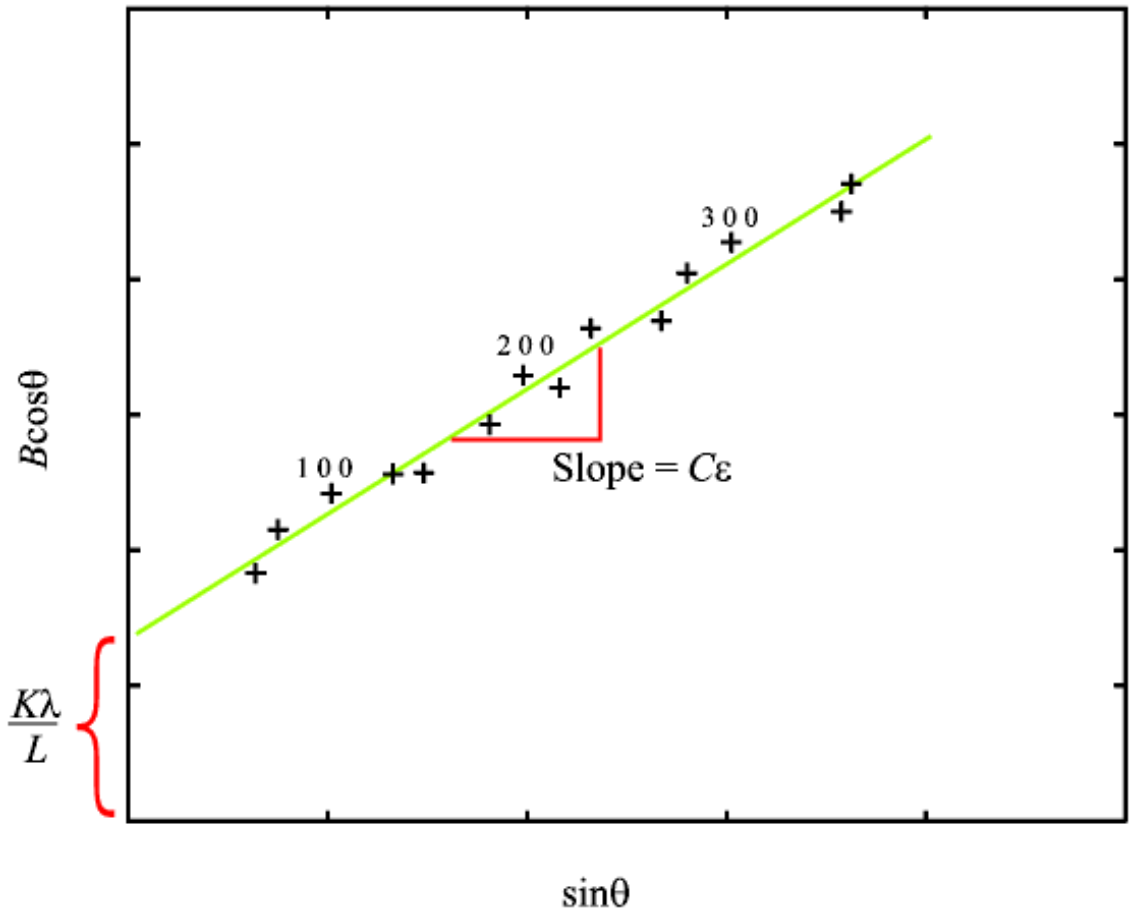

Class Outline

- Crystal structure (using VESTA software)
- Surface diffraction and surface structure
- Powder diffraction methods
- Williamson-Hall analysis of size and strain
- Pair Distribution Function (PDF)

Pair Distribution Function

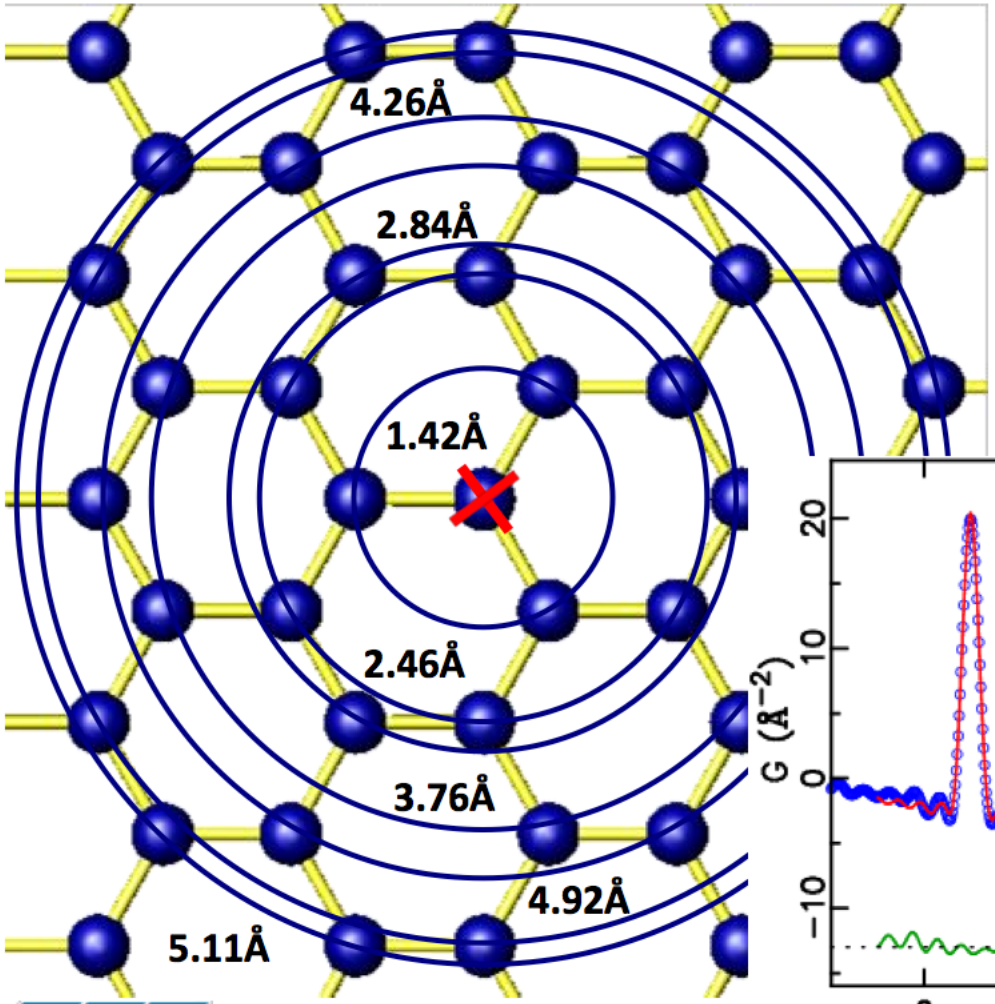

Radial atomic **p**air **d**istribution function (PDF) gives the interatomic distance distribution, or "probability" of finding atomic pairs distance *r* apart

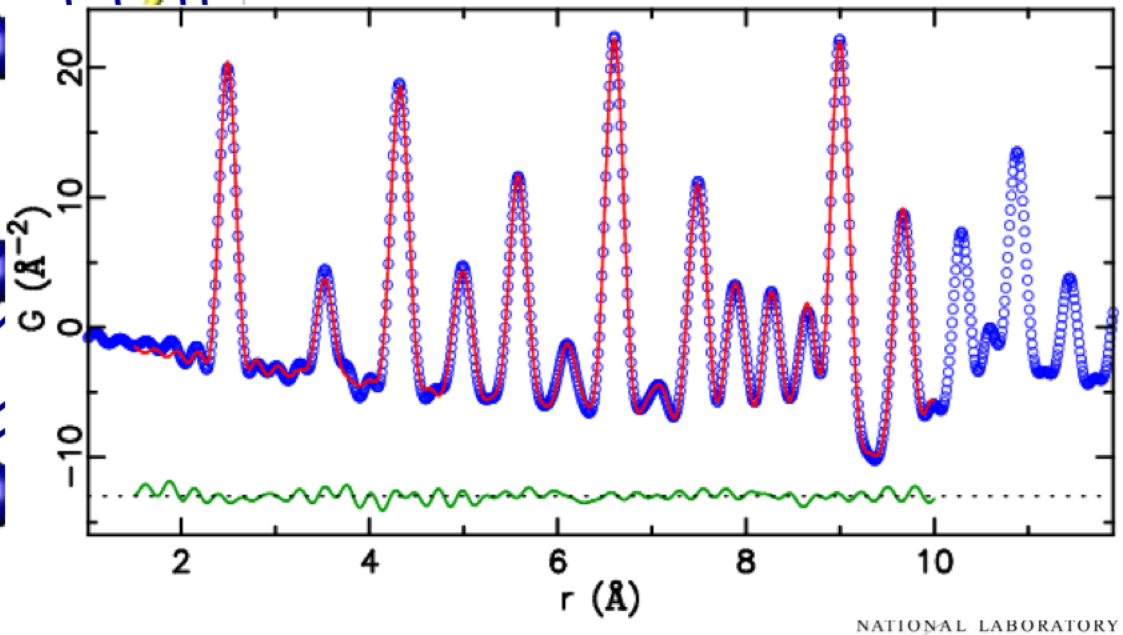

NEUTRONS

NATIONAL LABORATORY

PDF is scattering based Fourier Transform technique

Fourier Pair

$$G(r) = (2/\pi) \int_0^\infty F(Q) \sin(Qr)\, dQ \quad \Longleftrightarrow \quad F(Q) = \int_0^\infty G(r) \sin Qr\, dr$$

DERIVED
(directly from experimental data)

MEASURED
(Experimentally accessible from scattering intensities)

average number density
(number of atoms in symmetrized unit cell per unit cell volume)

$$G(r) = 4\pi r[\rho(r) - \rho_0]$$

"PDF"

pair density function

NOTE:
Many algebraic relatives are called PDF, more later!

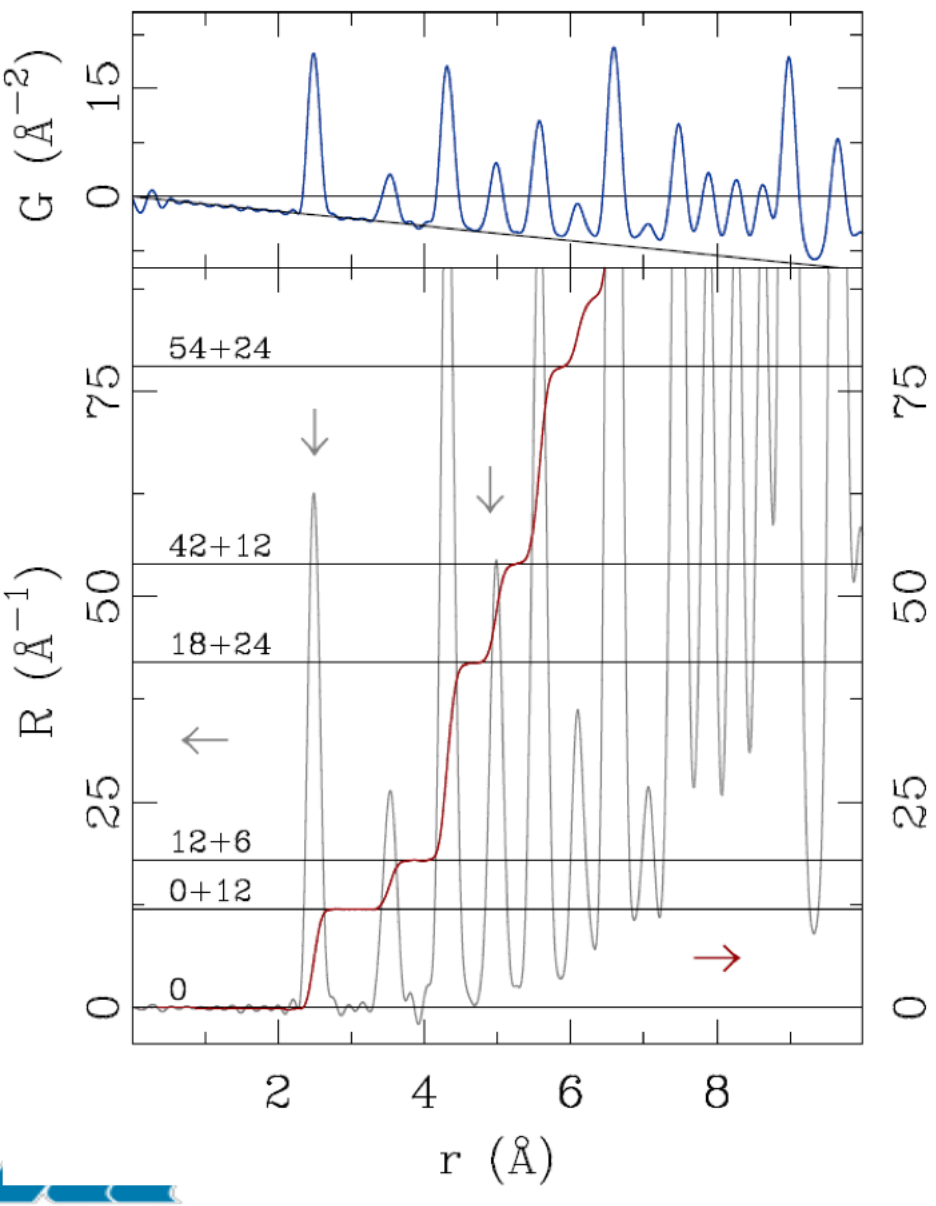

Fitting the Fm-3m model:

Top fit: 3 parameters (a, U_{ISO}, Scale)

Bottom fit: 4 parameters (a, U_{ISO}, Scale, δ)

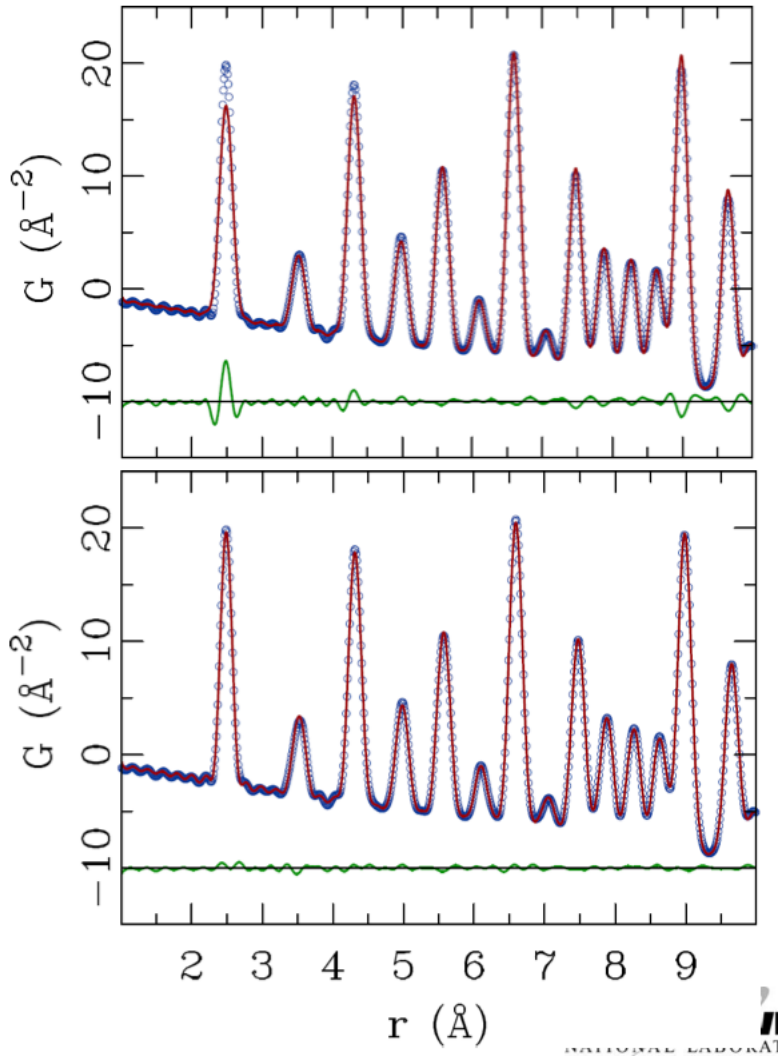

The case of ScF_3

dramatic negative thermal expansion

B. K. Greve *et al*, JACS **132**,15496 (2010).

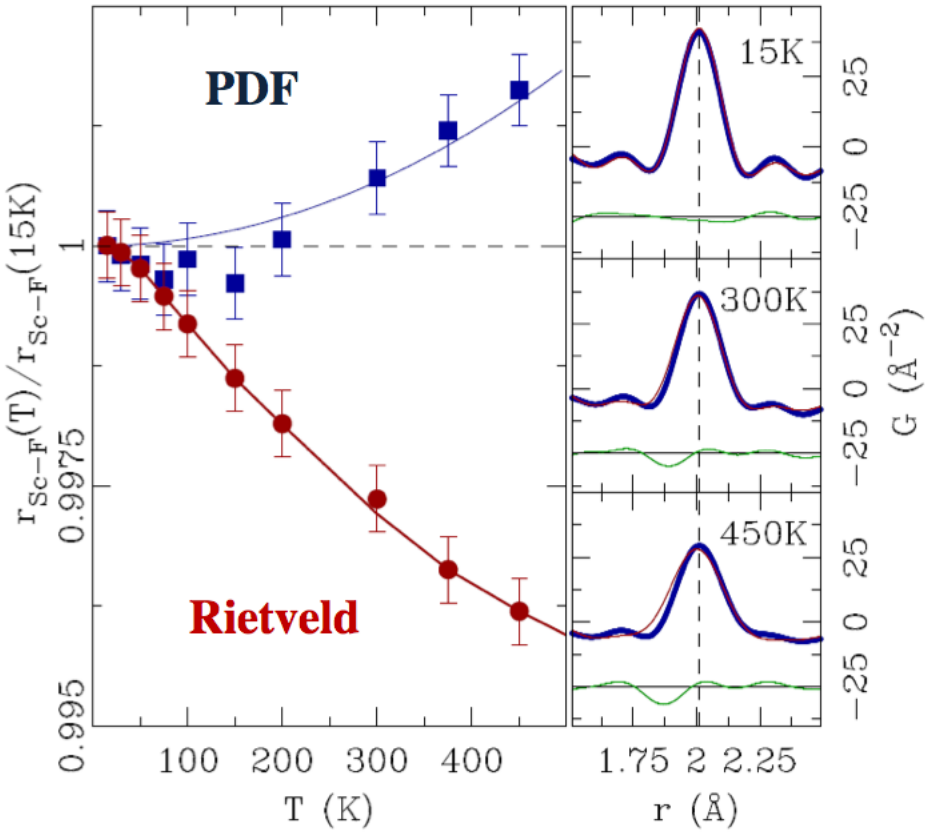

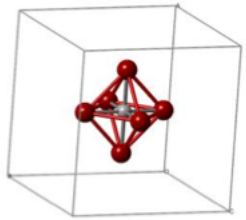

The case of PbTe

local offcentering of Pb at high T

E. S. Bozin *et al*, Science **330**,1660 (2010).

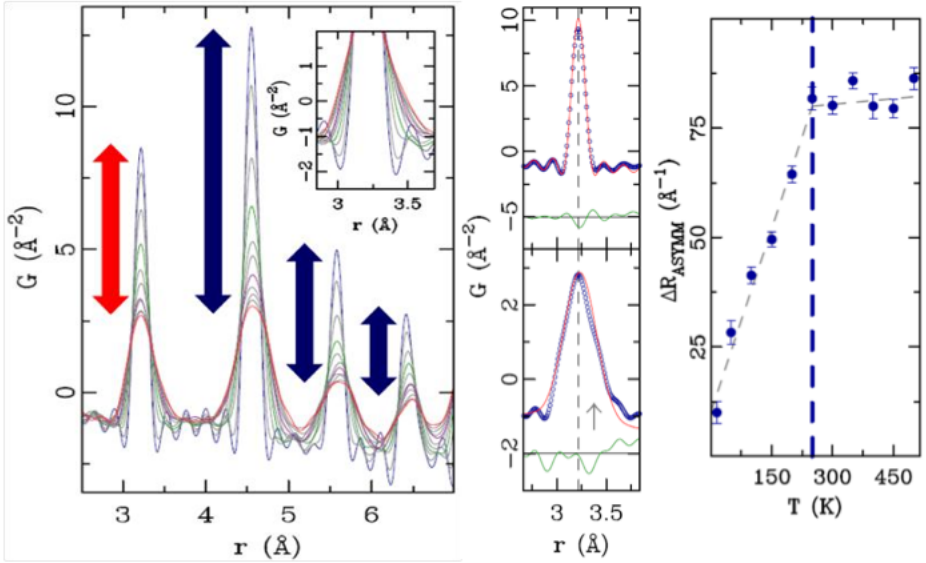

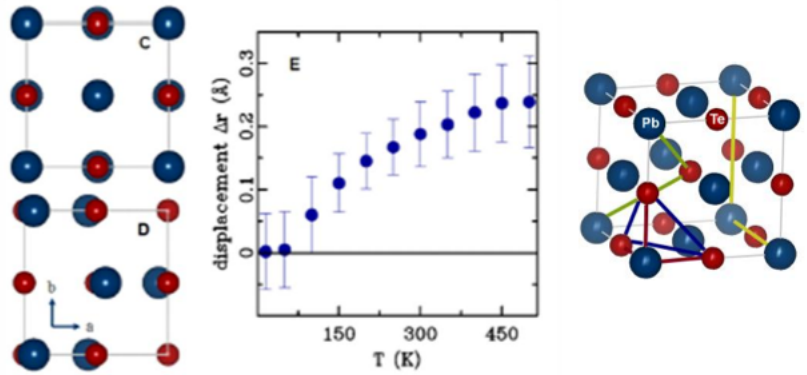

NEUTRONS

BROOKHAVEN NATIONAL LABORATORY

$$S(Q) = 1 + \left[I^{\text{el.}}(Q) - \sum c_i f_i^2(Q) \right] \Big/ \left[\sum c_i f_i(Q) \right]^2$$

$$S(Q) = \frac{1}{N|\langle b \rangle|^2} \langle \frac{d\sigma_{coh}}{d\Omega} \rangle - \frac{\langle |b|^2 \rangle - |\langle b \rangle|^2}{|\langle b \rangle|^2}$$

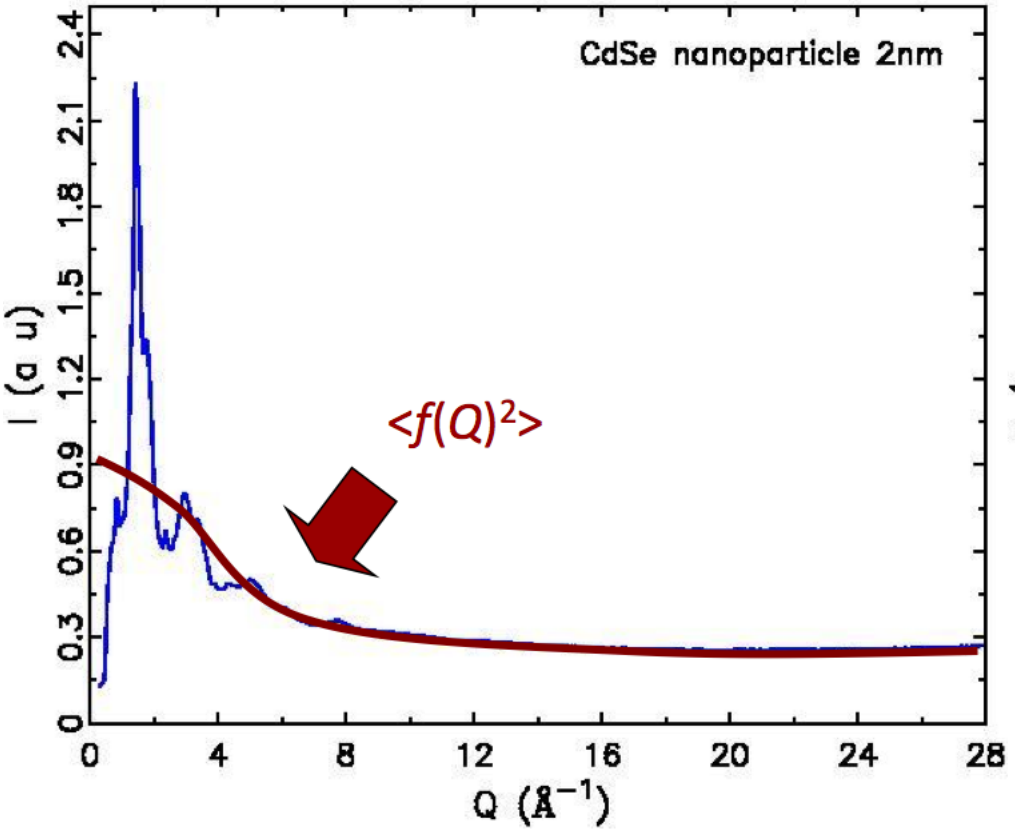

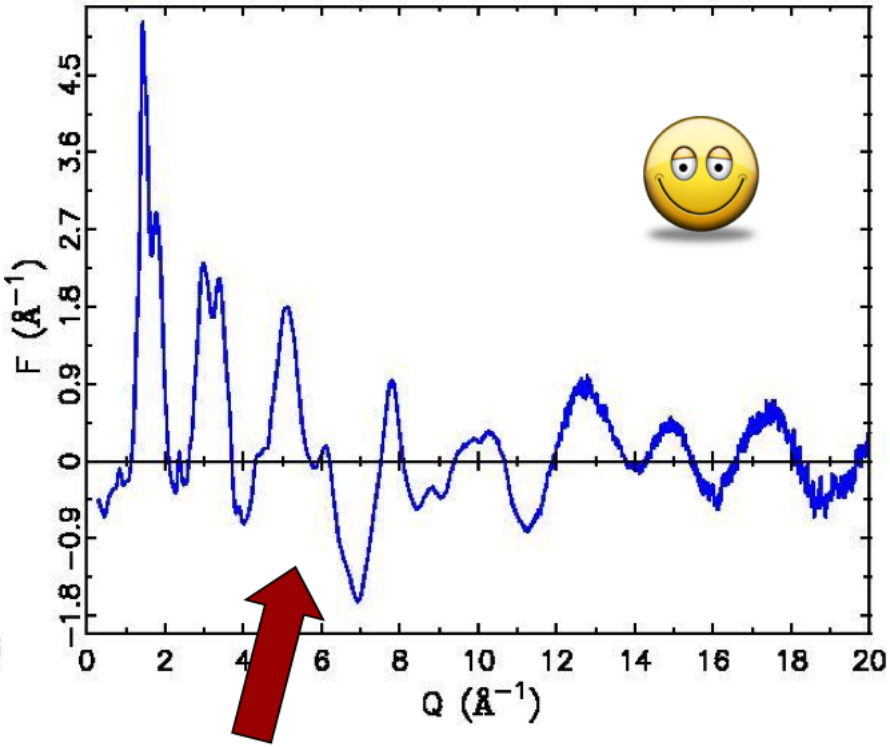

$$G(r) = \frac{2}{\pi} \int_0^\infty Q[S(Q) - 1] \sin Qr \, \mathrm{d}Q$$

Lanthanum Aluminate glass

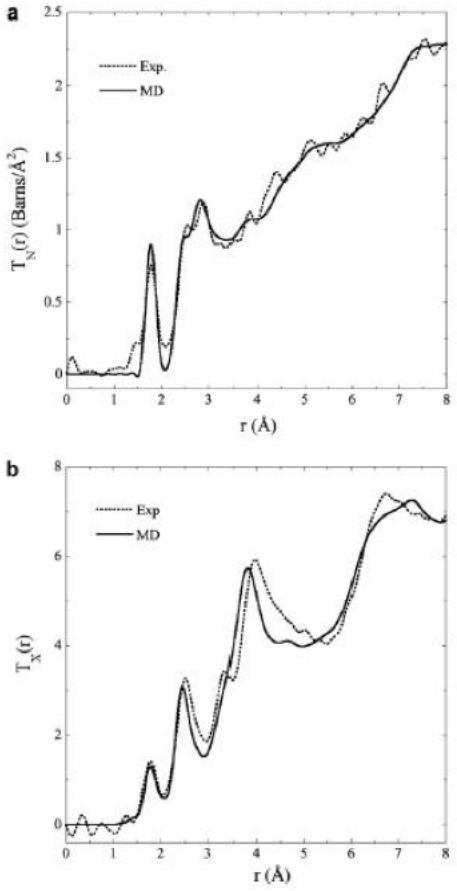

J. Du and L.R. Corales, J. Non-Cryst. Solids (2007)

Gold: bulk vs nanoparticle

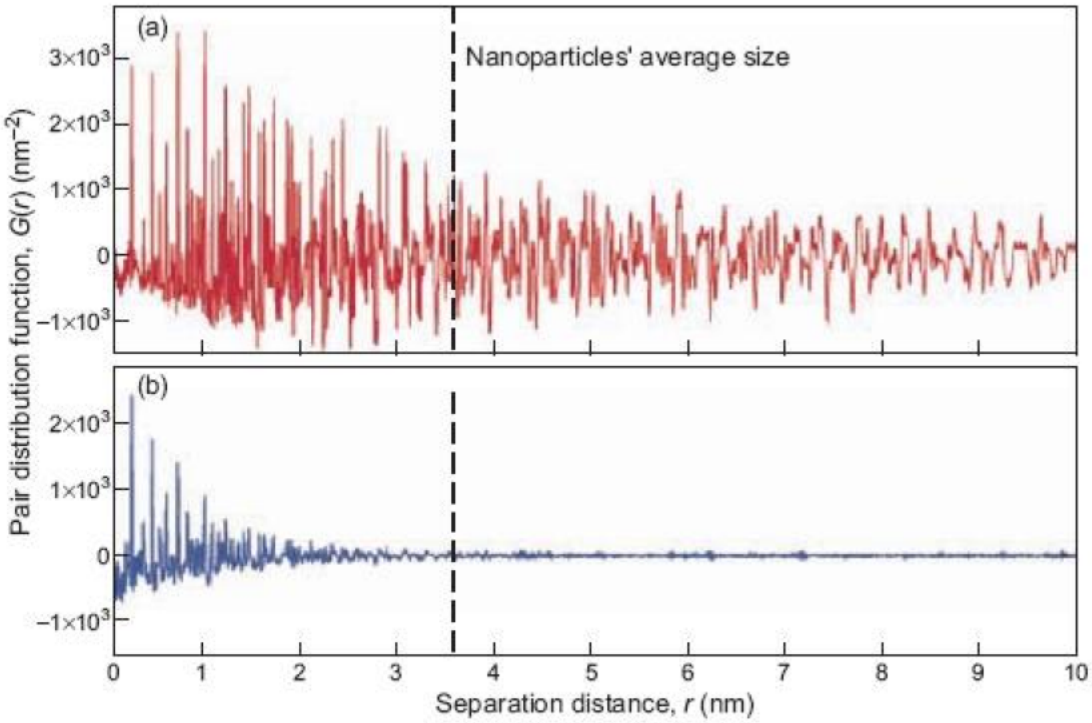

Th. Proffen et al, Los Alamos Science (2006)

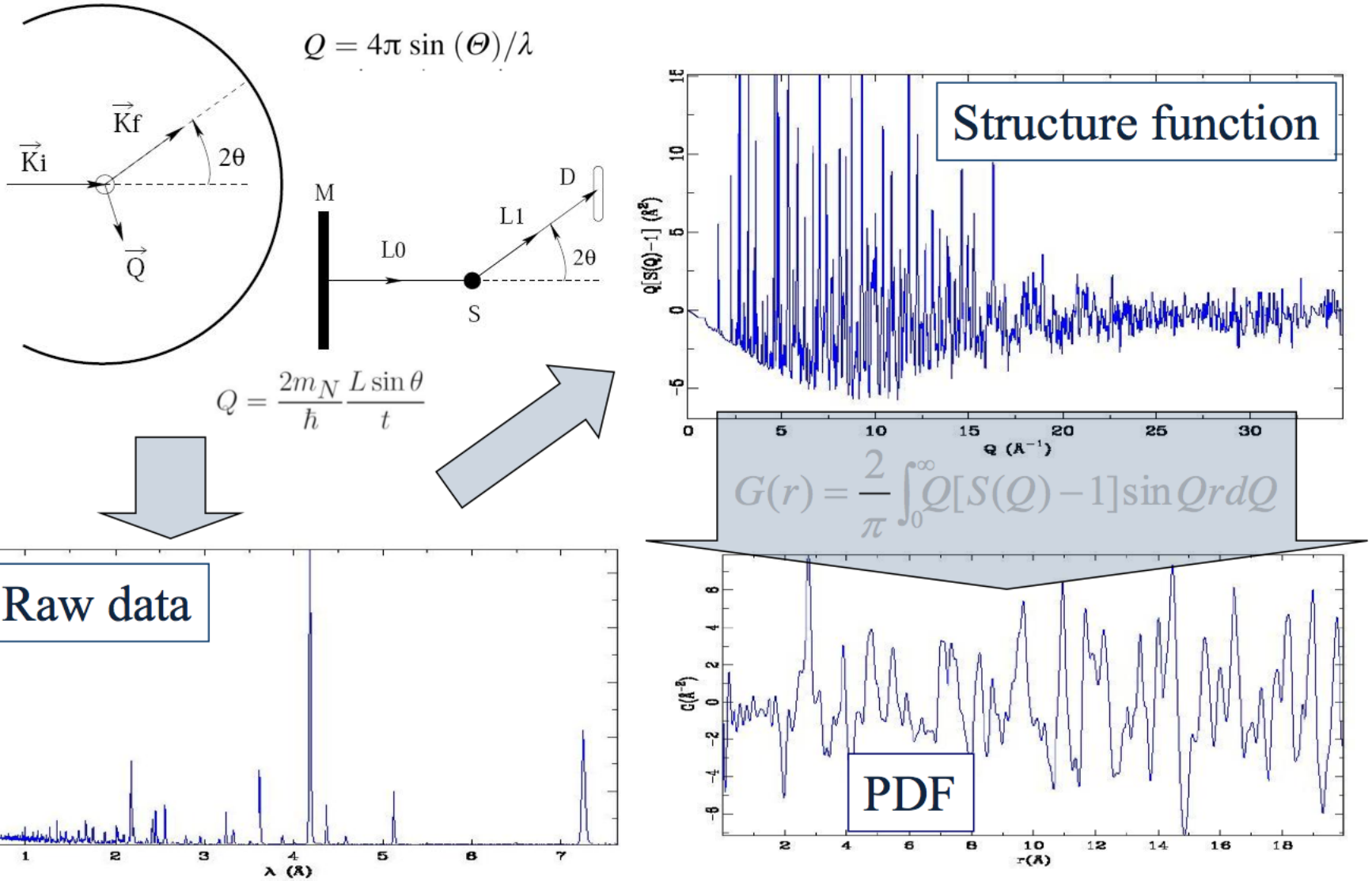
$Q = 4\pi \sin(\Theta)/\lambda$
Ki
Kf
2θ
Q
M
L0
L1
D
2θ
S
$Q = \frac{2m_N}{\hbar}\frac{L\sin\theta}{t}$
Structure function
$G(r) = \frac{2}{\pi}\int_0^\infty Q[S(Q)-1]\sin QrdQ$
Raw data
PDF
Counts
λ (Å)
Q (Å^{-1})
r(Å)

How do we get short range structural information?

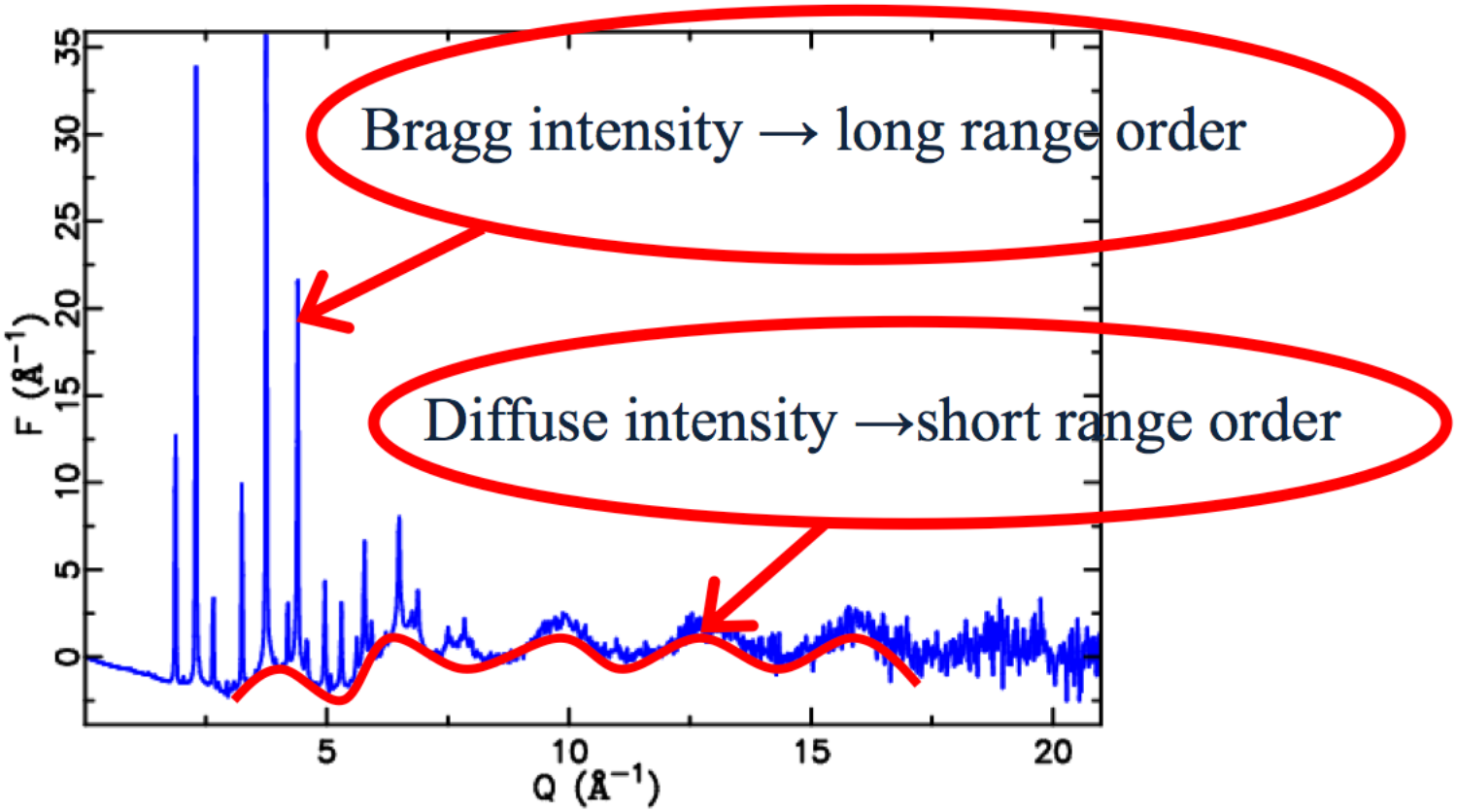

$$G(r) = \frac{2}{\pi}\int_0^\infty Q[S(Q)-1]\sin(Qr)dQ$$

Strength of the Pair Distribution Function Method

short range information

intermediate range information

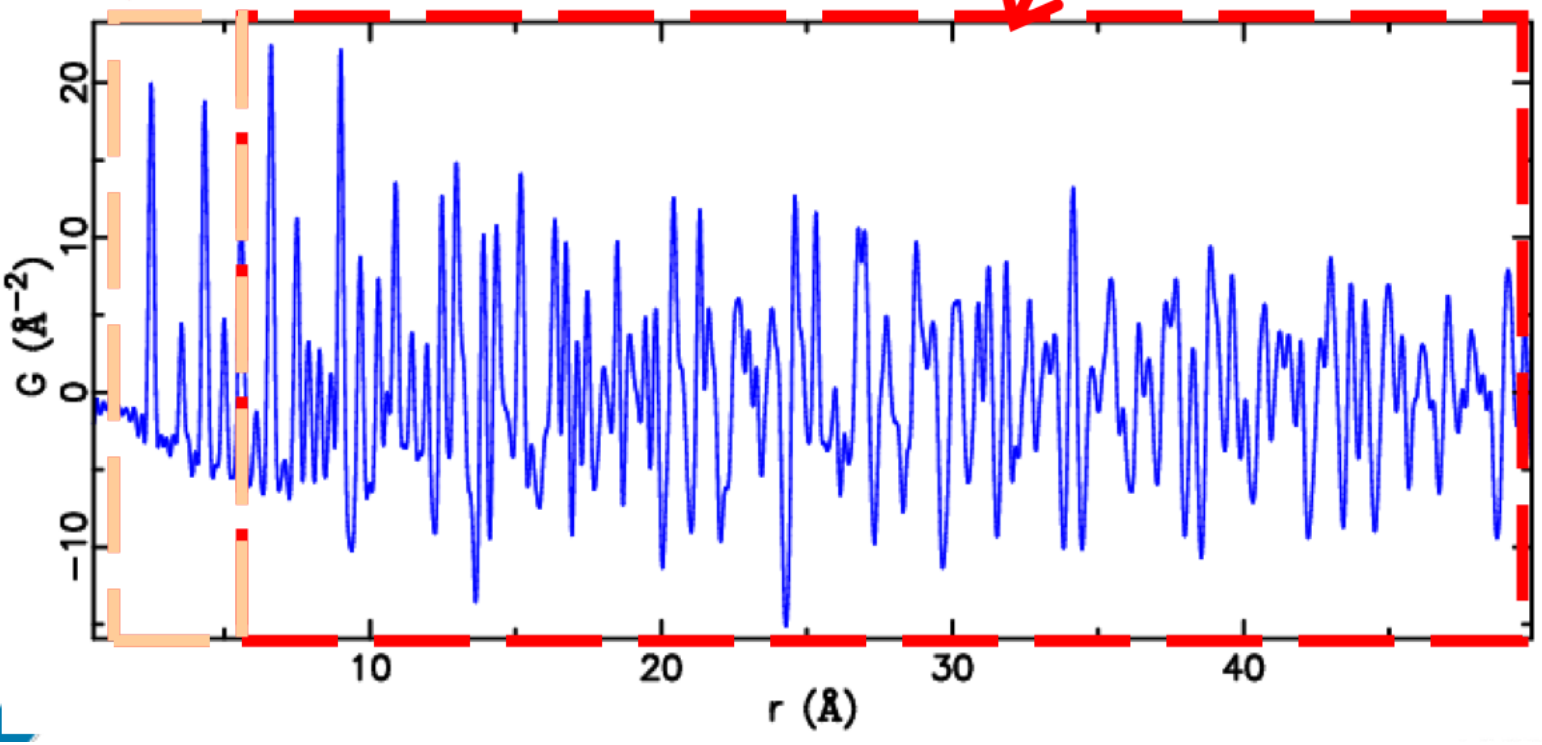

Effect of limited Q_{MAX} on PDF resolution
(real space resolution effects)

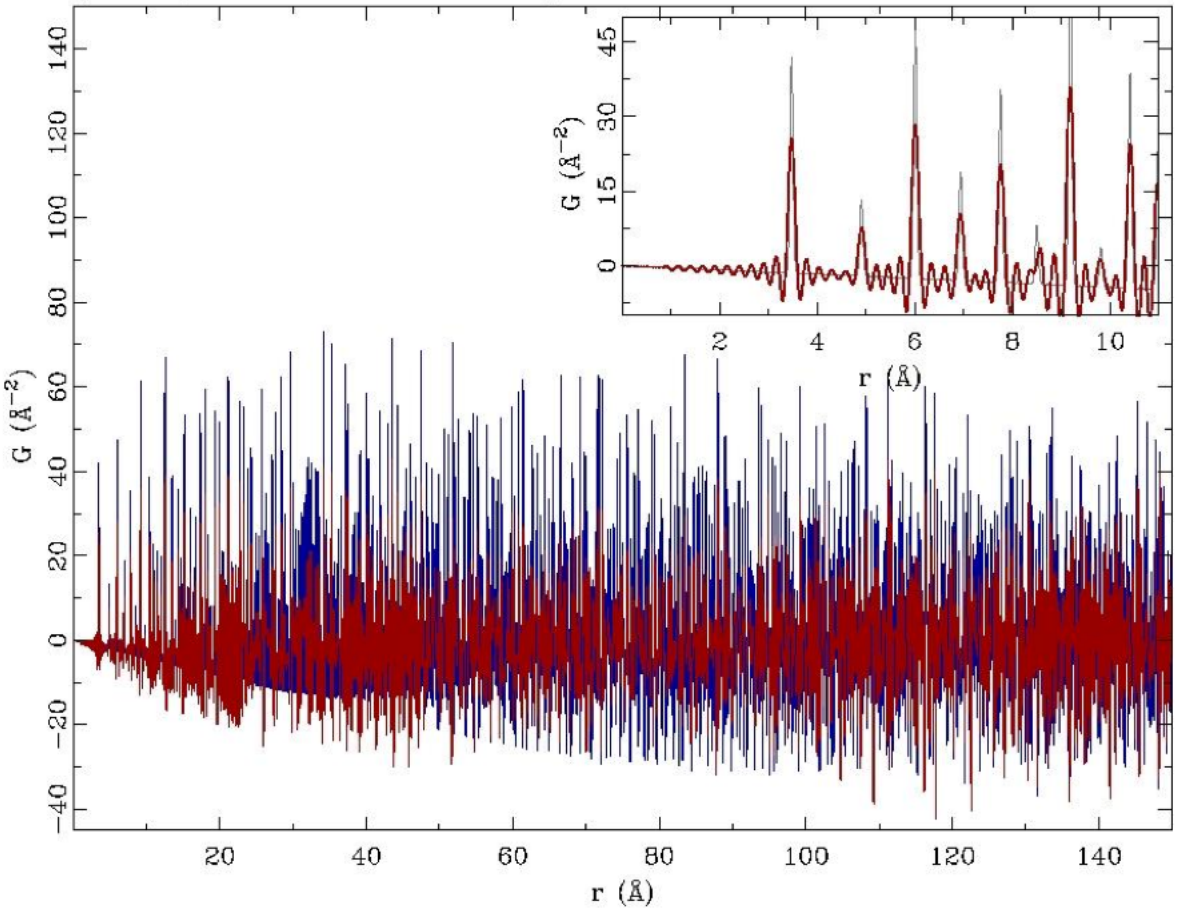

$$G(r) = \frac{2}{\pi}\int_0^{Q_{\max}} F(Q)\sin Qr\ \mathrm{d}Q$$

Q_{MAX}=12Å^{-1}

Q_{MAX}=24Å^{-1}

Q_{MAX}=36Å^{-1}

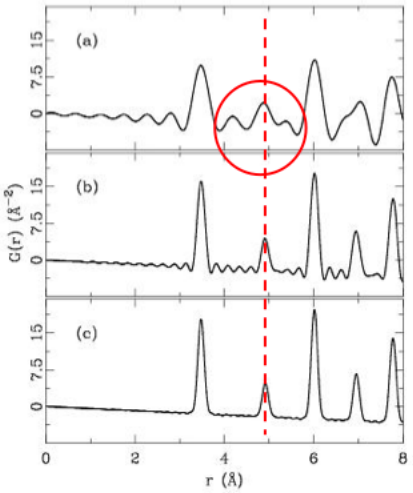

Figure 2.1: Effect of the termination ripples: simulated PDF of lead using Q_{max} values of (a) 12 Å^{-1}, (b) 24 Å^{-1}, and (c) 36 Å^{-1}.

$$G_{exp}(r) = \frac{1}{\pi}\int_0^{\infty} G(r')\left[\frac{\sin Q_{max}(r-r')}{r-r'} - \frac{\sin Q_{max}(r+r')}{r+r'}\right]dr'.$$

BROOKHAVEN

PDF primer: C60

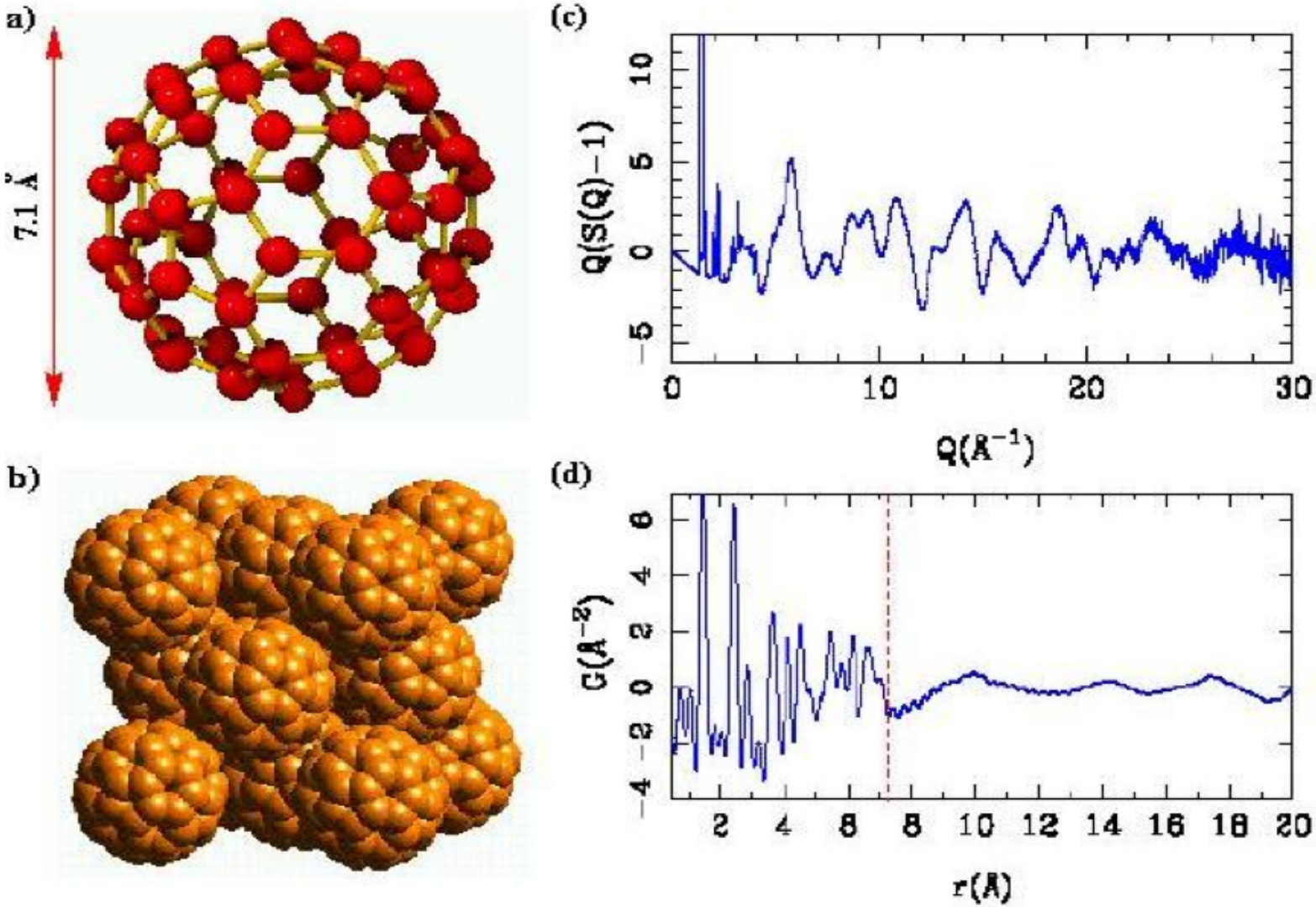

Summary

- Crystal structure (using VESTA software)
- Surface diffraction and surface structure
- Powder diffraction methods
- Williamson-Hall analysis of size and strain
- Pair Distribution Function (PDF)